2015-03-01

Experimental Testing of Shallow Embedded Connections Between Steel Columns and Concrete Footings

Nicholas Valgardson Barnwell
Brigham Young University - Provo

Experimental Testing of Shallow Embedded Connections Between Steel Columns and Concrete Footings

Nicholas Valgardson Barnwell

A thesis submitted to the faculty of
Brigham Young University
in partial fulfillment of the requirements for the degree of

Master of Science

Paul W. Richards, Chair
Fernando S. Fonseca
Richard J. Balling

Department of Civil and Environmental Engineering

Brigham Young University

March 2015

ABSTRACT

Experimental Testing of Shallow Embedded Connections
Between Steel Columns and Concrete Footings

Nicholas Valgardson Barnwell
Department of Civil and Environmental Engineering, BYU
Master of Science

Shallow embedded column connections are widely used for columns resisting gravity loads in current design methods. These connections are usually considered “pinned” for structural analysis. In reality these connections fall in between a fixed and a pinned condition. Although methods exist to estimate the stiffness and strength of exposed columns or embedded columns under lateral loads, little research has been done to determine the strength of shallow embedded columns.

An experimental study was carried out to investigate the strength of these connections. A total of 12 specimens with varying orientation, embedment depth, and column size were loaded laterally until failure or significant loss in strength. The results showed that shallow embedded connections are 86%-144% stronger in yielding and 32%-64% stronger in ultimate strength than current design methods would predict. This strength comes from a combination of the embedment depth and the resistance from the base plate and anchor rods. A model is proposed to explain the strength of the specimens and to conservatively estimate the strength of specimens with different variables. The specimens also exhibited stiffness ranging from 50%-75% of what would be expected from fully embedded columns.

Keywords: Steel columns, spread footings, baseplates, anchor rods, lateral stiffness

ACKNOWLEDGEMENTS

This research would not have been possible without the aid of numerous people, to whom I am very grateful. I would first like to thank Dr. Paul Richards for his constant support, encouragement, and advice throughout this process. He has been an incredible mentor and has put in a great amount of time and labor into this research. I would also like to thank my wife, Katelyn, who has been extremely patient and encouraging throughout this process. She has an incredible amount of faith in my abilities and constantly inspires me to do things that I thought were out of reach. Lastly I would like to thank the American Institute of Steel Construction which provided the funding for this project.

TABLE OF CONTENTS

LIST OF TABLES

LIST OF FIGURES

1 INTRODUCTION

1.1 Base Column Connections

In steel buildings there are three commonly used base connections for steel columns. These include: exposed, embedded, and shallow embedded column connections, all of which are shown in Figure 1-1. Exposed base connections are typical used in industrial facilities where the aesthetics of the connection are not important. Embedded base connections are used in moment frames to resist moment and shear loads. Shallow embedded base connections are the most widely used connection type and are typically used steel buildings for gravity columns (columns that are only designed to support the weight of the building). Shallow embedded connections for gravity columns are considered "pinned" for structural analysis and are only designed to resist the gravity load applied axially to the column.

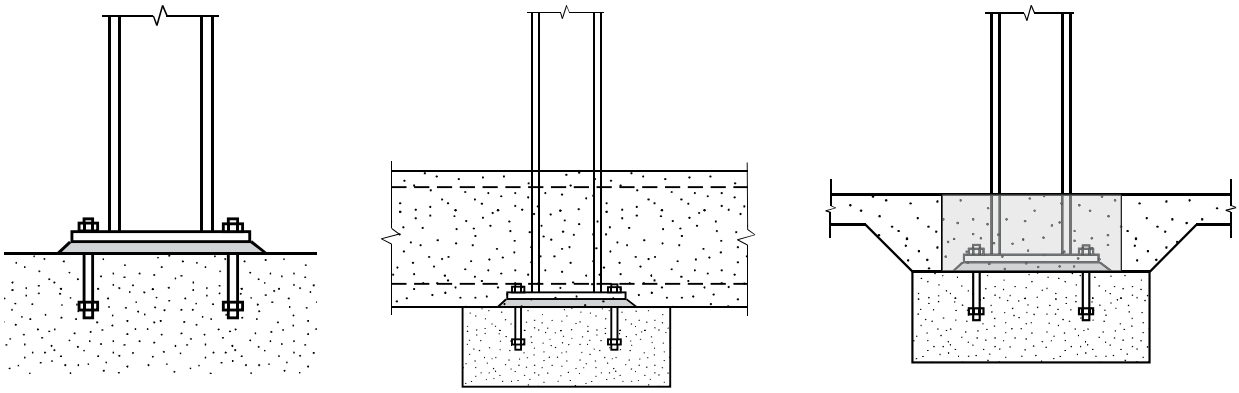

(a) Exposed **(b) Embedded** **(c) Shallow Embedded**

Figure 1-1: Base Column Connections

In typical construction practice, shallow embedded base connections are built in a block-out. This is a region of the floor slab that has not been filled with concrete around the column base, and allows the workers to build the connection [Figure 1-2]. After the connection is finished and the leveling grout underneath the baseplate has set, the block-out is filled in [Figure 1-1(c)]. These connections are considered to be pinned and have no flexural strength, this however is not entirely correct. The connection actually "falls" in between a pinned and a fixed connection.

Figure 1-2: Typical Block-out

1.2 Significance of Research

Little research has been done on shallow embedded column connections to determine the actual stiffness and strength they may have, but recently there has been more discussion about

shallow embedded connections. In tests performed by Xiao et al. [1] on HP pile-to-cap connections with shallow embedment, the results showed that although this shallow embedment was modeled as a pinned connection, it was able to resist a large moment at the connection. Although this phenomenon has occurred and been documented in other research, it has not been explored in greater detail.

It is important that an accurate model be developed to account for the strength and stiffness of these connections in the design of steel buildings. If significant strength and stiffness is discovered in these connections it could assist the lateral force resisting systems throughout the building. This could reduce the amount of steel used on a project because the amount of lateral force resisting systems could be reduced.

1.3 **Outline**

This chapter has discussed the types of column connections that are typically used today. It has also touched on the lack of research that exists on shallow embedded connections. Chapter 2 will go into detail on the research that has been done on embedded columns. Chapter 3 will lay out the testing procedures that were followed for this research. Chapters 4-6 will present and discuss the results obtained from the experimental testing.

2 LITERATURE REVIEW

2.1 Existing Strength Design

While methods exist for computing the strength of embedded steel shapes, little research has gone into determining the strength of shallow embedded base connections. The existing methods today may calculate the strength of just an embedded column or just an exposed base plate but they do not account for the combination of the two. This literature review will go into the existing methods and research for designing these connections, the lack of research for the specific connections being explored, and the need for more research on this topic.

2.1.1 Base Plate Guide Design Capacity

The columns studied in this research are only designed to resist axial loads due to gravity loads throughout the structure. These types of connections are designed using the Base Plate Design Guide [2]. The guide allows the designer to specify a base plate for gravity loads, small moments, or large moments. Figure 2-1 displays the current model for designing base plates for large moments. This model will be used to compare the test results from this research. These types of connections are used when the bending moment in the column is relatively large in comparison to the axial load. As it states in the design guide, the anchor rods need to be designed to prevent the column from tipping or causing the concrete to fail in compression [2]. That is, the

only resisting forces in this model come from the anchor rods and the concrete in compression. It does not account for added resistance of the bending moment from surrounding concrete.

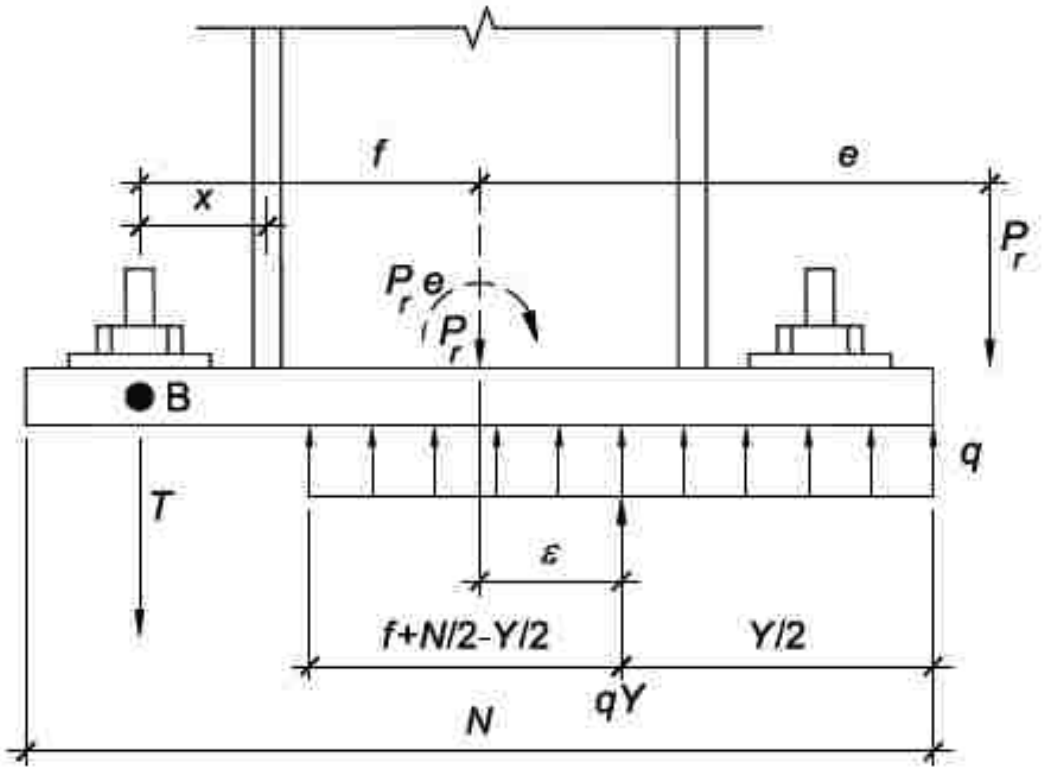

Figure 2-1: Base Plate Guide Design Model [2]

2.1.2 Precast and Prestressed Concrete Institute Design Handbook

The Precast and Prestressed Concrete Institute (PCI) Design Handbook [3] was one of the first texts to address the strength of embedded steel connections. Figure 2-2 shows the original model that appeared in this text. This model was based on an assumption that there was an embedment mechanism acting about a constant neutral axis. The model gave an estimated shear capacity, $V_{c,}$ that is based on the moment capacity of the connection and is given by equation 2-1 [3].

$$V_c = \frac{.85 f'_c b l_e}{3.67 + 4\frac{a}{l_e}} \qquad (2\text{-}1)$$

where:
f'_c = compressive strength of concrete in the pile cap
b = width of the embedded member
l_e = embedment depth
a = shear span of the pile

Although this was a conservative estimate of the strength of embedded columns, later research showed that the model was not sufficient.

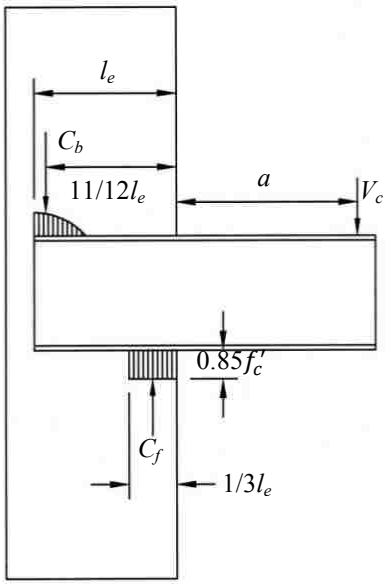

Figure 2-2: Original PCI Model

In 1980, Marcakis and Mitchell [4] performed experimental research on 25 different embedded specimens to determine a more accurate equation. Based on this research a new equation was proposed with some modifications. One of these modifications was that the width used in the equation could be taken as the confined column width, or the distance to the outside

of the column ties, but that it was limited to 2.5 times the width of the embedded shape. The new shear capacity is given by equation 2-2.

$$V_c = \frac{.85f'_c b_{eff} l_e}{1 + 3.6\frac{e}{l_e}} \tag{2-2}$$

where:
f'_c = compressive strength of concrete in the pile cap
b_{eff} = effective width of compression block
l_e = embedment depth
$e = a + l_e/2$
a = shear span of the pile

This equation appears in the most recent edition of the PCI Design Handbook and is used today to determine the strength of embedded steel members [3].

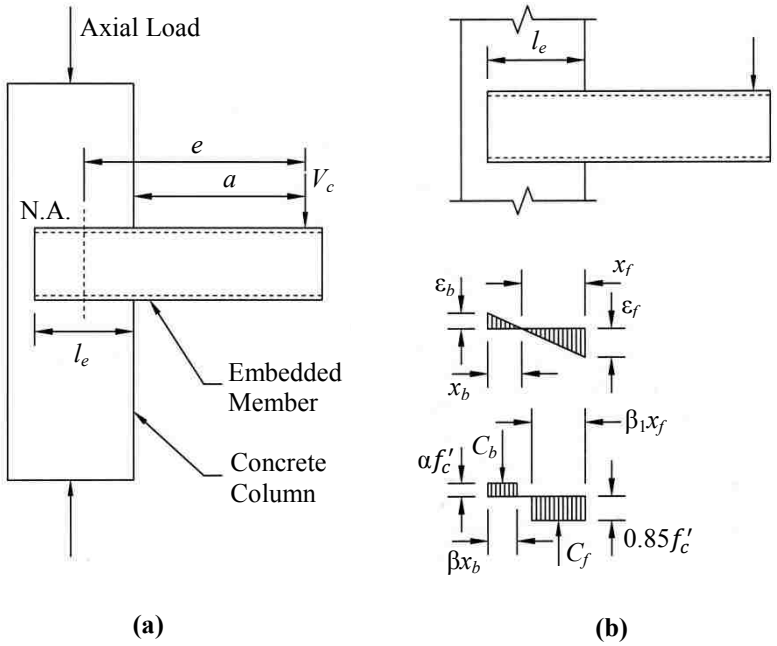

Figure 2-3: Current PCI Model [3]

2.2 Previous Research on Steel Column Connections

2.2.1 Embedded Steel Members

Embedded steel columns are widely used for steel moment resisting frames, but these connections are designed to fix the connection. Many tests have been performed to determine what actually makes an embedded column a fixed connection. Cui et al. [5] performed experimental research to determine if shallowly embedded columns could also function as fixed connections. In order to create this fixity, more rebar reinforcing was placed around the base plate. As part of the research a column with an exposed base plate connection was tested as well as columns with an unreinforced slab covering the connection. The research found that for a 100 mm slab and a 200 mm slab the strength of the specimen was 1.1 and 1.5 times stronger, respectively, than the exposed base plate. Although this research was mostly focused on how to make these shallow connections fully fixed, elements of the research showed that the existing models for determining the strength of these connections are inadequate.

In research performed by Pertold et al. [12], a model was proposed to determine the embedment length required to transfer moment and shear forces through an embedded connection. The embedment length determined by this model was smaller than what is used in practice today. One of the limitations of the research is that it is only valid for embedment depths ranging between b_{eff} and $2b_{eff}$, where b_{eff} is given by equation 2-3.

$$b_{eff} = min\begin{pmatrix} b_c + 0.5h_c \\ 2b_c - t_{wc} \end{pmatrix} \quad (2\text{-}3)$$

where:
b_c = width of the column section
h_c = depth of the column section
t_{wc} = thickness of the column web

In the case of shallow embedded columns the embedment depth will typically lie outside of this range. Although this model has shown that shallower embedment depths can resist more load than is currently expected, it does not provide a model that will work for columns with embedment less than or equal to the depth of the member, h_c, as defined in equation 2-3.

In research done on steel pile-to-pile-cap connections, which also demonstrated unexplained strength, Shama et al. [6], developed an equation to determine the capacity of these shallow embedded connections. This research was focused on finding an embedment depth that would allow the column to form a plastic hinge. A formula was derived that allows the designer to specify an efficiency of the connection with respect to the plastic hinge moment of the column, and find the required embedment depth. To accomplish this, an equation to estimate the moment capacity of the concrete in the joint was derived assuming that the connection was limited by the compressive strength of the concrete at the extreme fiber in the front face of the connection. This capacity is given by equation 2-4.

$$M_j \leq \frac{.85f'_c b_f {l_e}^2}{\left(6 + \frac{l_e}{L^*}\right)} \tag{2-4}$$

where:
L^* = distance from the point of application of the lateral load to the neutral axis of the joint

Xiao et al. [1] also performed research on steel pile-to-pile-cap connections. These connections typically have rebar attached to the embedded member which deviates from the model outlined in the PCI Design Handbook. This model is comparable to the base connections researched in this paper, as the strength of the attached rebar can be comparable to the strength of the anchor rods in a base plate. An example of these connections can be seen in Figure 2-4.

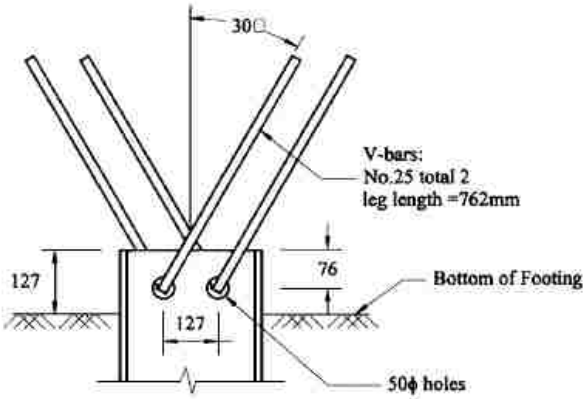

Figure 2-4: Pile-to-Pile-Cap Connections [1]

In this study the specimens were able to develop large moment resistance that could not be explained. Using the equation derived by Shama et al. [6] the expected strength of the columns were computed as $.06M_p$, where M_p is the plastic moment of the steel member. However, the connections were able to resist moments ranging from 0.25 to $0.66M_p$. This is much greater than the estimated strength which means there were other mechanisms contributing to the moment resistance. Figure 2-5 shows the two different mechanisms that were believed to be creating the moment resistance.

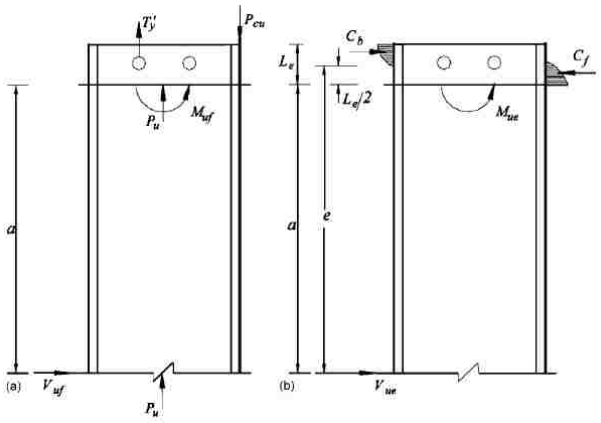

Figure 2-5: Moment Resistance Mechanism [1]

In the research the equation proposed by Marcakis and Mitchell [4] for embedment resistance was used in combination with the flexural resistance mechanism shown in Figure 2-5. Using this model the strength of these connections was able to be estimated very closely. The equations from the PCI Design handbook were reduced to equation 2-5 by simply multiplying the shear by the distance, as shown in the PCI model. The flexural mechanism resists the load through tension in the rebar and a compressive block underneath the steel shape (that is equal to the force in the rebar).

$$M_{ue} = \frac{.85 f'_c b_{eff} l_e}{1 + 3.6 \frac{e}{l_e}} a \qquad (2\text{-}5)$$

where:
M_{ue} = nominal strength provided by the embedment mechanism
f'_c = compressive strength of concrete in the pile cap
b' = effective width proposed by Marcakis and Mitchell (1980)
L_e = embedment depth
$e = a + L_e/2$
a = shear span of the pile

While this approach seems reasonable, it has been shown in other tests that these connections still have unexplained strength even after taking into account the mechanism in the concrete and the flexural mechanism resisting the moment. In experimental tests performed by Richards et al. [7] on pile-to-cap connections for pipe piles, it was discovered that these connections had much more strength than anticipated from the methods mentioned above. Figure 2-6 shows the mechanisms that were used to calculate the expected strength of the connection before the tests were performed.

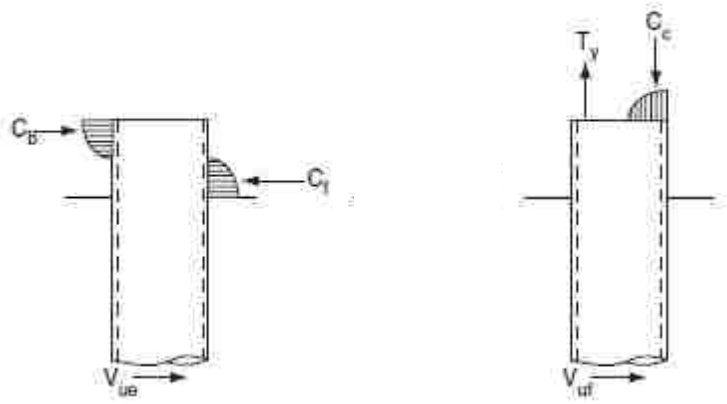

(a) Embedment Mechanism **(B) Flexural Reinforcement Mechanism**

Figure 2-6: Moment Resisting Mechanisms [7]

In these tests, the specimens consisted of two pipe piles embedded into a pile cap. One of the most intriguing specimens exhibited strengths much higher than predicted, and was able to pull the trailing pile out of the ground before any failure occurred in the pipe or the pile cap. It was suggested in the paper that unexplained strength of the specimens could be attributed to the friction force between the concrete and the pipe pile. This friction mechanism is shown in Figure 2-7. These friction forces could be calculated using the forces C_b and C_f from the embedment mechanism, multiplied by the friction coefficient for concrete poured against steel. In the calculations it was assumed that the force F_f would only become as large as F_b so that the forces were balanced, but that F_b would be developed fully. With these assumptions, the moment due to the friction could be calculated with equation 2-6.

$$M_{friction} = F_d d \qquad (2\text{-}6)$$

where:
$F_b = \mu C_d$
μ = coefficient of friction
$C_d = .85 f'_c b_{eff} a$
d = diameter of steel pipe

When added resistance was applied to the model used to predict the strength, it produced strength much higher than was exhibited in the specimen. As was stated before, the mode of failure for this specimen was that the trailing pile was pulled out of the ground, so it could have been possible for the specimen to reach this capacity had the pile stayed in the ground.

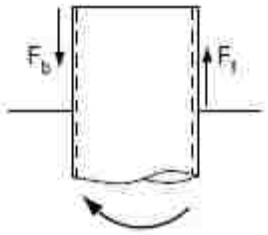

Figure 2-7: Friction Mechanism [7]

In recent research performed by Eastman R.S. [8], an experimental test was performed on steel piles with shallow embedment. This research consisted of three specimens. For each specimen the cap was 3×3×5' with typical cap reinforcement. The piles used in the tests were 12.75" in diameter. All three piles extended approximately 5' out of the concrete and the embedment depths were 17.9", 6.25", and 4.56", respectively. These depths were chosen as fractions of the pile diameter, the fractions being, 1.5, 0.5, and 0.4, respectively. All the specimens had a steel cover plate welded to the embedded end of the pile cap. The specimen with the deepest embedment yielded the column, while the other two specimens experienced failure in the concrete. All three specimens exhibited larger strength than expected.

From this research a model for elastic strength was proposed to explain the unexpected resistance. This model is essentially an elastic version of the model developed by Marcakis and

Mitchell, which is used in the PCI design handbook, with an added bearing force underneath the cover plate. The overall model is shown in Figure 2-8.

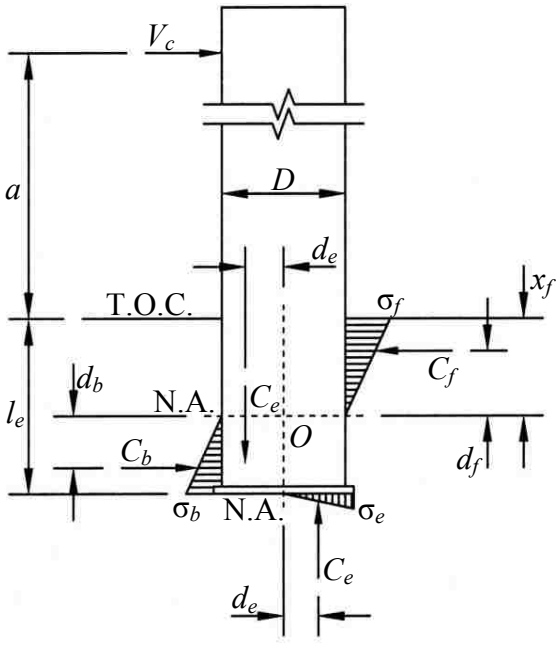

Figure 2-8: Elastic Strength Method Developed by Eastman, R.S. [8].

With a few assumptions the values shown in this model can be determined. The first assumption is that the maximum stress at the front of the connection corresponds to a strain of 0.001. This assumption means the concrete strain is still in the elastic region. The stress at the front of the connection, σ_f, can be determined from equation 2-7.

$$\sigma_f = \varepsilon_e E_c \qquad (2\text{-}7)$$

where:
$\varepsilon_e = 0.001$
$E_c = 4731\sqrt{f'_c}$, MPa
f'_c = compressive strength of concrete, MPa

Using this stress, the magnitude of the resultant acting on the front of the connection, C_f, can be determined from equation 2-8.

$$C_f = \frac{1}{2} x_f D \sigma_f \tag{2-8}$$

Using the elastic linear relationship between the stress at the front and back of the connection, the stress at the back of the connection can be determined using equation 2-9.

$$\sigma_b = (l_e - x_f)\left(\frac{\sigma_f}{x_f}\right) \tag{2-9}$$

The magnitude of the resultant acting at the back of the connection can be determined with equation 2-10.

$$C_b = \frac{1}{2}(l_e - x_f) D \sigma_b \tag{2-10}$$

The distance from the neutral axis to the location of the resultants associated with these two stresses can be found from equations 2-11 and 2-12, respectively.

$$d_f = \frac{2}{3} x_f \tag{2-11}$$

$$d_f = \frac{2}{3}(l_e - x_f) \tag{2-12}$$

Once these forces have been determined, force equilibrium gives us equation 2-13.

$$V_c = (C_f - C_b) \tag{2-13}$$

The remaining forces acting in the y-direction, shown in Figure 2-8, could be limited by two factors that will be described here. The end bearing stress is assumed to be zero in the middle of the pile and increases linearly to the edge stress, σ_e. This stress is given by equation 2-14 and states that the magnitude of the bearing triangular stress block is similar to that of the back end stress block, σ_b but limited to be less than it.

$$\sigma_e \leq \sigma_b \tag{2-14}$$

The resultant vertical force can then be determined from equation 2-15.

$$C_e = \frac{1}{6} D^2 \sigma_e \tag{2-15}$$

The distance from the vertical neutral axis to the location where the resultant acts was derived and is given by equation 2-16.

$$d_e = \frac{3\pi D}{32} \tag{2-16}$$

A balancing vertical force that can be seen in Figure 2-8 is also assumed to exist in the model. This force could be due to friction between the pile and the concrete. Since this value must be equal to the vertical bearing stress, the value of C_e would be limited by the friction force. The second limitation put on the bearing force is given by equation 2-17. This resultant is assumed to act at the same distance d_e given by equation 2-16.

$$C_e = .75\mu_k \tag{2-17}$$

where:
$\mu_k = 0.35$ for kinetic friction between steel and concrete

Once the limiting factor for the vertical bearing stress is determined, the location of the neutral axis can be found from equation 2-18. Then, the maximum elastic load can be found using equation 2-13.

$$V_c(a + x_f) = C_f d_f + C_b d_b + C_e d_e + C_e d_e \tag{2-18}$$

The methods for computing the maximum elastic load are compared in Figure 2-9. In this figure the lowest curve assumes no end bearing stress, the middle curve assumes the bearing force is limited by friction, and the upper curve assumes the bearing stress is equal to stress at the back of the column ($\sigma_e = \sigma_b$). The elastic strength of the specimens is also plotted.

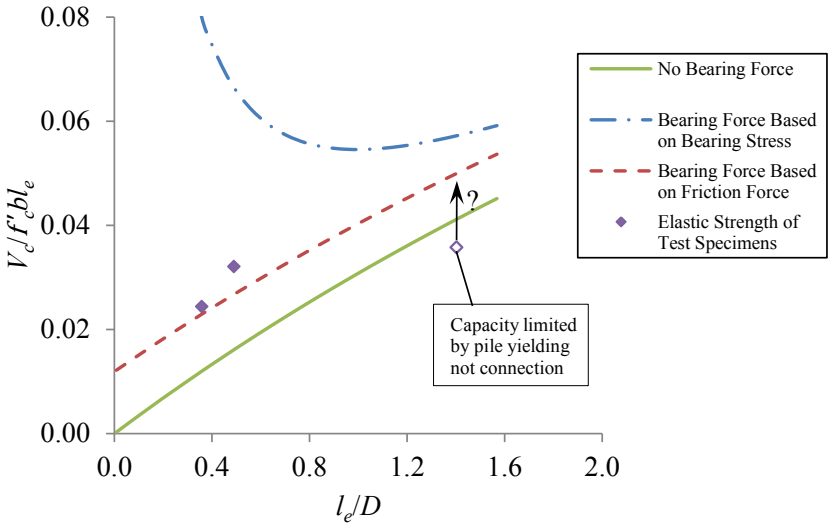

Figure 2-9: Model for Elastic Strength Compared with Elastic Strength of Specimens [8]

2.2.2 Exposed Base Plate Connections

Other research has been conducted on exposed base plate connections as well. Recently Kanvinde and Deierlein [9] performed tests on standard exposed steel base connections. In these tests, base plates were designed according to the design guide and tested to determine how the moment resistance compared to the expected moment resistance. One of the most interesting aspects of this research was that the specimens showed little strength degradation up through 7%-10% drift cycles. This was surprising as other structural elements are typically designed to have little strength degradation up until about 4% drift. Also, on average the specimens were 80% stronger than the design guide estimates. In the experiment, yielding in the base plate was primarily responsible for the energy dissipation that allowed the specimens to show little strength degradation. An example of this yielding is shown in Figure 2-10. In todays practice much design is put into making sure the base plate remains elastic, although the base plate can dissipate a large amount of energy through yielding. While the research presented herein is

mainly focused on the effect embedment has on strength, the fact that existing models are not sufficient to estimate the moment resistance of these connections will be addressed.

Figure 2-10: Base Plate Yielding [9]

Other research performed by Thambiratnam and Paramasivam [10] also showed that base plate connections were able to develop more moment resistance than expected. In this experiment, one of the variables was the eccentricity at which the load was applied. The research showed at the lowest eccentricities the specimens failed from concrete cracking but for the rest of the tests, at medium to high eccentricities, the mode of failure was base plate yielding. In the end these connection had a factor of safety ranging from 1.09-1.89 with a mean value of 1.35 when compared to the allowable strength method.

The existing methods for designing shallow embedded columns have been shown to be insufficient. It is important that these connections be tested and quantified so that they can be accurately represented in design.

3 METHODS

3.1 Overview

This study investigated three different factors to determine their effect on the flexural strength and stiffness of typical steel gravity column base connections. These factors include: embedment depth, column shape, and column orientation, with the main focus on embedment depth. There were eight specimens designed to specifically test these factors. Four more specimens were created to test the effect having the anchor bolts disengaged and the floor slab braced from movement had on the strength. The first eight specimens are listed in Table 3-1 and the four modified specimens are listed in Table 3-2 with their respective variables.

Table 3-1: Standard Specimen Parameters

Specimen	Embedment [in]	Orientation	Shape
A1	8	Strong	W8×35
A2	8	Strong	W8×48
A3	8	Weak	W8×35
A4	8	Weak	W8×48
B1	16	Strong	W8×35
B2	16	Strong	W8×48
B3	16	Weak	W8×35
B4	16	Weak	W8×48

Table 3-2: Modified Specimen Parameters

Specimen	Embedment [in]	Orientation	Shape	Braced Slab
CA2	8	Strong	W8×48	Y
DA2	8	Strong	W8×48	N
CB2	16	Strong	W8×48	Y
DB2	16	Strong	W8×48	N

The test setup consisted of the frame, the actuator and a test specimen as shown in Figure 3-1. The frame was constructed out of a W12×72 column that was bolted to the floor and then laterally braced by two W8×31 struts. This frame was designed to resist the force that came from the actuator as it pushed on the test columns. The actuator (110 kips capacity) was placed at two different heights depending on the specimen. This was done to keep the distance between actuator and the top-of-slab similar for different embedment depths. The actuator was connected to the test column through a connection piece that was bolted through the shape to a plate on the opposite side of the shape. This allowed the actuator to push and pull the shape back and forth. The connection piece was designed with a specific length so the actuator would begin testing at mid stroke, allowing it to reach its maximum displacement (+/- 10") in both directions.

The specimen consisted of a steel column, slab-on-grade concrete, footing concrete, and block-out concrete. The slab-on-grade concrete was first poured around the block-out and then the column was connected to the footing through the anchor bolts embedded in the footing. The block-out was essential to create the connection. The embedment depths of the specimens were determined by the thickness of the slab-on-grade concrete. Typical slab-on-grade is 12" thick but in some cases can be up to 24" thick. The columns were designed on a ⅔ scale, thus the embedment depths of the columns were also based on a ⅔ scale which yielded depths of 8" and 16".

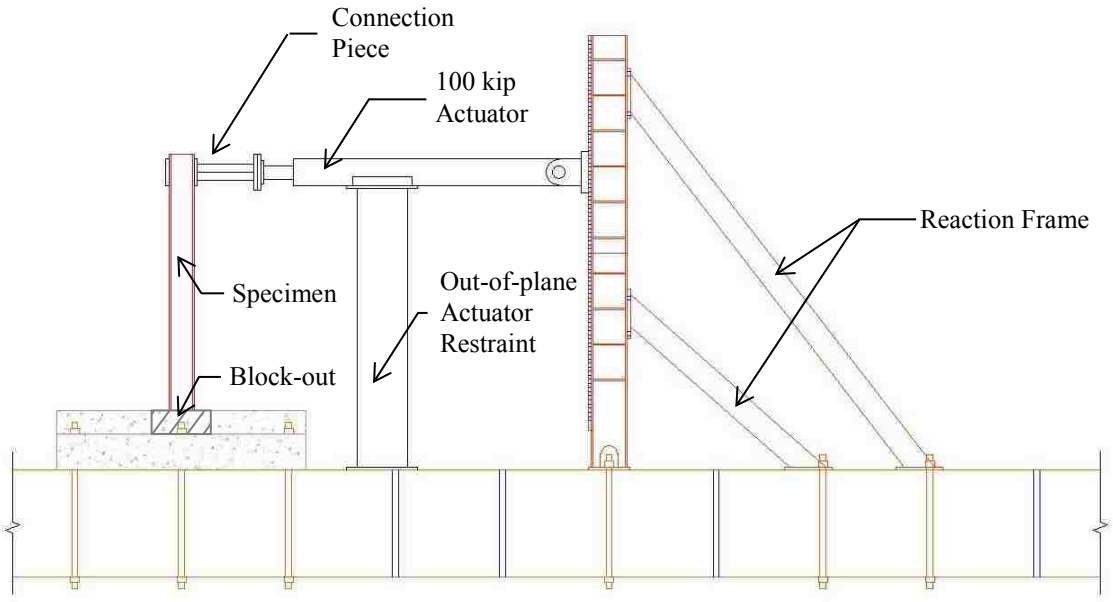

Figure 3-1: Test Overview

3.2 Specimen Design

3.2.1 Steel Design

The base plate design and column layout can be seen in Figure 3-2. The specimens consisted of four W8×48 columns and four W8×35 columns all with identical base plates. The columns for the 8" embedment were 7'8" tall, and the columns for the 16" embedment were 8'7" tall. The base plate was designed as a PL 1"×13"×1'1" plate with four 1 $^{5}/_{16}$" diameter anchor rod holes spaced 1 ¼" from the edge of each side of the base plate. A grout hole with the same diameter as the anchor rod holes was placed on the centerline perpendicular to the web of the column and 2" from the centerline parallel to the web of the beam. All the columns were welded

to the base plate with ¼" welds on the outside of the top and bottom flange. The calculations that were used to determine the plate size can be found in Appendix B.

The column sizes were selected based on columns that would typically be found in steel buildings. Different shape property ratios were taken from W14× and W12× columns and were used to find W8× columns that had similar property ratios. The justification and explanation for this selection can be found in Appendix A. The calculations used to determine the ratios can be found in Appendix B.

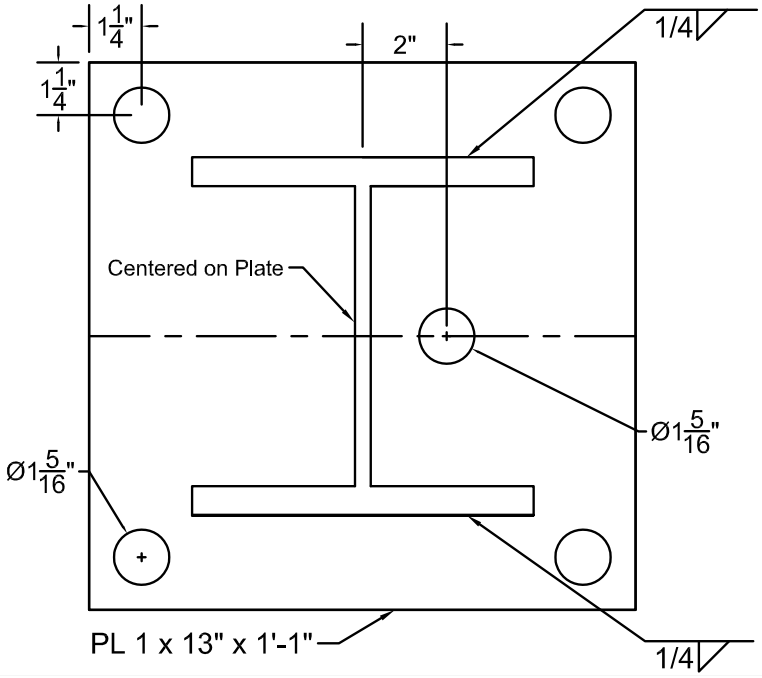

Figure 3-2: Base Plate Design

3.2.2 Concrete Design

The concrete part of the test specimens was intended to represent a footing and slab-on-grade, and have the capacity to be lifted and moved. The bottom layer of concrete, representing

the footing, was 7'×7'×1' [Figure 3-3 and Figure 3-4]. The bottom reinforcement consisted of six, 6'9" #5 bars in both directions. The outside bars were designed to guide the PVC that went through the footing and therefore the exact dimensions were set during the construction process. The remaining bars were evenly spaced from the outside bars with a spacing of 14 ⅜". The inside bars were spaced 11 ⅞" apart in order to guide the column anchor rods during the construction process. The bottom mat of rebar sat on 2" chairs. Four #5 bars with 90-degree bends were designed to pick up the specimens. Both legs of the bars extended down to the bottom layer of reinforcement with the 90-degree bend wrapping underneath the rebar.

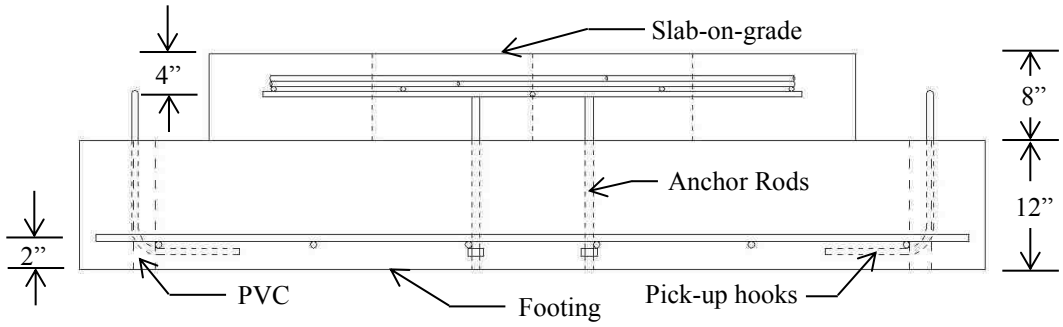

(a) Shallow Embedment

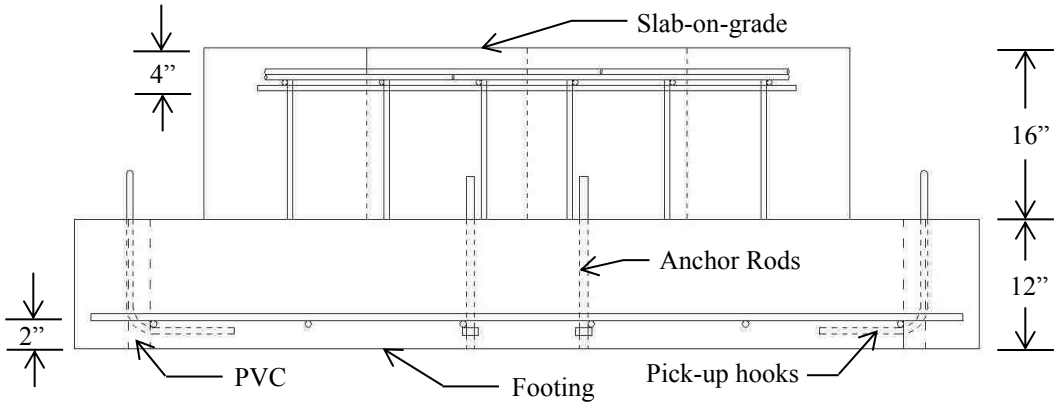

(b) Deep Embedment

Figure 3-3: Concrete Elevations

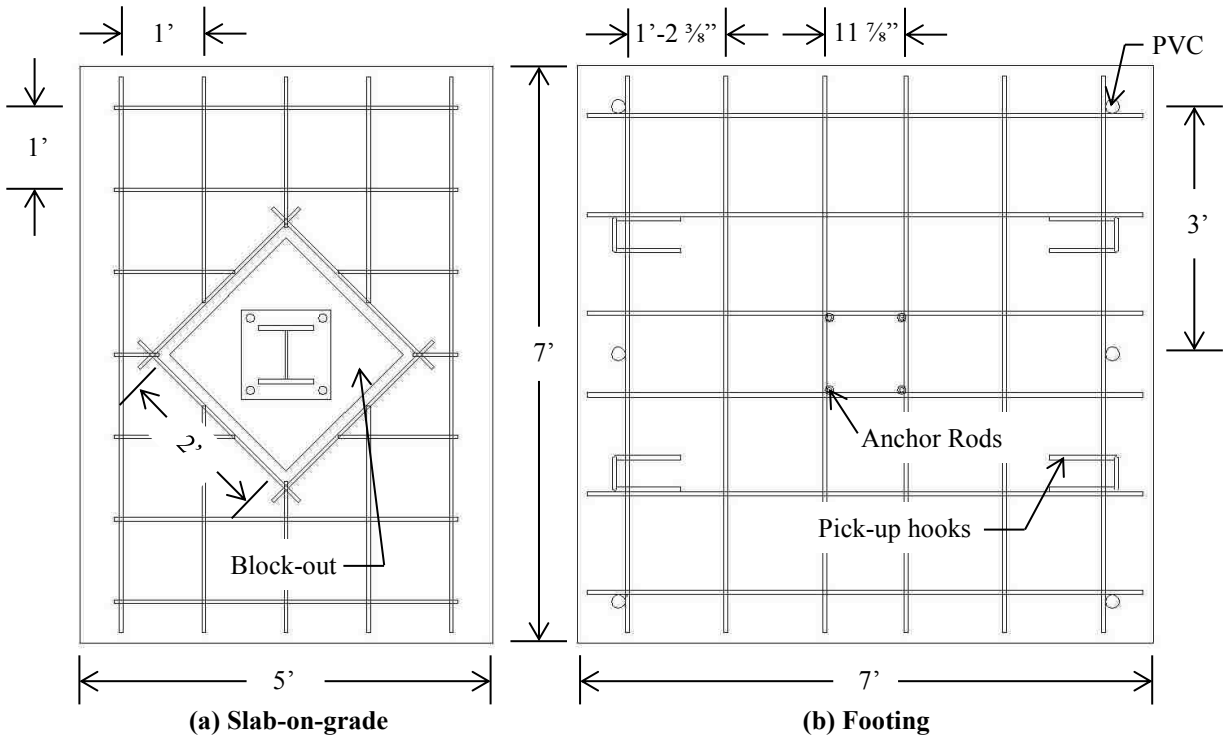

Figure 3-4: Rebar Layout

The second layer of concrete represents the slab-on-grade. For the first four specimens a 7'×5'×8" thick slab was poured on top of the footing and for the other specimens the slab was 16" thick. Around where the column would be placed a 2'×2' diamond block-out was provided, centered on the slab and over the anchor bolts. To make up for the interrupted reinforcement at the block-out #4 bars were placed 1 ½" from the edge of the block-out. The remaining reinforcement consisted of # 4 bars evenly spaced at 1' in both directions. The specific lengths and layout of the bars varied and can be seen in Figure 3-4. For both embedment depths the bottom layer of the top reinforcement mat was placed about 4" from the top of the slab. An elevation view of the rebar in the slab and footing is shown in Figure 3-3.

The justification for the concrete design is discussed in Appendix A. All the necessary calculations for the concrete design are found in Appendix B.

3.3 Construction Process

3.3.1 Specimen Construction

The overall construction process is shown in Figure 3-5 through Figure 3-19. The process will be described for one specimen, but all eight specimens were constructed in the same way. The construction process began by laying out the bottom layer of rebar and tying it together in a mat for each specimen [Figure 3-5]. This process was repeated for rebar in the second layer of concrete as well [Figure 3-6]. The top layer was set aside until after the bottom concrete had been poured. Next eight 7'×7' forms with plywood bases were assembled. Figure 3-7 shows the completed form and the placement of the PVC and anchor rods. Using the rebar to guide the placement of the PVC and anchor rods as was discussed before proved to be too difficult. In order to guide the PVC pipe, six plywood disks with the same inside diameter as the PVC were nailed in the locations where the PVC pipe would be placed [Figure 3-8]. To guide the anchor rods a plywood guide was fastened in the center of the base [Figure 3-9]. Then the rebar mat was placed in the form on 2" chairs and the rebar designed to pick the specimen up was tied into it [Figure 3-7]. Next the anchor rods were placed in the guide and a second guide was placed at the top of the bolts with nuts on both sides of the plywood, which prevented the bolts from drifting out of place [Figure 3-7].

Figure 3-5: Tying the Footing Rebar

Figure 3-6: Tying the Slab Rebar

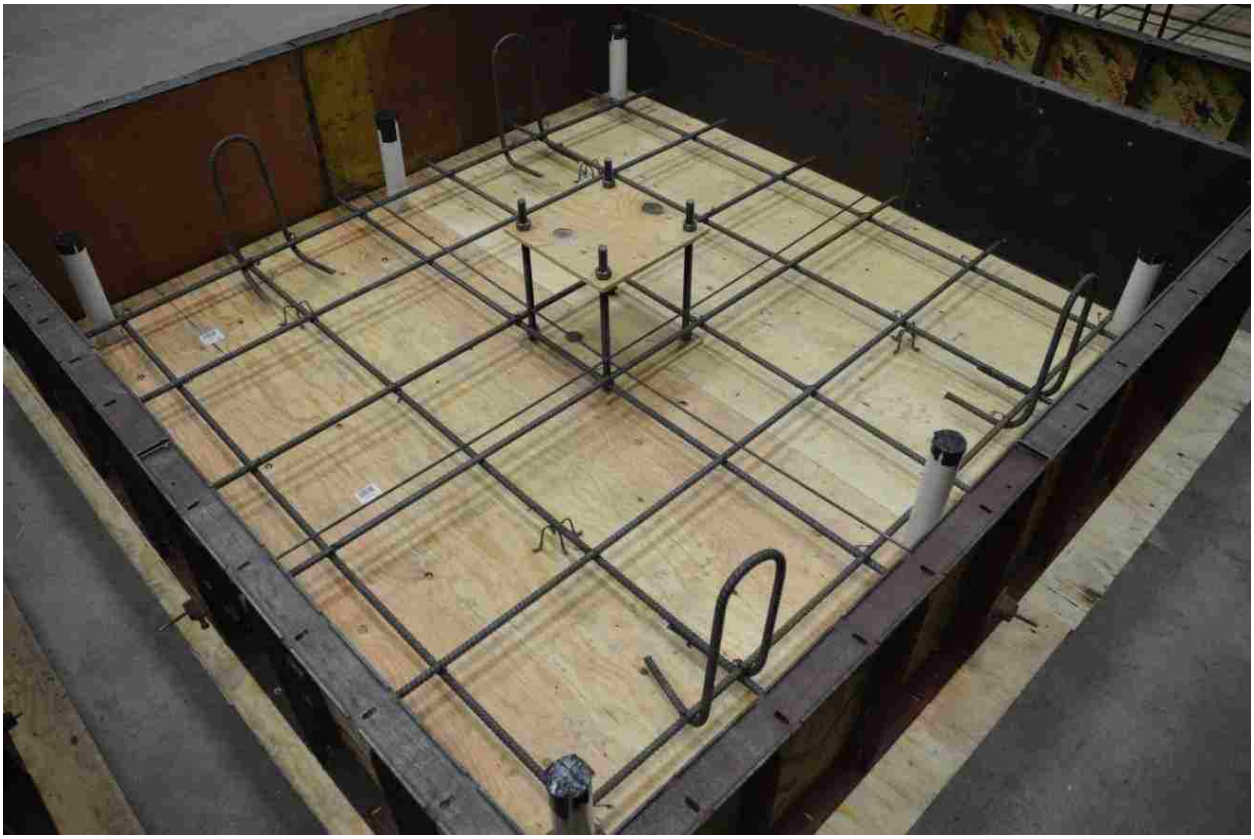

Figure 3-7: Completed Footing Form

Figure 3-8: PVC Guide

Figure 3-9: Anchor Rod Guide

After the rebar, anchor rods, and PVC were in place the footing concrete was poured into the forms. Concrete was placed into the forms and shoveled into place until it reached the 1' line drawn on the side of the forms [Figure 3-10]. Any excess concrete was placed in the next form and this process was continued until all the forms were filled up to 1'. No finish was put on top of the footing because this would not be representative of what would be done in practice. Figure 3-11 shows one of the completed footings after the first pour.

Figure 3-10: Footing Concrete Pour

Figure 3-11: Completed Footing

In preparation for the next pour, plywood walls were formed inside the existing form and on top of the footing. The forms permitted the slab-on-grade concrete to be poured while maintaining the block-out area free of concrete. Figure 3-12 shows the completed slab forms. For the shallow embeds the rebar was placed on 4" chairs so the mat would sit in the middle of the slab. For the deeper embeds, 12" rebar rods had to be welded to the mat so that the rebar would sit at the same distance from the top of the slab as the shallow embeds [Figure 3-13]. Lastly a form for the block-out was built from plywood that had 2' × 2' outside dimensions, and placed so the anchor bolts were centered inside the block-out [Figure 3-14]. A brace was used across the block-out to prevent the concrete from pushing it around [Figure 3-12]. Next the concrete for the slab-on-grade was poured following the same steps outlined for the footing concrete pour. Figure 3-15 shows two of the specimens after the concrete pour. A brush finish was put on this layer of concrete as is done for a typical floor slab.

(a) Shallow Embedment

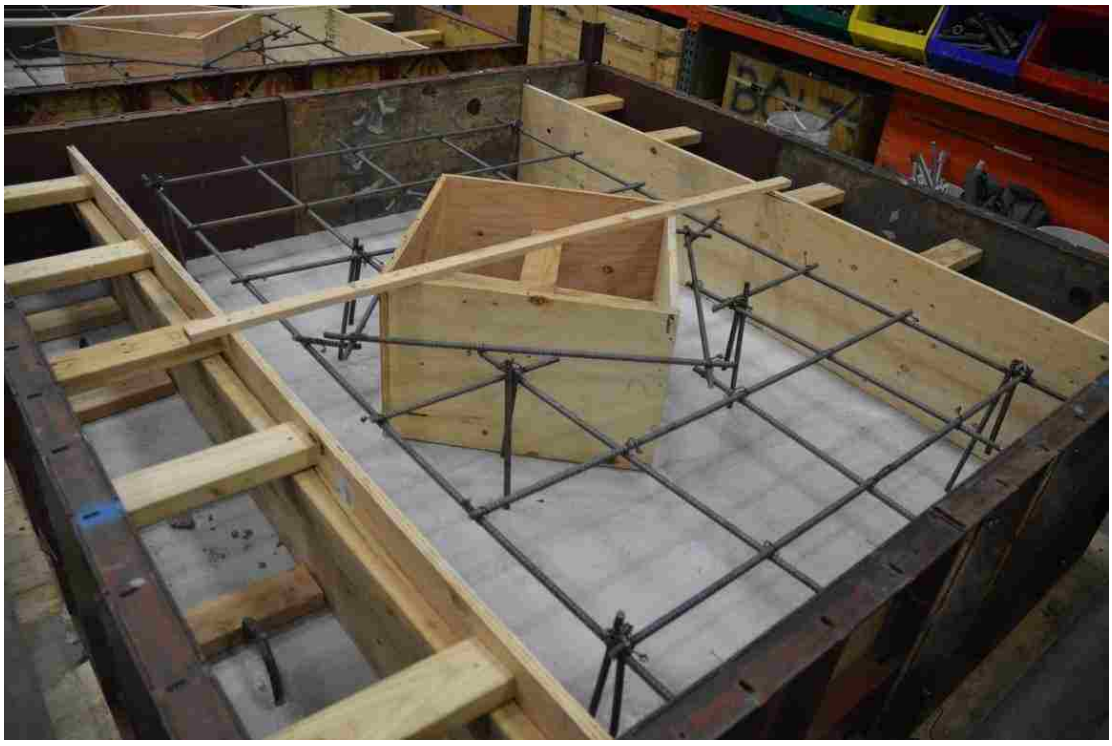

(b) Deep Embedment

Figure 3-12: Completed Slab Forms

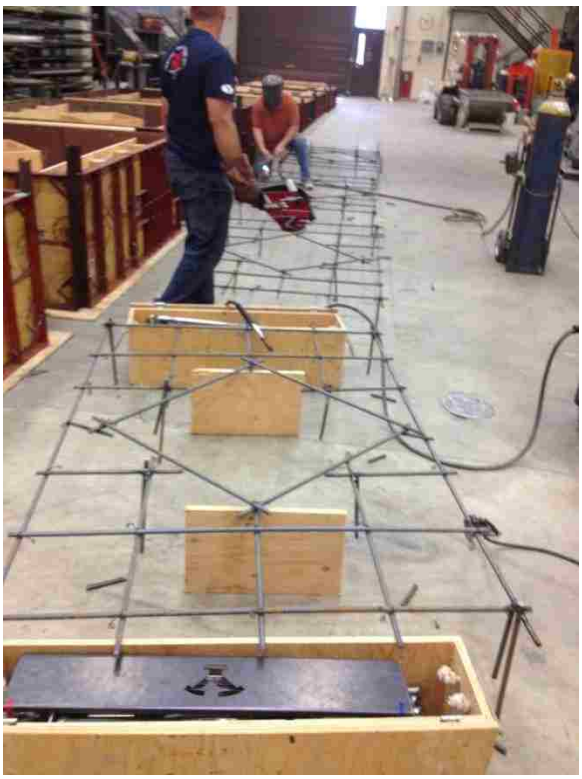

Figure 3-13: Welding on Rebar Chairs

(a) Shallow Embedment

(b) Deep Embedment

Figure 3-14: Block-out Forms

(a) Shallow Embedment

(b) Deep Embedment

Figure 3-15: Finished Slab

Once the concrete had set, the columns were placed into the block-outs. Leveling nuts and washers were screwed onto the anchor rods so that the top of the washer was about 1 ½" from the concrete footing [Figure 3-16]. The columns were then oriented and placed on top of the washers and leveling nuts [Figure 3-17]. With the column in place, the nuts were adjusted until all four sides of the column were level. Next 2" × 2" × ¼" plate washers with a 1 $^{5}/_{16}$" hole were placed on each anchor rod and then another ¾" bolt. The bolts were tightened by hand and then another ½ turn with a wrench.

Figure 3-16: Leveling Nuts and Washers

Figure 3-17: Column on Leveling Nuts and Washers

Once the columns were placed and leveled, high strength non-shrink grout was poured underneath the columns to fill the void needed for the leveling nuts. When the grout had set, the

block-out was filled in with concrete. During this process a vibrator was used to consolidate the concrete, making sure that there were no voids in the block-out. Once again a brush finish was placed on the block-outs as may be done in practice. The specimens were tested 28 days after the block-out concrete was poured.

Figure 3-18: Bolt and Washer Installed on Grouted Column

Figure 3-19: Column After Filling the Block-out

Measurements were taken on each specimen to find the as-built dimensions. This was done to determine the exact location of the column with respect to the block-out, the slab-on-grade, and the footing. Table 3-3 shows the dimensions and Figure 3-20 shows how the dimensions were labeled on the different specimens.

Table 3-3: As-built Dimensions

Actual Dimensions [in]

Specimen	A	B	C	D	E	F	G	H	I	J	K	L
A1	24.75	29.5	29.5	13.25	12.75	16	17.125	12.5	12.875	29.25	29.5	25.25
A2	25.5	29	29.75	12.25	12	17	16.75	12.75	13	29	29.75	25
A3	25.5	29	30	16.75	12	13	13	12.75	16.5	29.25	29.75	25
A4	25.25	29.75	29.25	12.75	12.5	12	13.25	12.75	12.5	29	29.5	25.25
B1	28	29.5	29.5	11.5	12.75	16.25	17	13	15	29.5	29.5	23.25
B2	26.25	30	29.75	11.75	13	16	17.25	13	13.75	30	29.75	24.5
B3	25.5	29	31.5	15.75	11.75	14.5	11.25	15	18	28	32.25	24.25
B4	26.25	29.5	30	12	12.5	12.75	12.75	13	13.5	29.5	30	24.5
CA2/DA2	25.25	29.75	29.25	12.75	12.5	16	17.25	12.75	12.5	29	29.5	25.25
CB2/DB2	26.25	29.5	30	12	12.5	16.75	16.75	13	13.5	29.5	30	24.5

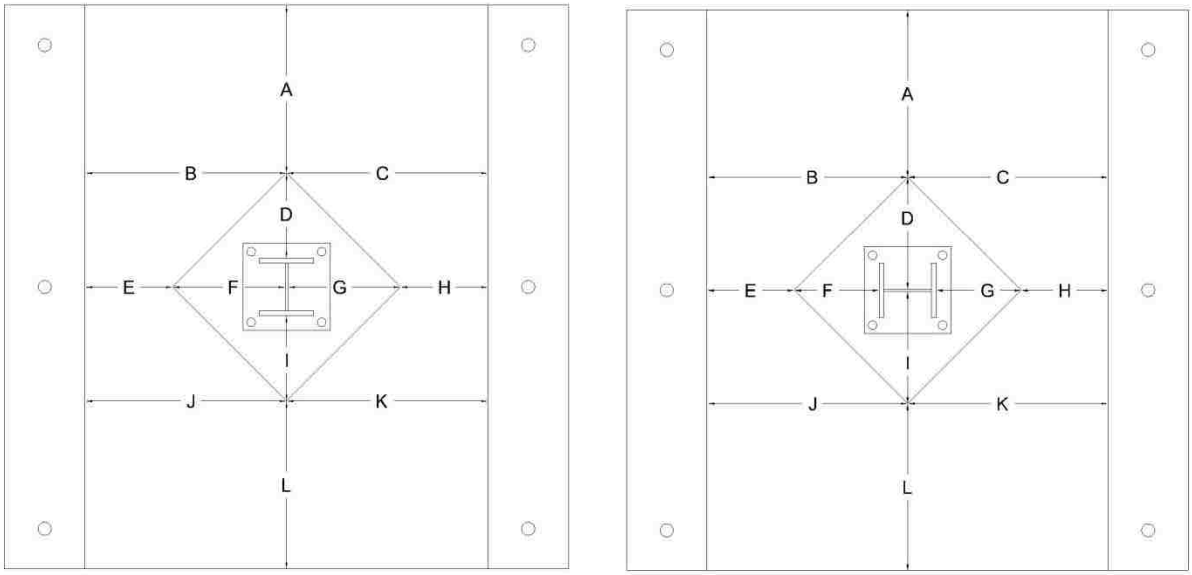

(a) Strong Axis **(b) Weak Axis**

Figure 3-20: As-built Dimension Labels

There are a few things that occurred during the construction process that should be noted. On specimen B1 the form began to bow out during the pour which created a large void around the end of the specimen [Figure 3-21]. Also, on specimen B3, the brace on top of the block-out form broke during the pour and the form shifted. Figure 3-22 shows where the off-center block-

out ended up relative to the anchor bolts (centered). Even with the offset, the column was able to be placed in the block-out without modification. See Table 3-3 for the as-built dimensions. These issues during construction did not seem to impact the final results.

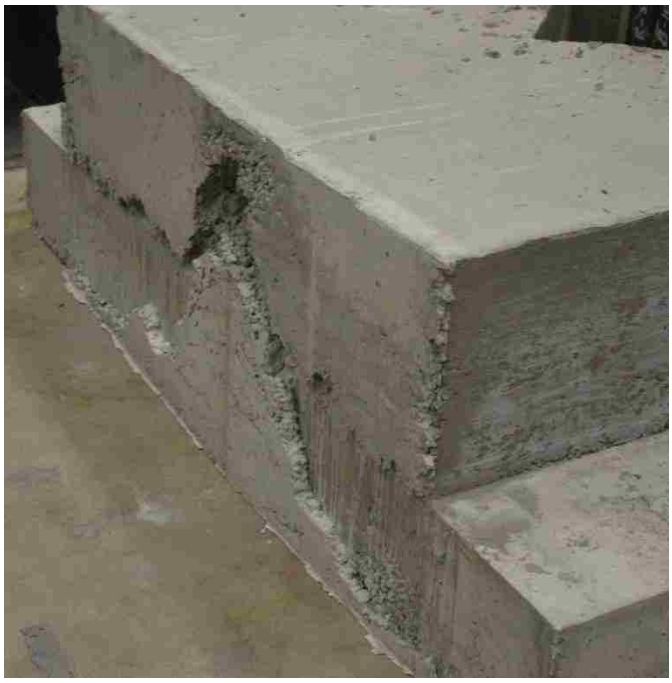

Figure 3-21: Void between the Slab and Footing of Specimen H

Figure 3-22: Shifted Block-out on Specimen E

3.3.2 Specimen Set Up

The specimen set up involved fastening the specimen to the lab floor, connecting the actuator to the column, and setting up the instrumentation.

The first step in the process was placing the specimen in the testing location and post-tensioning it to the lab floor. Where the specimen needed to be placed, the floor was not level and tensioning down the specimen would cause the concrete to crack. In order to prevent this, a HYDROCAL mixture was poured underneath the specimen to form a level base. To do this the

specimen was put into place but not lowered all the way. Then form release was applied to the floor so the HYDROCAL could easily be removed after each test [Figure 3-23]. Next the HYDROCAL was mixed and poured it inside the testing area [Figure 3-24]. Before the paste set the specimen was lowered into place [Figure 3-25]. Figure 3-26 shows the specimen immediately after being placed into the HYDROCAL mixture. Once the HYDROCAL had set for 4 hours, it had gained sufficient strength that the test setup could proceed. This was typically done the day before the test to give ample time for testing the following day. When the HYDROCAL was dry, the specimen was anchored down with six 1 ¼" rods that were tensioned to approximately 50 kips each.

Figure 3-23: Applying Form Release to Lab Floor

Figure 3-24: HYDROCAL Mix Preparation

Figure 3-25: Lowering Specimen into Place

Figure 3-26: Specimen Immediately after Being Placed in HYDROCAL

After the specimen was tensioned to the floor, the actuator was connected to the column face. For the strong axis tests, four ¾" bolts were placed through the connector and the column face [Figure 3-27]. Nuts were placed on the outside and inside of the column flange and the inside of the flange and outside of the connection piece, for the side connected to the actuator connection piece. For the weak axis test four ¾" bolts were placed through the connection piece, through the holes in the web of the column and through the endplate. The plate on the end of the connection piece and the end plate were also bearing on the flanges of the column. Nuts were placed on the back sides of the end plate and the plate on the connection piece, as well as on both sides of the web [Figure 3-27]. This allowed the force to be transferred through the web as well as through bearing in the flanges. These nuts were snug tight. For the deeper embedment, plate washers were placed on the back of the plate on the connection piece [Figure 3-28]. This was a precautionary measure to ensure that prying did not produce forces in the bolts that would cause them to break suddenly. Lastly the instrumentation was connected, which will be explained in further detail in the next section.

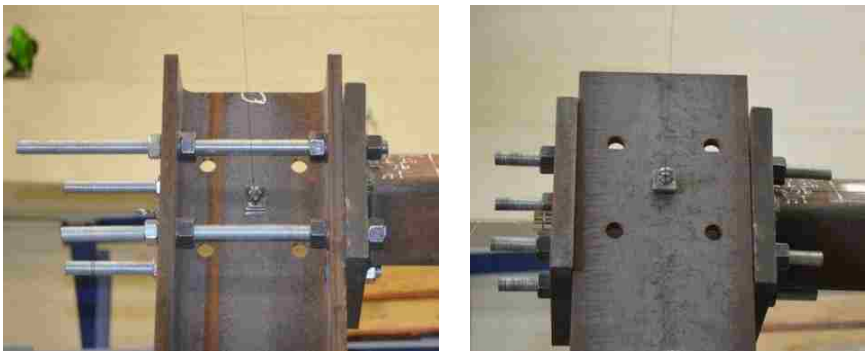

(a) Strong Axis **(a) Weak Axis**

Figure 3-27: Connection Piece to Column Connection

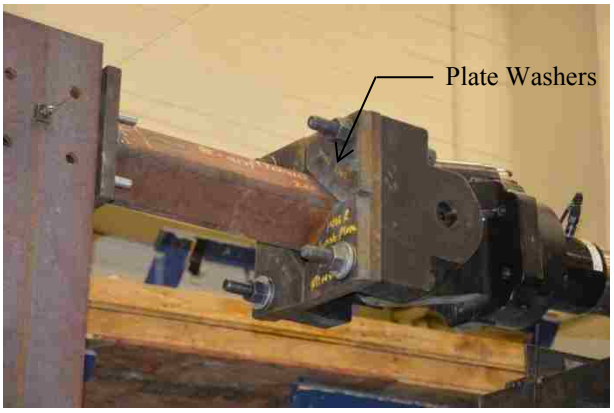

Figure 3-28: Plate Washers

3.3.3 Modified Specimen

Two specimens were prepared that did not have a top nut on the anchor bolts, so the anchor rods were not engaged during the test. These specimens were labeled CA2 and CB2, where CA2 had the same parameters (orientation, shape, and embedment) as specimen A2 and CB2 had the same parameters as specimen B2. As will be discussed later, the slab began to rock back and forth during the test. After the test, the specimens were modified to prevent the slab from rocking back and forth, and tested again. Two steel beams were placed on top of the outside

edges of the slab and bolted to the rods already being used to fasten the specimen to the lab floor [Figure 3-29]. For the second test the specimens were named DA2 and DB2 respectively.

(a) Specimen DA2 **(b) Specimen DB2**

Figure 3-29: Modified Specimen Design

Once the tests were complete, the block-outs were jackhammered out so the orientation of the columns could be changed. The columns were switched to be tested in the weak axis, bolted, and then the block-outs were re-filled with fresh concrete. These specimens were then named A4 and B4 and tested as the other standard specimens had been tested.

3.4 **Instrumentation**

Three main forms of instrumentation were used during the test. Strain gages were placed in various locations on the steel column to measure the strain as the loads were applied. String

pots were also placed in different locations in order to measure specific displacements. Lastly a Digital Image Capture (DIC) system was used to record specimen response during testing. For each specimen the instrumentation was kept as similar as possible.

3.4.1 Strain Gages

All strain gages were placed 2" to the inside the flanges of the steel columns. Elevations of the gages depended on the specimen depth. The shallow specimens (A1-A4, CA2, and DA2) had two gages on each flange [see Figure 3-30(a)]. The first gage was placed 2" above the top of the base plate. The next gage was placed with a spacing of 5" O.C. which resulted in it being placed 1 ½" above the concrete.

For specimens B1-B4, CB2, and DB2, which all had 16" embedment, three strain gages were placed on each flange [see Figure 3-30(b)]; one 2" above the steel base plate and the other two placed at 6 ½" O.C. This resulted in the top strain gage being located 1 ½" above the surface of the concrete. For specimens B1, B2, CB2, and DB2 extra strain gages were placed on the south flanges between the bottom two gages so they were 5 ¼" from the top of the base plate. On specimens B2, CB2, and DB2, extra strain gages were placed between the top two strain gages on the same flange where the other extra gages were placed. This meant the spacing of all the strain gages (standard and extra) was actually 3 ¼" O.C. for those two flanges.

Both strong and weak axis instrumentation can be seen in Figure 3-30. In the figure the plain text are the gages on the east facing flange for the strong axis, and south facing flange for weak axis. The gages in parenthesis are the gages opposite these. Figure 3-31 shows some of the strain gages after they were placed on the columns.

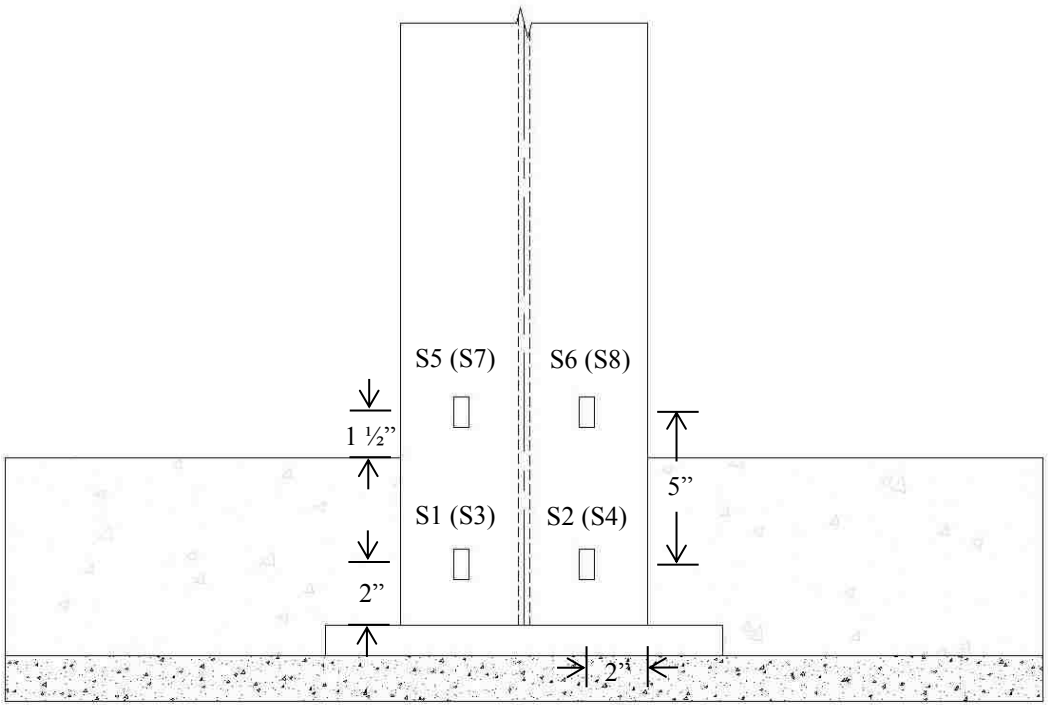

(a) Shallow Embedment

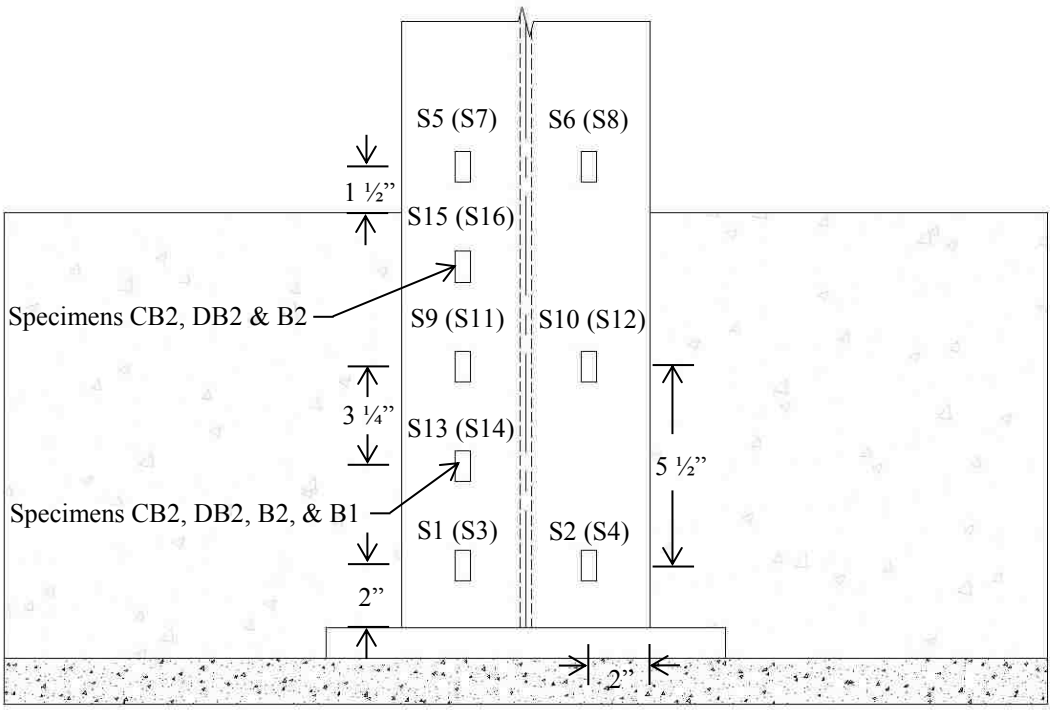

(b) Deep Embedment

Figure 3-30: Strain Gage Locations

Figure 3-31: Installed Strain Gages

3.4.2 String Pots

String potentiometers (pots) were used to measure important displacements throughout the test. Each specimen had the same number of pots. The first two pots were centered on the east side of the footing and the slab, respectively, to measure any horizontal movement in either direction [see Figure 3-32]. The next five pots were placed along the steel column. The first one was placed 2" from the top of the concrete and the rest were spaced at 20 $^{9}/_{16}$" O.C. for the deeper embeds and 19 $^{13}/_{16}$" O.C. for the shallower embeds. This left the last string pot lined up with the line of action of the actuator. The next one was placed at the same elevation as the top string pot on the column but on the face perpendicular to the other pots. The purpose of this string pot was to measure any out-of-plane displacements at the top of the column. The last two string pots were placed on top of the slab, centered at the edge of each end. These pots were placed to measure any uplift in the slab. The overall layout of the string pots can be seen in Figure 3-32.

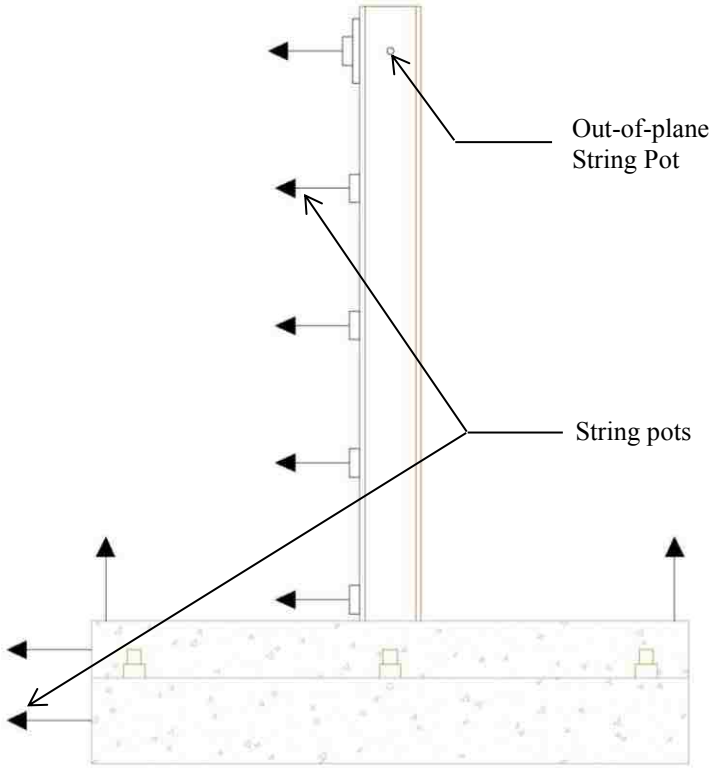

Figure 3-32: String Pot Locations

3.4.3 Digital Image Capture System

A Digital Image Capture (DIC) system was also used to record our tests. Although the collected data will not be included in this report, the system was very helpful as it was a stationary recording apparatus and the changes in the specimen could be seen from a fixed location. This helped identify that the slab was rocking back and forth early on in the test which will be discussed later on.

3.4.4 Instrumentation Setup

The strain gauge wires were first connected to the module that would read the data. They were then labeled in the computer with the labels shown in Figure 3-30. The pots that measure the column movement were attached to the column with strong magnets that would not move as the column deflected. To connect the pots to the concrete, holes were drilled in the desired locations and I-hooks were epoxied into the holes. The string pot bases were all fastened to objects that would not move during the testing. Figure 3-33 shows the installed string pots and how they were connected to the specimen and to fixed locations.

Figure 3-33: Installed Potentiometers

3.5 Testing Equipment

The actuator used is an MTS model 244.41 110 Kip actuator with 20" of displacement and the system to control the actuator is called MTS TestStar IIm. The data acquisition system used is National Instruments, which uses the LabView 2013 software. Four Analog Input Bridge NI-9237 Strain Gauge modules were used. The main block that holds the modules is called NI cDAQ-9172. To complete each Strain Gauge channel an NI 9944 (120 ohm) was used. To read

the string pots an NI-9206 Analog Input Fuel Cell module was used. Firstmark Controls Analog-Output Miniature Position Transducers, model 160-1705-C6SU, were used to measure the movement of the samples.

3.6 Loading Protocol

The loading protocol was based on story drift. The actuator was programed to push with the load required to get to each drift. The test was typically stopped after each drift cycle to take photographs and inspect the specimen for damage. The loading protocol is listed here with the drift first and the number of cycles run at that drift in parenthesis: 0.00375(6), 0.005(6), 0.0075(6), 0.01(4), 0.015(2), 0.02(2), 0.03(2), 0.04(2), 0.05(2), 0.06(2), 0.07(2), 0.08(2), 0.09(2), .10(2), .11(2). Not all of the specimens were tested up to a drift of .11, but all of the tests followed the same loading protocol until it was decided to end the test. A graphical representation of the loading protocol can be seen in Figure 3-34.

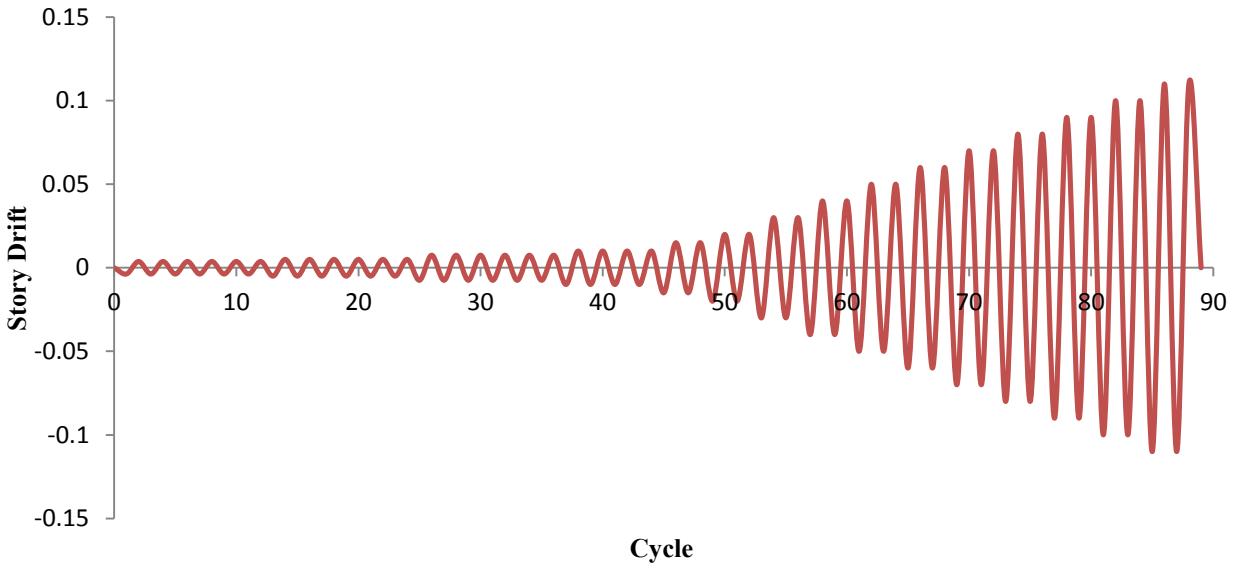

Figure 3-34: Loading Protocol

3.7 Data Reduction

The data was output as an excel file with the following data: time step, actuator load, actuator displacement, string pot displacements, and strain gage data. There were a few different methods used to interpret and draw conclusions from the data.

During the test the actuator began to pivot upward as it pushed on the column and downward as it pulled on the column [Figure 3-35]. To compensate for this in the data, as the actuator load was greater than it would have been to push the column directly perpendicular, the load was multiplied by the actual displacement, taken from a string pot at the same elevation as the actuator, and divided by the displacement measured from the actuator. This gave the component of the load that was strictly acting perpendicular to the face of the column.

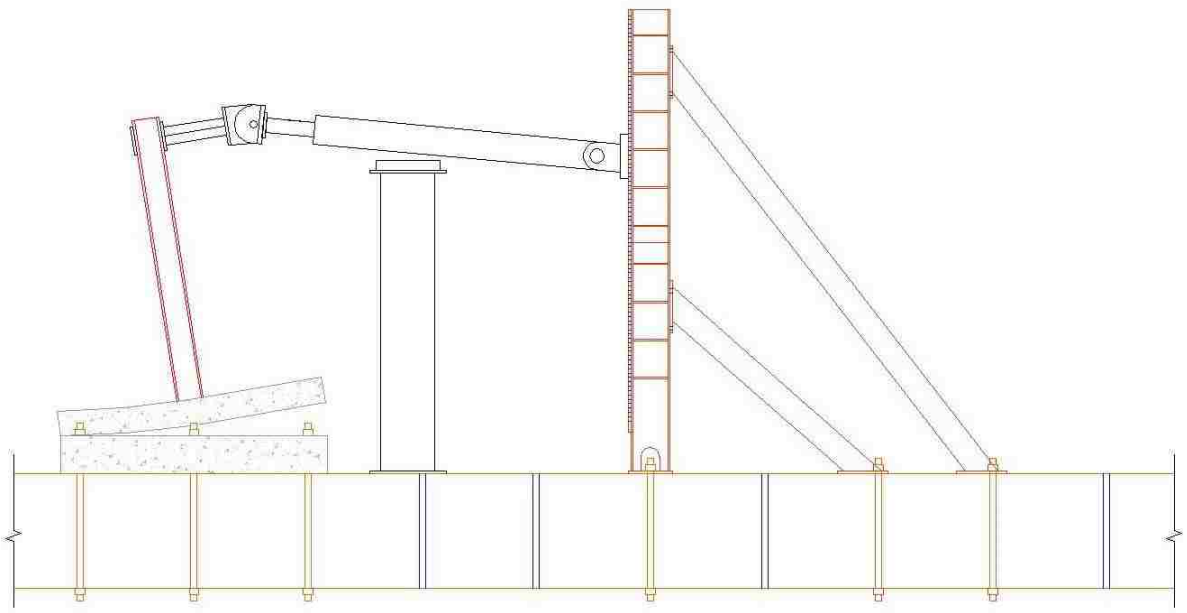

Figure 3-35: Actuator Pivot (Exaggerated)

After the load had been corrected for each specimen, the hysteretic force vs. displacement plots were plotted from the corrected load and the string pot at the line of action of the actuator. From these plots several factors were determined including: the initial stiffness, where the specimen connection began to yield, and the ultimate load the specimen could resist.

3.8 **Post-test Investigation**

After the tests the block-outs of most of the samples were jackhammered out to investigate what had happened around the base plate. The concrete was removed down to the grout level, which left the base plate uncovered. At this point most of the nuts could be taken off and the columns removed. Pictures are shown with the test observations in the next section.

4 RESULTS

4.1 Test Observations

For each individual specimen observations were recorded as the test progressed. Many of the observations and photos of the specimens were similar. Specimen A1 will be discussed in detail and photos of the specimen are included from the 0.01–0.06 drift cycle. Less detailed discussion is provided for the other specimens, which performed similarly. Photos of the block-out at 0.02 percent drift, 0.04 percent drift, and after the test have been included for all the specimens in Figure 4-1 through Figure 4-3. At 0.04 drift most of the specimens began to form visible cracks.

For most of the specimens the slab-on-grade separated from the footing, forming a gap at the edges of the footing. As the test progressed, the gap between the slab-on-grade and the footing widened. Figure 4-4 shows one of the specimens later on in the test once the separation was visible. This was initially discovered after reviewing the DIC results after the first few cycles of the first test. A similar crack pattern was observed on most of the specimens. These cracks typically formed from the corner of the flanges, propagated to the edge of the block-out, then followed the outline of the block-out to a corner, and the from the corner of the block-out to the edge of the slab.

(a) Specimen A1

(b) Specimen A2

(c) Specimen A3

(d) Specimen A4

(e) Specimen B1

(f) Specimen B2

(g) Specimen B3

(h) Specimen B4

(i) Specimen DA2

(l) Specimen DB2

Figure 4-1: Specimens at 0.02 Drift

(a) Specimen A1

(b) Specimen A2

(c) Specimen A3

(d) Specimen A4

(e) Specimen B1

(f) Specimen B2

(g) Specimen B3

(h) Specimen B4

Figure 4-2: Specimens at 0.04 Drift

(a) Specimen A1

(b) Specimen A2

(c) Specimen A3

(d) Specimen A4

(e) Specimen B1

(f) Specimen B2

(g) Specimen B3

(h) Specimen B4

(i) Specimen CA2

(j) Specimen DA2

(k) Specimen CB2

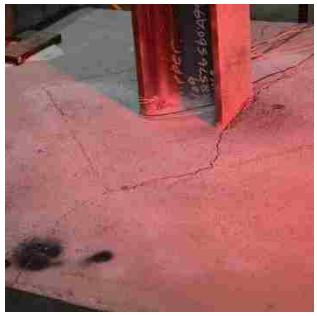

(l) Specimen DB2

Figure 4-3: Specimens after the Test

Figure 4-4: Slab Separation from Footing

4.1.1 Specimen A1

A progression of the specimen from the 0.01 drift cycle to the 0.06 drift cycle is shown in Figure 4-5 through Figure 4-10. During the initial cycles, 0.0375-0.01, there was no observable damage. The column connection at the 0.01 drift cycle is shown in Figure 4-5. During the 0.015 cycle the slab separated from the concrete footing and began to rock back and forth as is shown in Figure 4-4. During the 0.02 cycle there were no other changes. Figure 4-1(a) and Figure 4-6 show the column connection at 0.02 drift. In the 0.03 cycle a faint crack formed from the corners of the flange and propagated to the edge of the slab [Figure 4-7].There was also a small pop during this cycle. A large crack opened up on the edge of the slab during the 0.04 drift cycle and

the column at this drift is shown in Figure 4-2(a) and Figure 4-8. Throughout this cycle more cracks formed and began to widen. Little change was observed in the specimen throughout the 0.05 drift cycle which is shown in Figure 4-9. During the 0.06 drift cycle the concrete around the cracks also began to flake [see Figure 4-10]. Between the 0.07 and 0.09 drift cycle the actuator head started to swivel causing the column to twist as can be seen in Figure 4-11. Besides these observations, little new damage was detected during these cycles, although the existing cracks continued to widen and flake. During the 0.09 drift cycle the bolts broke during the first cycle. After the bolts broke the test was ended to prevent any more sudden and potentially dangerous failures in the specimen. Figure 4-3 shows the column connection after the test was finished.

Figure 4-5: Specimen A1 at 0.01 Drift

Figure 4-6: Specimen A1 at 0.02 Drift

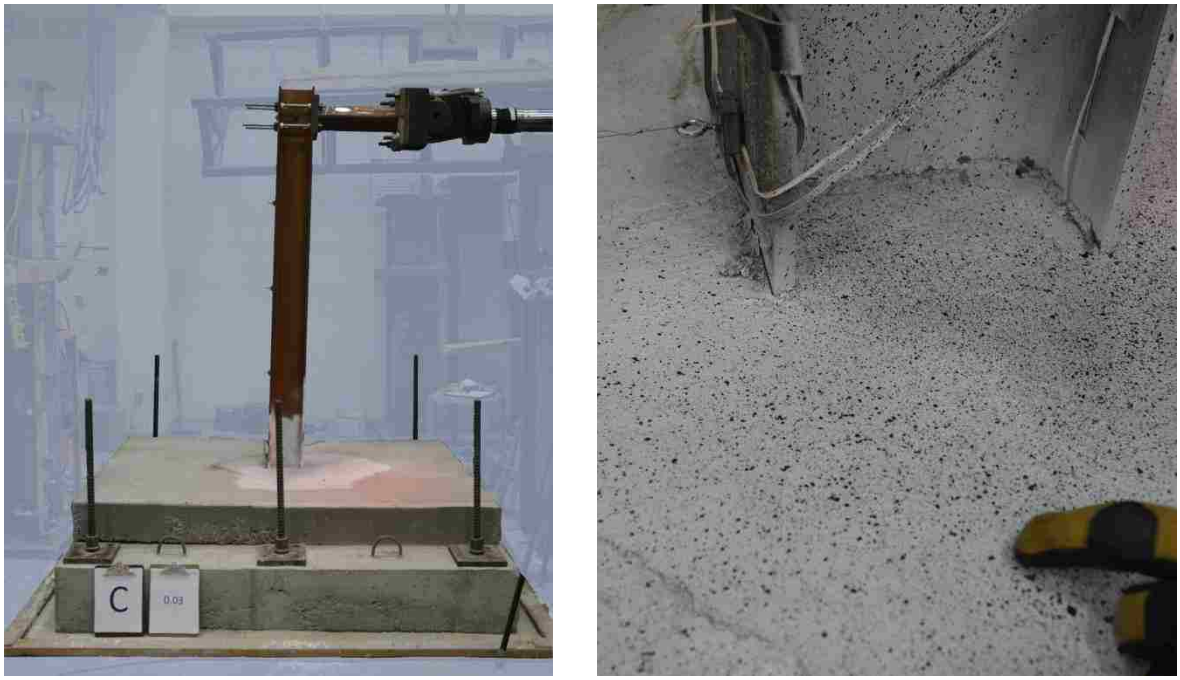

Figure 4-7: Specimen A1 at 0.03 Drift

Figure 4-8: Specimen A1 at 0.04 Drift

Figure 4-9: Specimen A1 at 0.05 Drift

Figure 4-10: Specimen A1 at 0.06 Drift

Figure 4-11: Column Twist

4.1.2 Specimen A2

Specimen A2 behaved in a similar way as specimen A1. During the 0.00375 drift cycle, no change was seen in the specimen. In the 0.005 drift cycle, the slab separated from the footing and began to rock back and forth throughout the remaining cycles. From the 0.005 to the 0.015 cycle there was minimal change in the specimen. During the 0.02 drift cycle, small cracks began to form from the corners of the flange but they did not reach to the edge of the block-out. Figure 4-1(b) shows the column connection during this drift cycle. These cracks spread to the edge of the block-out and to the edge of the slab during the 0.03 drift cycle. During the 0.04 drift cycle the cracks began to propagate vertically through the edge of the slab. Also during this cycle a crack formed between the cracks leading to the edge of the slab [see Figure 4-2(b)]. In the 0.05 drift cycle an arching crack formed between the flanges. From the 0.05 cycle to the 0.08 cycle the cracks continued to widen but no other new evidence of degradation was observed. During the 0.09 drift cycle there was a very large pop and it is believed that the bolts broke at this point. The test was ended on the 0.10 drift cycle. Figure 4-3(b) shows the specimen at the end of the test.

4.1.3 Specimen A3

Due to an actuator control error the column was pushed until it yielded on the first cycle. There was little damaged to the concrete surrounding the specimen and the test was able to be continued. Figure 4-12 shows the flaking of the paint indicating yielding of the flanges on the column. Once the actuator was brought back to the original position the correct loading protocol was input into the computer and the test was started over. Also during the initial push the slab separated from the footing and began to rock back and forth during the first drift cycle. During the 0.00375 cycle, a crack opened up from the flange of the column to the edge of the slab. This

crack may have formed during the first push but closed up when the column was brought back to the original position. From cycles 0.005 to 0.015 there was no change in the specimen. During the 0.02 rad drift cycle a small crack began to form the un-yielded flange [see Figure 4-1(c)]. There was little change between 0.02 and 0.07 except for some small cracks around the big cracks that had previously formed. Figure 4-2(c) shows the specimen at 0.04 drift. During the 0.07 cycle the concrete around the web opposite the yielded flanges began to flake. During the 0.08 drift cycle the cracks that formed second spread diagonally to the edge of the slab. The test was ended on the 0.09 drift cycle. Figure 4-3(c) shows the specimen after the end of the test.

Figure 4-12: Yielded Column Flanges

4.1.4 Specimen A4

The base for this specimen was used for the test of specimens CA2 and DA2 so there were existing cracks in the slab before the test started. These cracks are shown in Figure 4-3(j).

As this base had previously been used, the slab had already separated from the footing and consequently began to rock back and forth during the first drift cycle. Little change was seen in the specimen between the 0.00375 and 0.02 drift cycles. Figure 4-1(d) shows the specimen during the 0.02 drift cycle. During the 0.03 drift cycles, cracks formed about ⅓ of the way between the edge of the slab perpendicular to the applied load and the column, propagating out from the block-out and column. These cracks occurred on all four sides of the specimen. During the 0.04 drift cycle, cracks began to form from the corners of the flanges to the edge of the block-out as had occurred with previous specimens [see Figure 4-2(d)]. During the 0.05 drift cycle, the existing cracks from the previous test that occurred at the corner of the block-out to the edge of the slab began to open up. Throughout the 0.06 drift cycle, the concrete began to crush and flake on edge the footing where the slab was rocking up and down. By the 0.07 drift cycle, the cracks propagating from the corners of the flanges spread across the front of the flanges and to the other flange corners. The test was ending after the 0.08 drift cycle. Figure 4-3(d) shows the column after the test had finished.

4.1.5 Specimen B1

Specimen B1 had a very high bond strength between the slab and the footing, which allowed the specimen to gain considerable strength. Between the 0.00375 and 0.015 drift cycles there was little change observed in the specimen other than small gaps between the flanges and webs, and the concrete. During the 0.02 rad drift, cycle the bond between the slab and the footing broke and the specimen began to rock back and forth, as happened in previous tests. There was also a significant loss in strength during this cycle due to the break in the concrete bond. Also, during this cycle a crack formed on the edge of the slab in the middle of the specimen. This was interesting because the cracks that formed on the other specimens typically started in the block-

out and propagated out from the flanges of the column. This may have been due to the sudden break in the bond. Figure 4-1(e) shows the specimen during the 0.02 drift cycle. No change was observed during the 0.03 drift cycle, but in the 0.04 rad drift cycle the crack widened and it spread on top of the slab to the edge of the block-out and then two more cracks formed through the block-out to the corners of the column flanges. Also, a crack began to form from one of the flanges to the other flange [Figure 4-2(e)]. Throughout the 0.05 drift cycle the crack between the flanges grew until it was fully connected. During the last cycle (0.06 drift) the concrete began to flake and crush around the cracks.

4.1.6 Specimen B2

Specimen B2 also had a very strong concrete bond between the slab and the footing. Once again the specimen was able to receive much higher loads than the other specimens. From the 0.00375 to the 0.01 drift cycle, there was no change in the specimen. During the 0.015 drift cycle the concrete bond broke and the slab began to rock back and forth. There was no change during the 0.02 drift cycle, but in the 0.03 drift cycle the slab lift on each end became more visible and a crack began to open up in the middle of the side of the slab. Figure 4-1(f) shows the specimen during the 0.02 drift cycle. Also, during the 0.03 drift cycle as the concrete rocked back and forth, it began to crush on the edges of the concrete underneath the slab. No change was observed during the 0.04 drift cycle, but throughout the 0.05 drift cycle cracks opened up from the corner of the flange to the edge of the block-out, and then to the crack that had formed on the side of the slab. Figure 4-2(f) shows the specimen during the 0.04 drift cycle. The 0.06 drift cycle showed no new changes in the specimen. During the 0.07 drift cycle a crack opened up from each edge of the flange to the other flange. Through the remaining cycles, 0.08 drift and

0.09 drift, these cracks continued to widen and flake. The test was ended on the 0.09 drift cycle. Figure 4-3(f) shows the specimen at the end of the test.

4.1.7 Specimen B3

There were no visible changes in the specimen from 0.00375 drift to 0.02 drift. Figure 4-1(g) shows the specimen at 0.02 drift. During the 0.03 drift cycle flaking was observed in the column steel indicating that it had yielded. Throughout the remaining cycles of the test, the column continued to yield, but there was no evidence of degradation in the concrete. It appears that the bond between the concrete of the slab and the footing never broke because the column yielded before it could break the bond. The test was ended after the 0.08 drift cycle. Figure 4-2(g) and Figure 4-3(g) show the specimen at 0.04 drift and after the test, respectively.

4.1.8 Specimen B4

The base for this specimen was used for the test of specimens CB2 and DB2 so there were existing cracks in the slab before the test started. These cracks are shown in Figure 4-3(l). Because the slab base had already been used, the slab had separated from the footing and began to rock back and forth as soon as the test began. From the 0.00375 drift cycle up until the 0.05 drift cycle there was little change in the specimen. There were no cracks in the block-out but the existing cracks in the slab, from the previous test, opened up as the slab rocked back forth. Figure 4-1(h) and Figure 4-2(h) show the specimen at 0.02 drift and 0.04 drift. During the 0.06 drift cycle, a small crack formed perpendicular to the flange and out to the corner of the block-out. Also towards the end of this cycle a second crack formed in the block-out and propagated to the edge of the slab and then down the side of the slab. No change was observed in the 0.07 drift cycle but during the 0.08 drift cycle a third crack opened up in the block-out and much of the

concrete began to flake around the cracks. Also during this cycle the concrete cracked and began to flake between the flanges the test was ended on this cycle. Figure 4-3(h) shows the specimen after the end of the test.

4.1.9 Specimen CA2

There was no visible change in the specimen during the 0.00375 drift cycle. It became evident that the slab was rocking back and forth during the 0.05 drift cycle; however, it was not entirely clear exactly when the concrete bond broke. There were no other visible changes throughout the test which was ended on the 0.01 drift cycle. Figure 4-3(i) shows the specimen after the end of the test.

4.1.10 Specimen DA2

We tested specimen CA2 again with the modifications noted in the methods section (3.3.3 Modified Specimen) and it was renamed DA2. There were no changes in the specimen through the 0.0375 drift cycle but during the 0.005 rad drift cycle cracks began to form from the outside corners of the flange and spread to the edges of the block-out. Also a visible separation was observed between the flange and the concrete and became more noticeable throughout the cycles. As the drift increased to 0.0075, the existing cracks widened and new ones formed from the corners of the block-out to the side of the slab. Another large crack began to form from the outside of the block-out to the south east corner of the slab during the 0.01 drift cycle. There was no change in the specimen during the 0.015 drift cycle. Similarly during the 0.02 cycle two more cracks opened up, one from the middle of the block-out to the edge of the slab, in between the middle of the slab and the northeast corner, and the other between the middle of the slab and the

northwest corner. The test was ended after this cycle. Figure 4-3(j) shows the specimen after the end of the test.

4.1.11 Specimen CB2

There was very little change in the specimen from the 0.00375 drift cycle to the 0.0075 drift cycle. During the 0.01 drift cycle, the concrete bond between the slab and the footing broke. At this point the slab began to rock back and forth like the other specimen had done. After the 0.01 drift cycle the test was ended. Figure 4-3(k) shows the specimen after the test.

4.1.12 Specimen DB2

Specimen CB2 was tested again with the modifications noted in the methods section (3.3.3 Modified Specimen) and was renamed DB2. Little change was seen during drift cycles 0.00375 - 0.0075. During the 0.01 drift cycle, a crack formed from the corner of the block-out to the edge of the slab and there were also a few small cracks that began to propagate out from the column flanges. During the 0.015 drift cycle, those small cracks began to open up and an obvious path could be traced from the column flanges to the edge of the block-out and then from the edge of the block-out to the edge of the slab. Throughout the 0.02 rad drift cycle, these cracks widened and the crack on the edge of the slab began to grow down the side of the slab and towards the foundation. After this cycle the test was ended. Figure 4-3(l) shows the specimen after the test was completed.

4.1.13 Post-test Investigation

The post-test investigation was performed to determine if anything could be found out about what was going on inside the concrete and around the base plate. After jackhammering out

the specimen similar patterns were noticed with most of the specimens. For many of the specimens a triangular cracking pattern was observed around the bolts as shown in Figure 4-13. On the columns that the bolts broke, the break happened just underneath or just inside the leveling nut in all cases. This is shown for one of the specimens in Figure 4-14. It was also noticed that there was no evidence of yielding in the base plates. This was particularly interesting because the loads that were reached during the test would have resulted in failure in the baseplate according to the baseplate design guide.

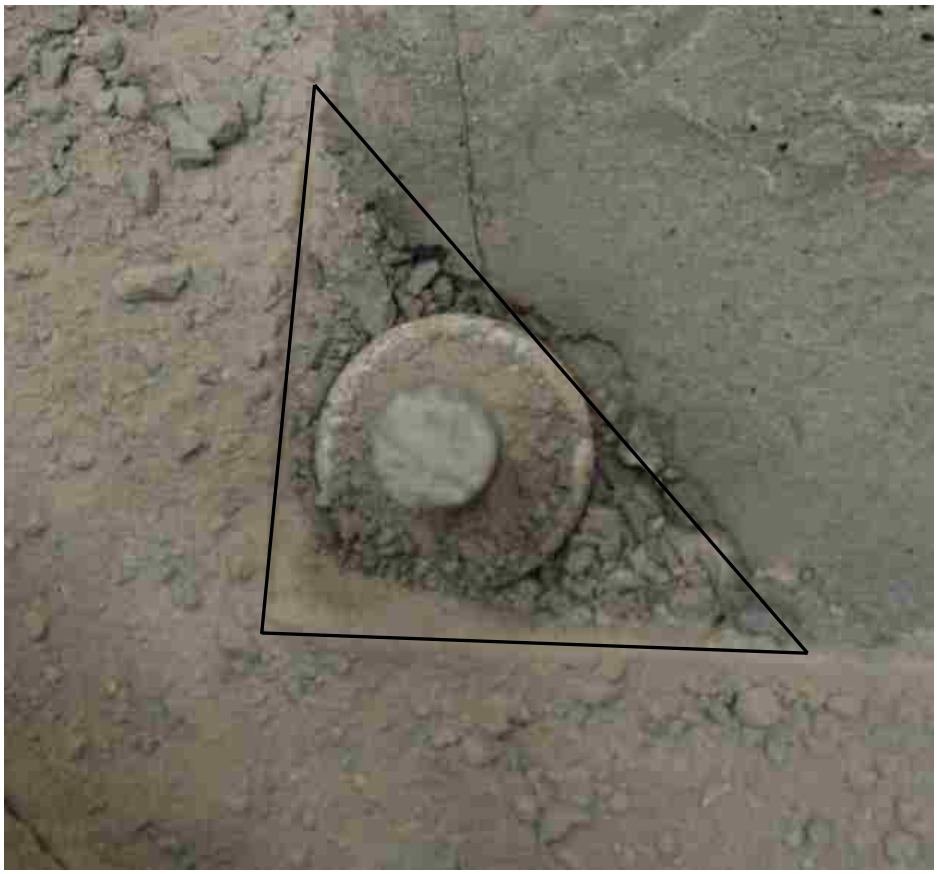

Figure 4-13: Triangular Cracking Pattern

Figure 4-14: Broken Anchor Bolt

4.2 Global Results

4.2.1 Backbone Curves

Backbone curves were developed based on the corrected data. To create the curves the maximum load at each drift cycle was plotted versus the recorded displacement at that load for each specimen. For the deeper embeds, a high initial strength can be seen. This strength can be attributed to the strong concrete bond between the slab-on-grade and the footing. The backbone curves are shown in Figure 4-15. At drifts greater than 0.04, all of the specimens with bolts, had similar strength.

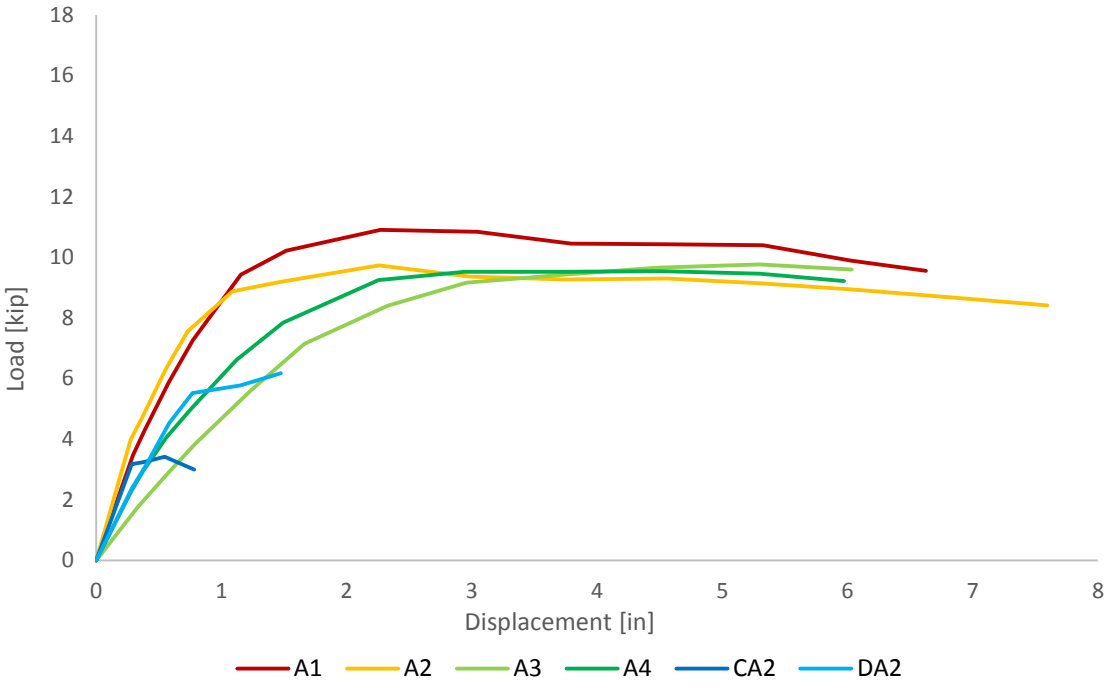

(a) Shallow Embedment

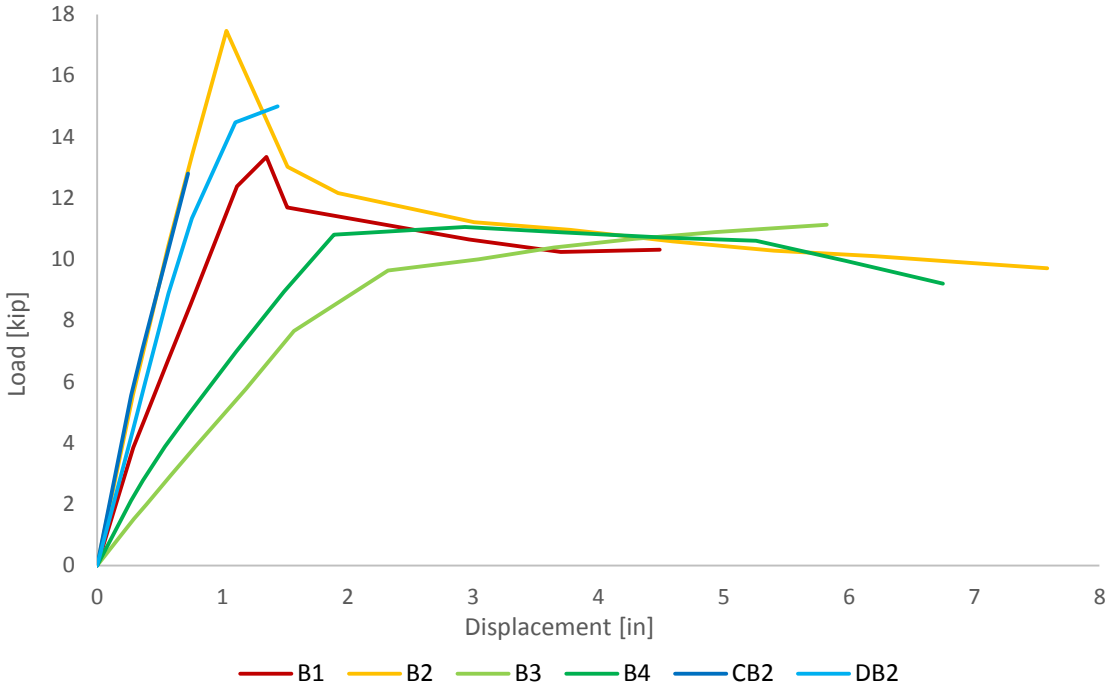

(b) Deep Embedment

Figure 4-15: Backbone Curves

4.2.2 Hysteretic Plots

For each of the specimens global hysteretic plots were made with the corrected force and the displacement from the string pot at the line of action of the actuator. On these plots specific events such as a break in the concrete bond or a broken bolt are pointed out directly on the plot. In some cases it was evident from the observations and from the data that there were two separate instances when the bolts broke. The points are separately called out on the plots. For the most part, there was only one obvious data point when the bolts broke. These points are labeled on the plots and it is assumed that both bolts broke at the labeled data point. These are shown in Figure 4-16 through Figure 4-27 .

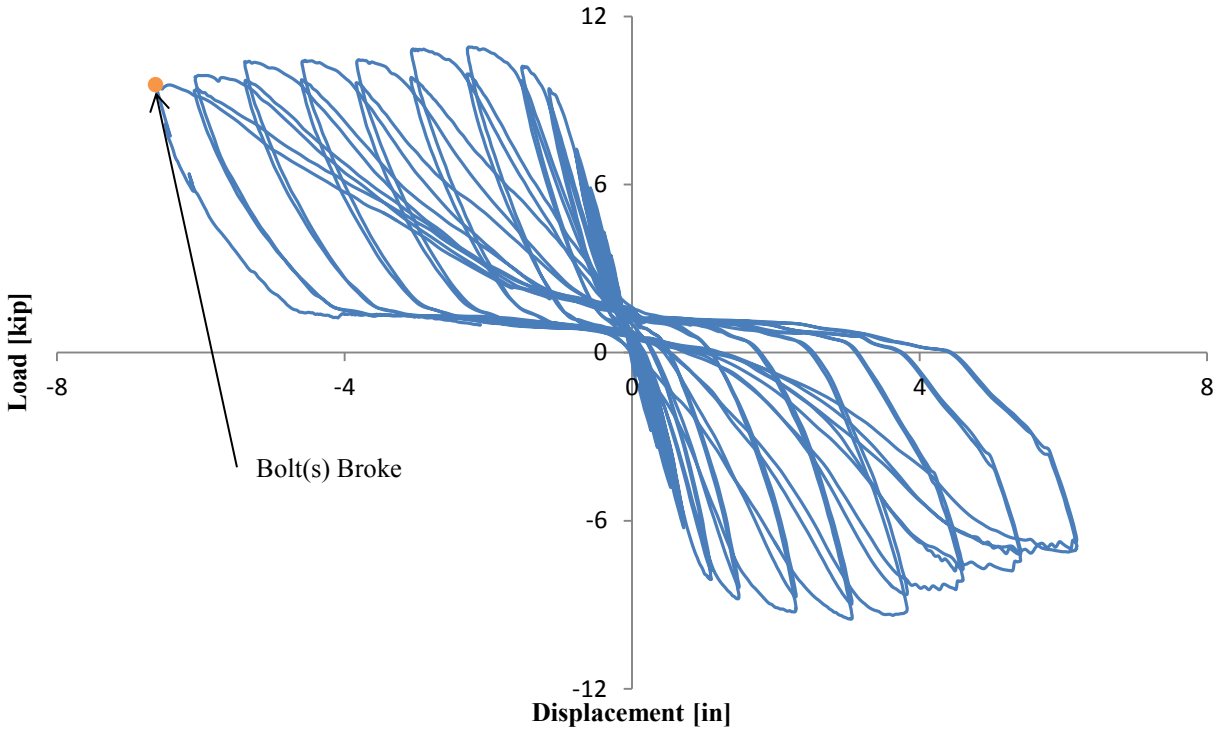

Figure 4-16: Specimen A1 Global Hysteretic Plot

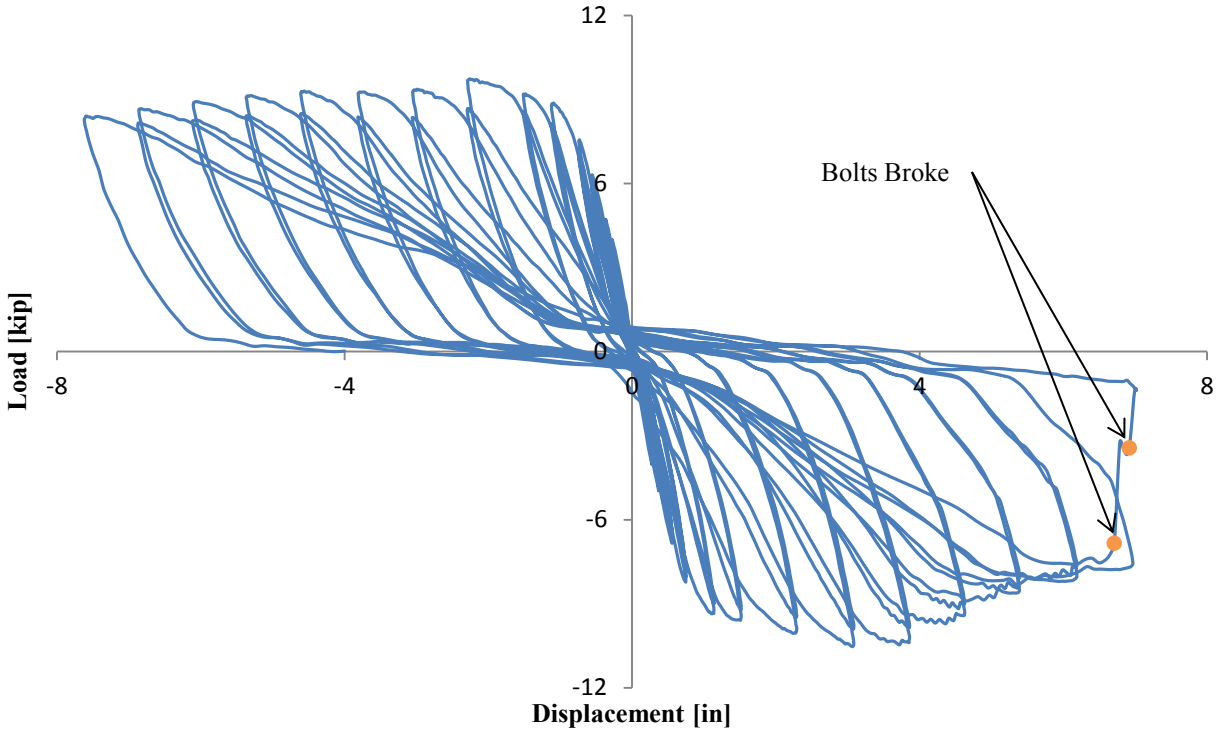

Figure 4-17: Specimen A2 Global Hysteretic Plot

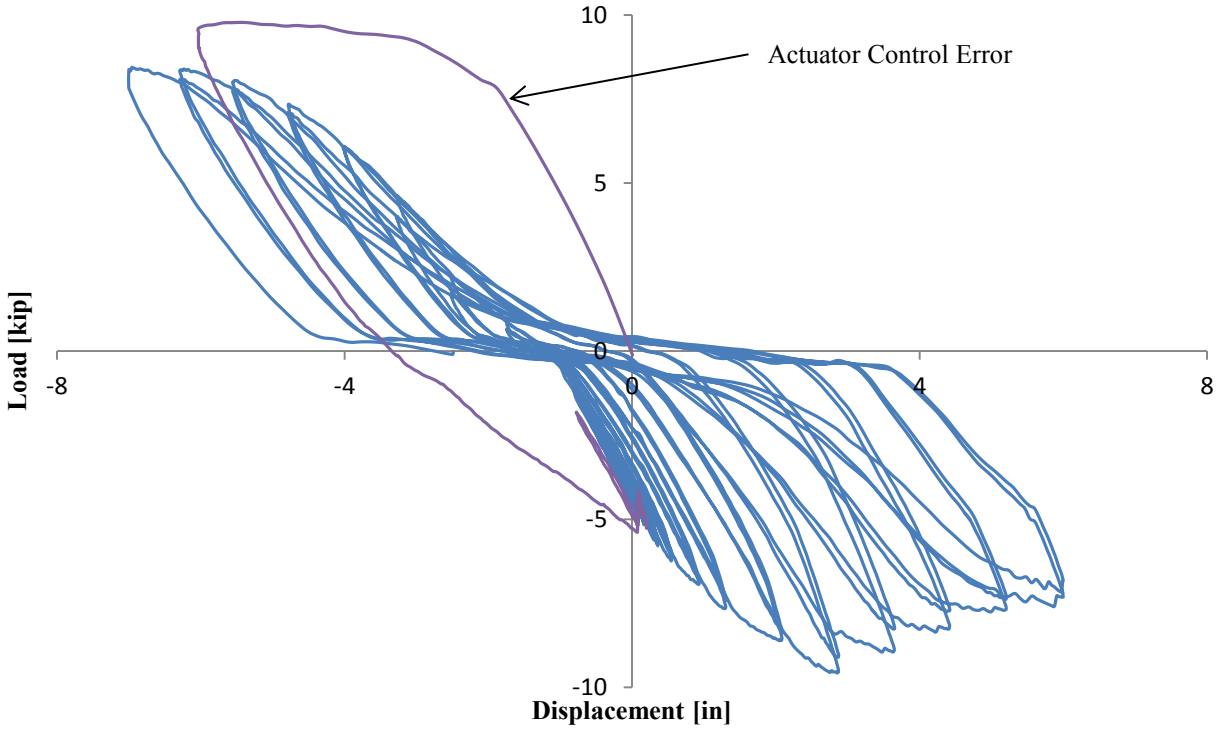

Figure 4-18: Specimen A3 Global Hysteretic Plot

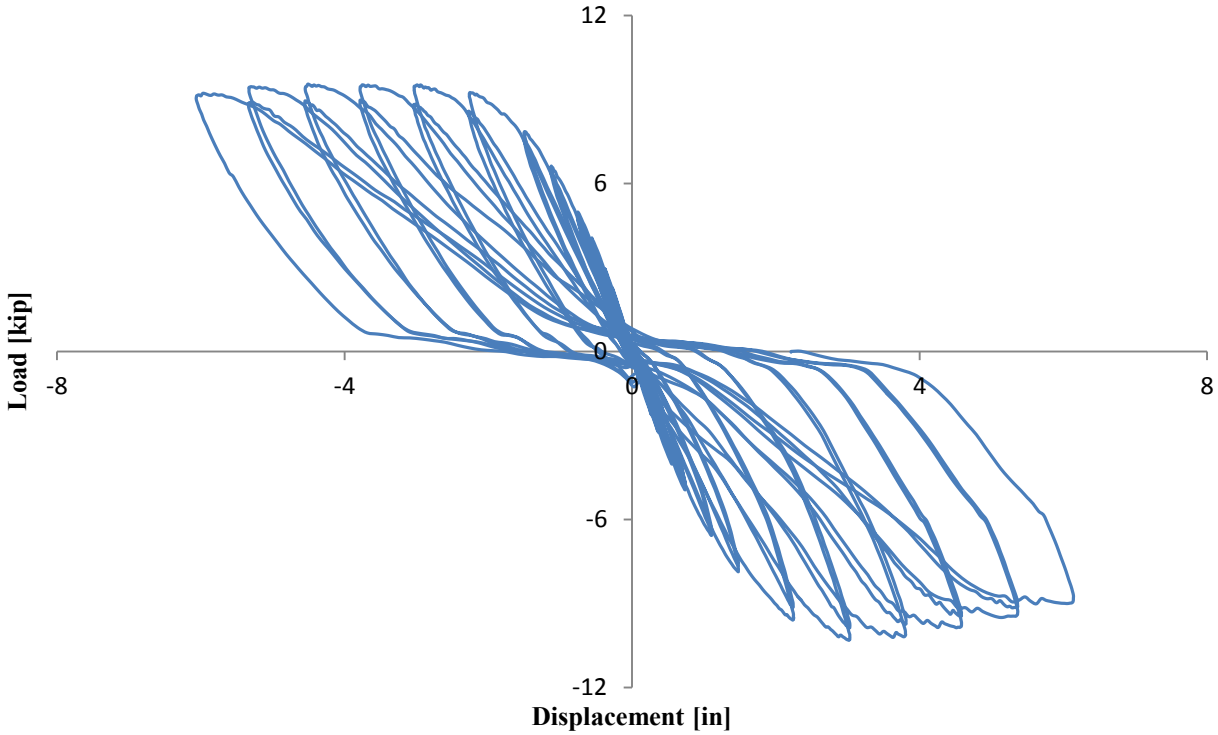

Figure 4-19: Specimen A4 Global Hysteretic Plot

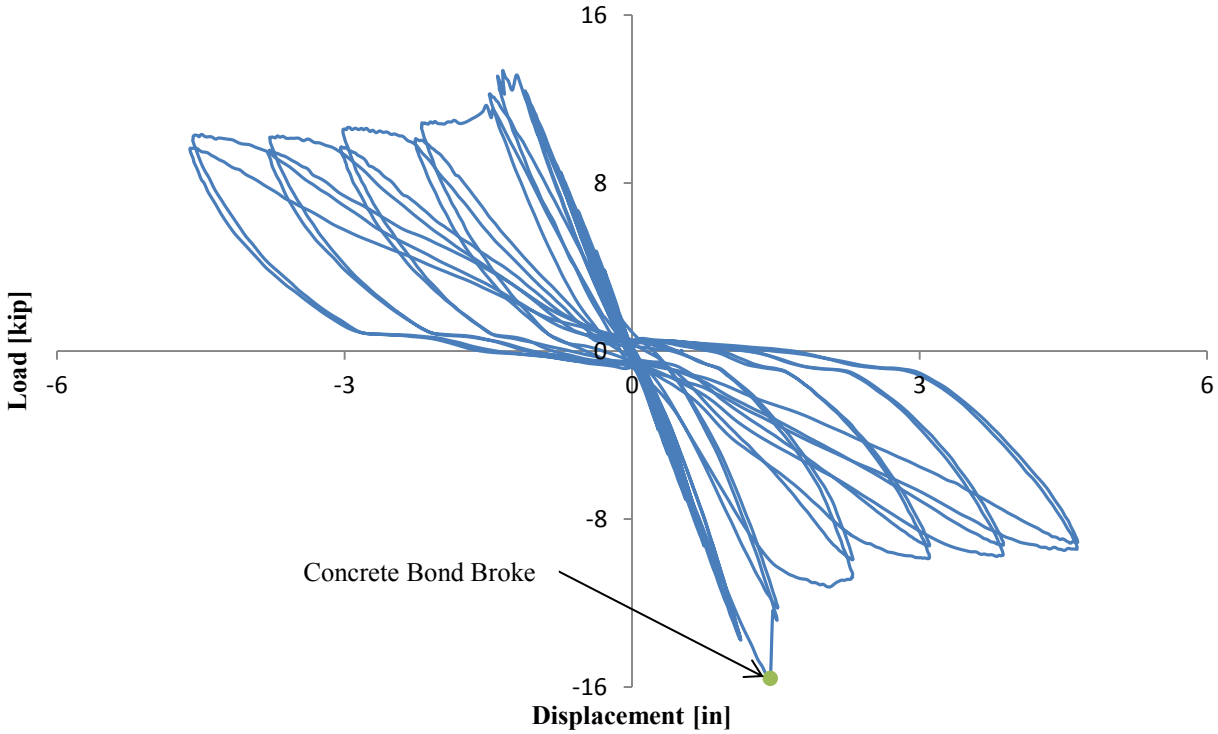

Figure 4-20: Specimen B1 Global Hysteretic Plot

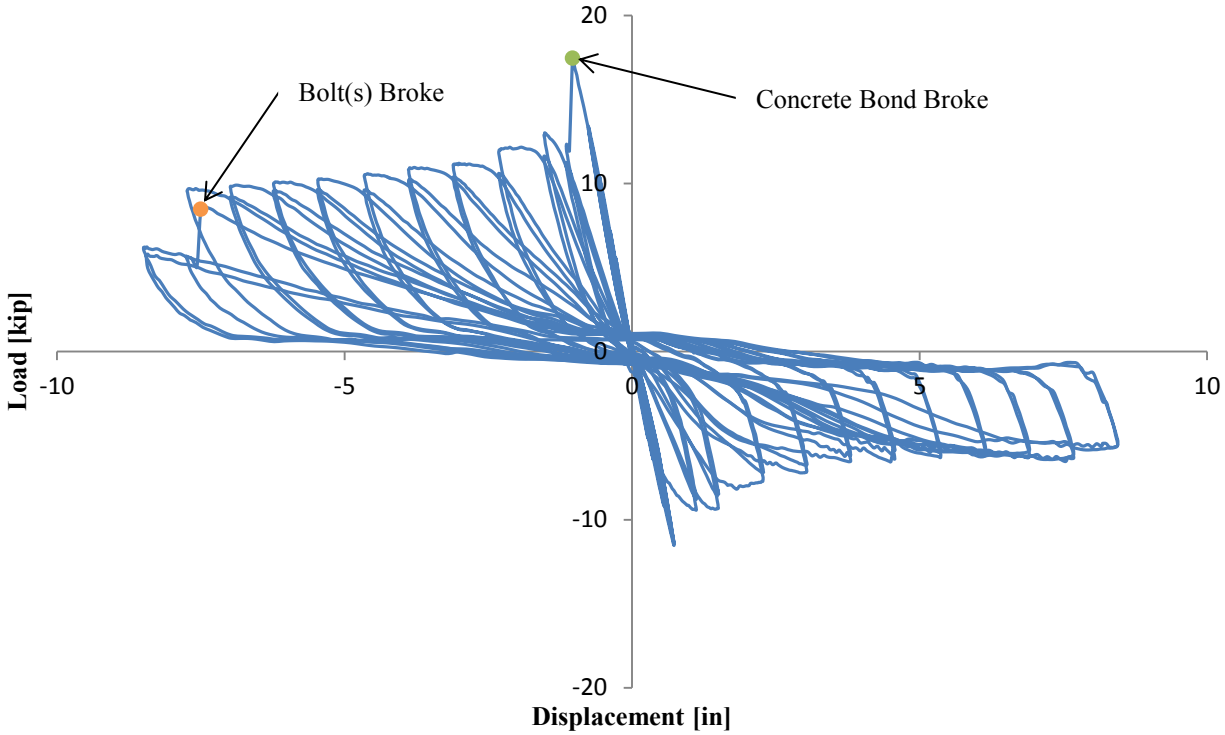

Figure 4-21: Specimen B2 Global Hysteretic Plot

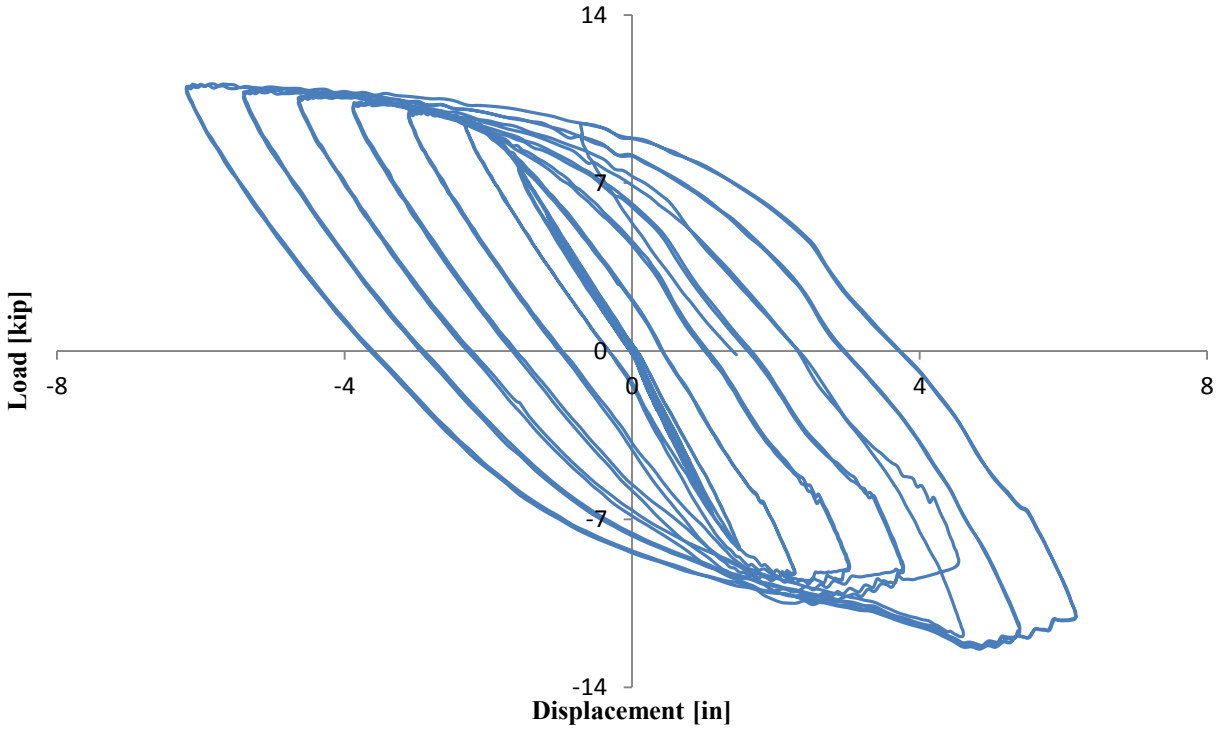

Figure 4-22: Specimen B3 Global Hysteretic Plot

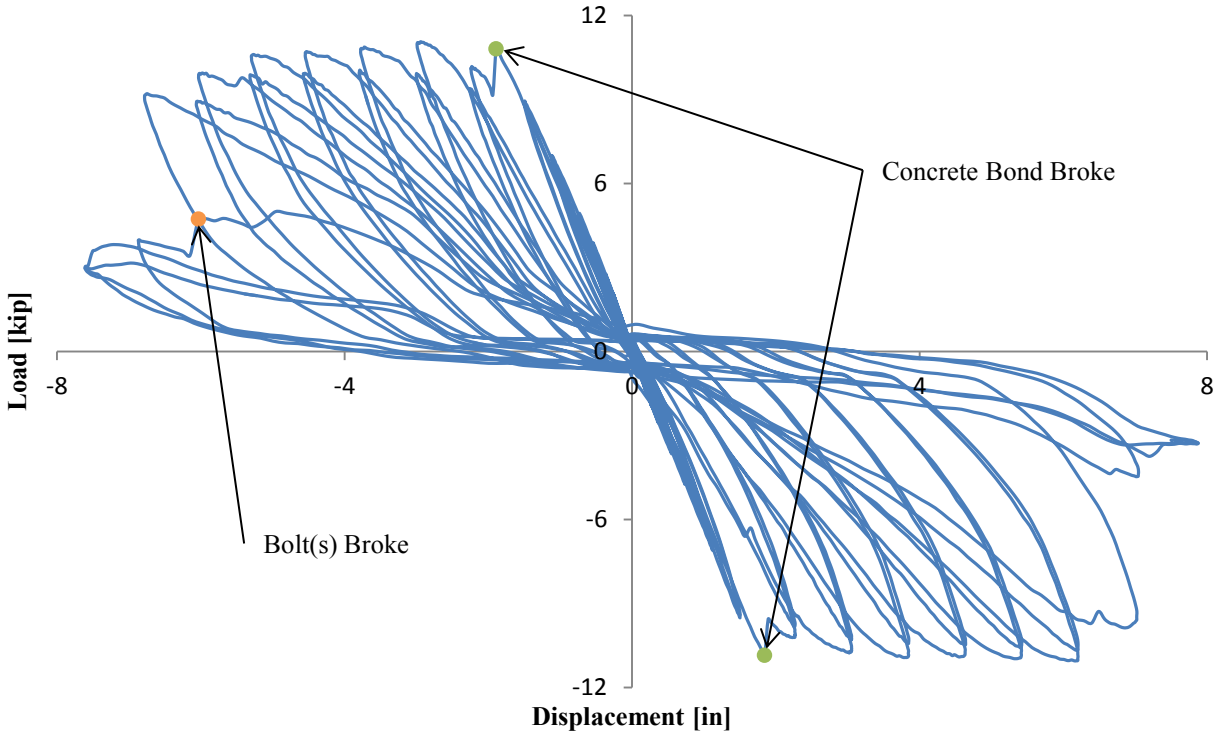

Figure 4-23: Specimen B4 Global Hysteretic Plot

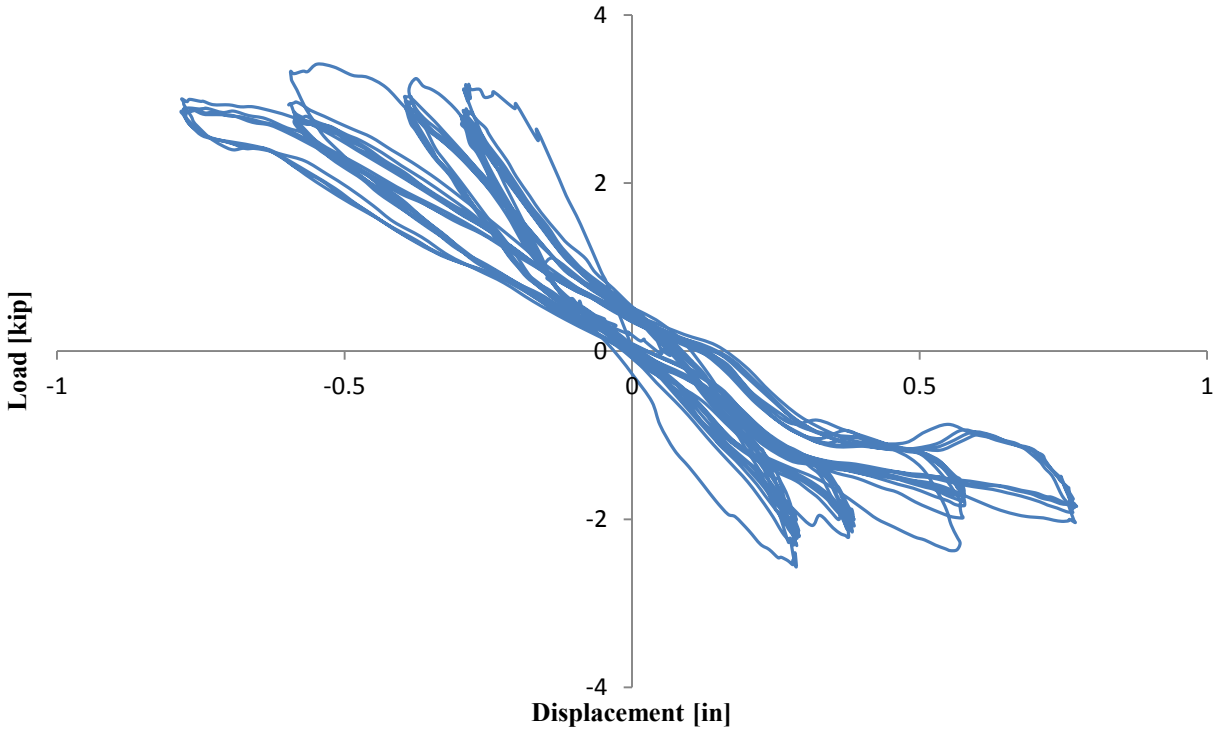

Figure 4-24: Specimen CA2 Global Hysteretic Plot

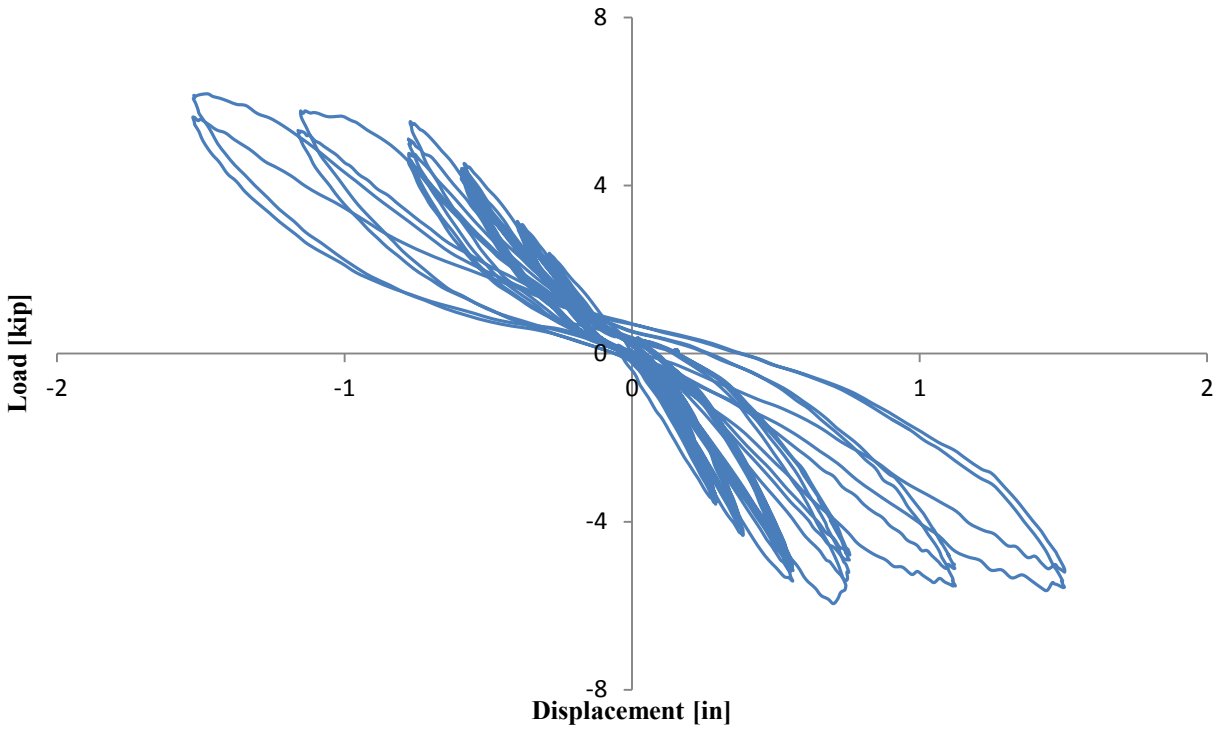

Figure 4-25: Specimen DA2 Global Hysteretic Plot

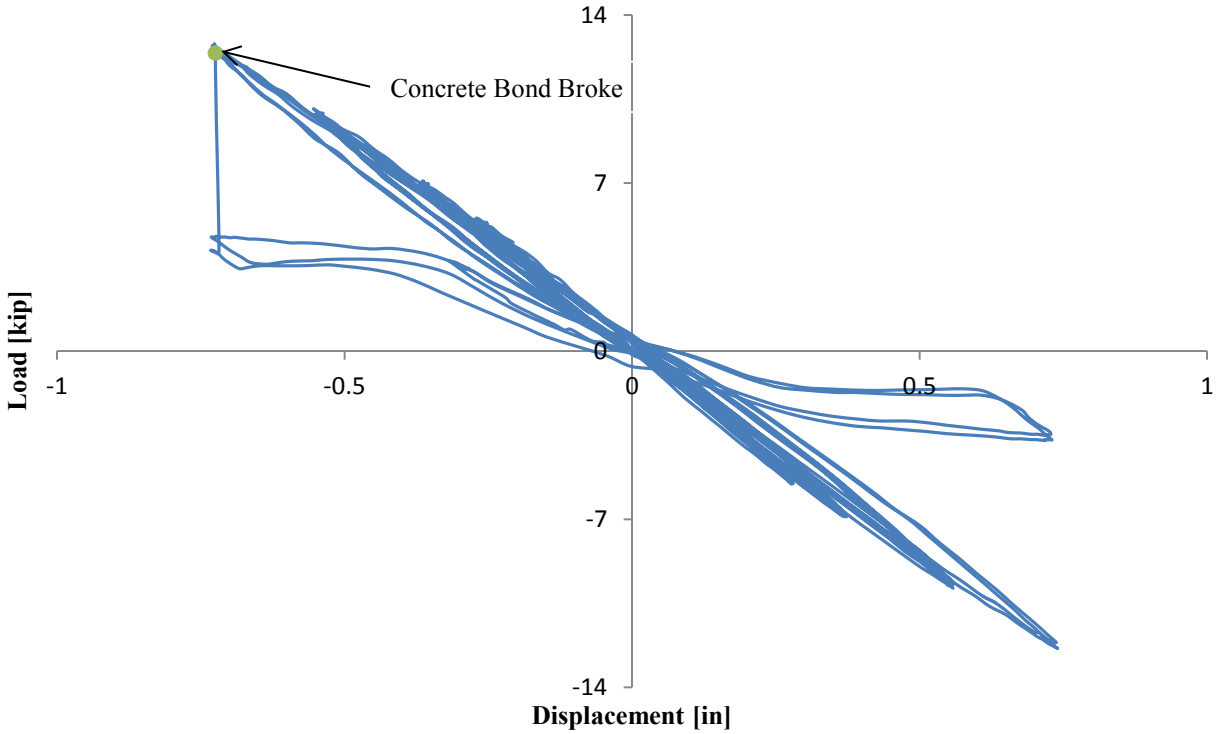

Figure 4-26: Specimen CB2 Global Hysteretic Plot

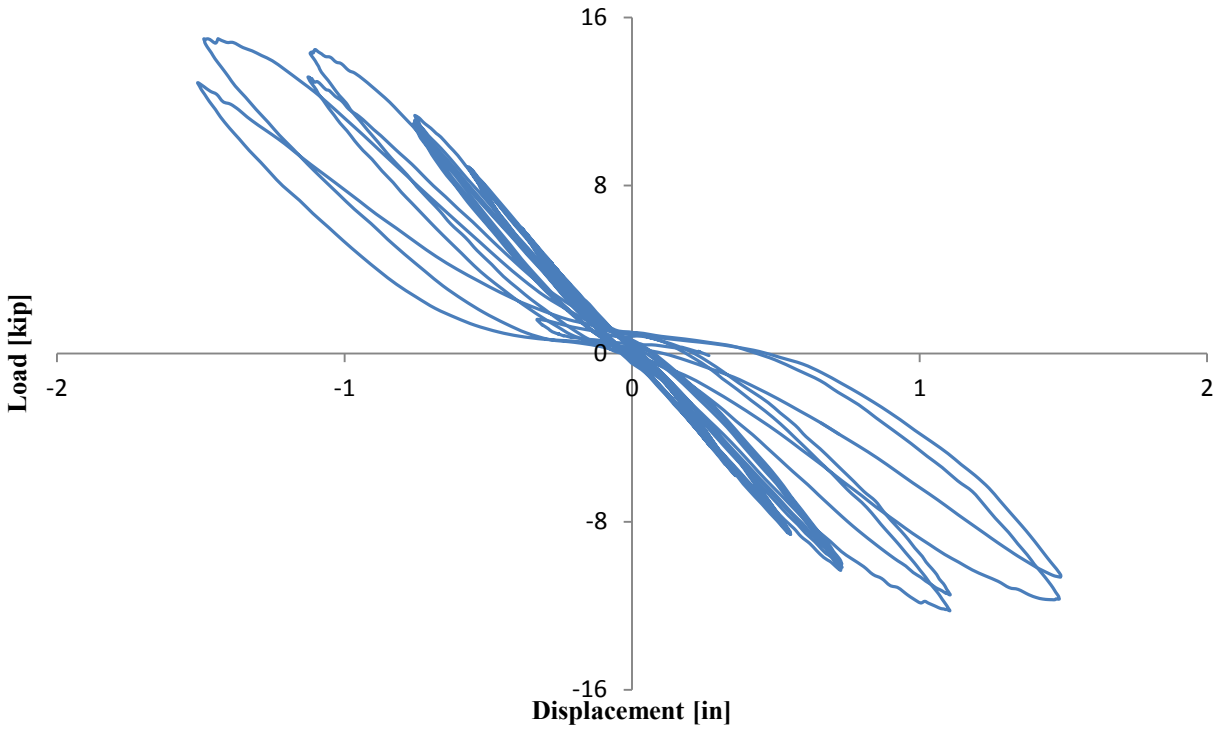

Figure 4-27: Specimen DB2 Global Hysteretic Plot

4.3 Specimen Stiffness

At the beginning of each cycle we plotted the hysteretic corrected force vs. displacement plots. From these plots we could estimate the specimen stiffness, which was taken as the slope of three or more points from the most linear portion of the plots before visible yielding could be detected. The plots for each specimen up to the 0.02 drift cycle can be seen in Figure 4-28 through Figure 4-39. After the actuator control error on specimen A3 there was a permanent displacement. For this reason the stiffness plots start at a non-zero displacement. For specimens CA2 and CB2 we only plotted up until the 0.01 drift cycle since that was as far as they were tested.

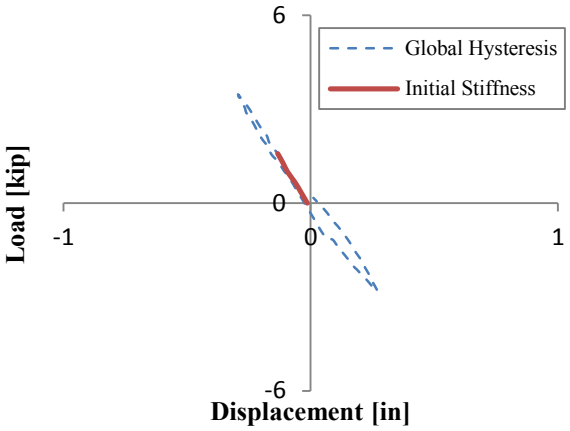

(a) 0.00375 Drift Cycle

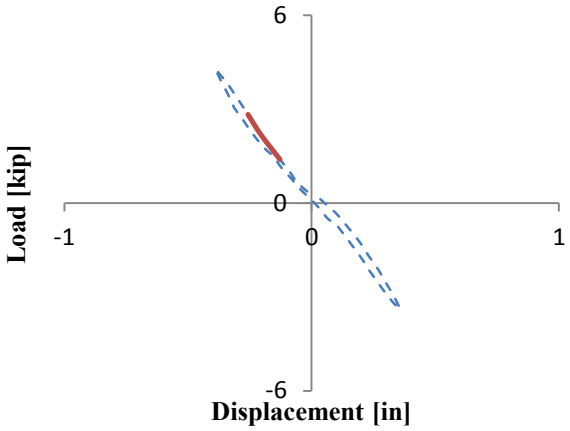

(b) 0.005 Drift Cycle

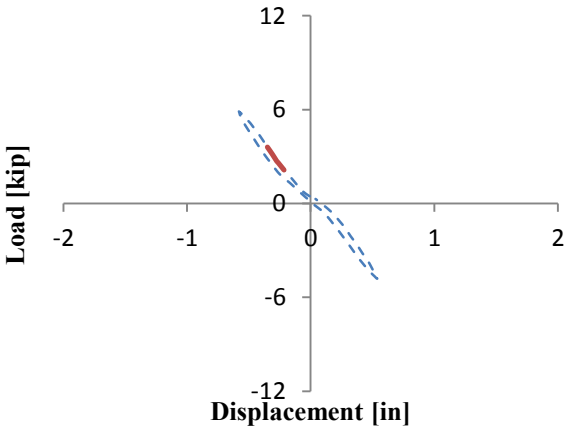

(c) 0.0075 Drift Cycle

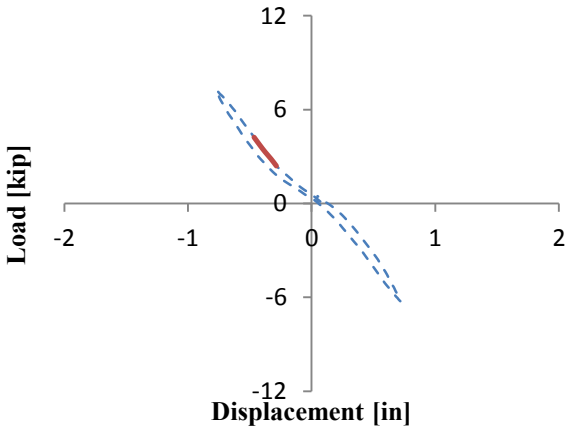

(d) 0.01 Drift Cycle

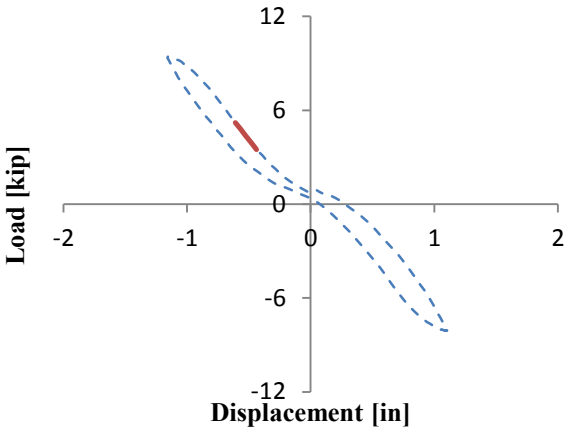

(e) 0.015 Drift Cycle

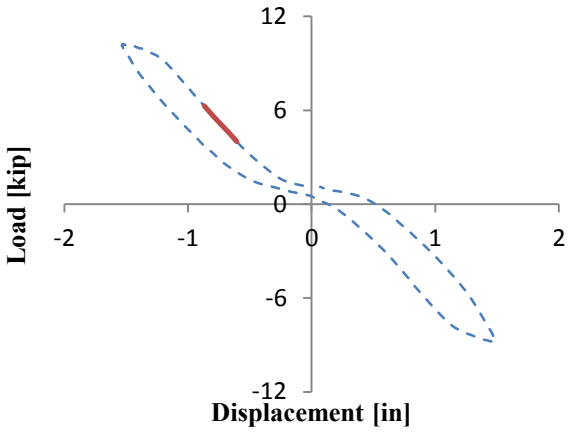

(f) 0.02 Drift Cycle

Figure 4-28: Hysteretic Progression of Specimen A1

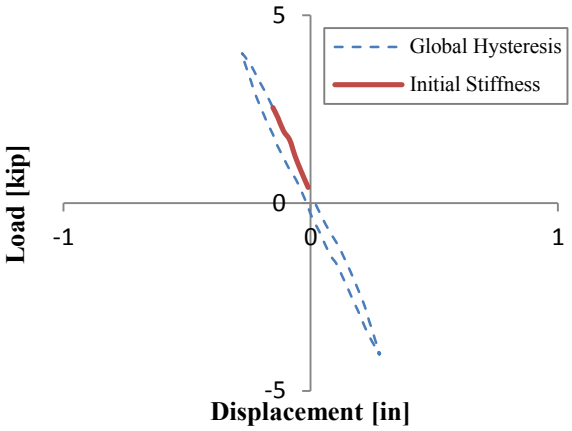

(a) 0.00375 Drift Cycle

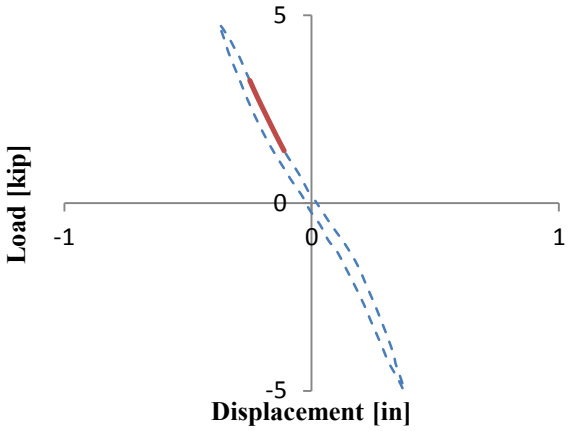

(b) 0.005 Drift Cycle

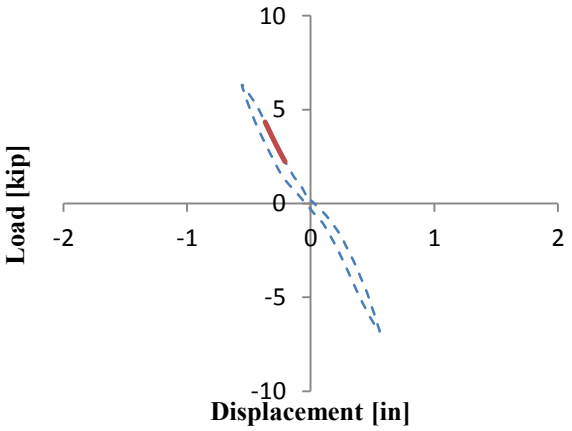

(c) 0.0075 Drift Cycle

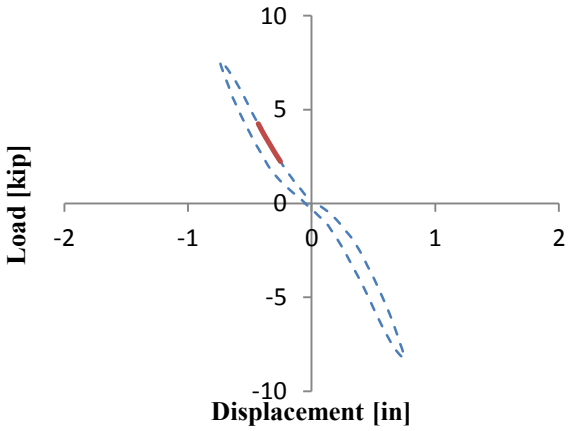

(d) 0.01 Drift Cycle

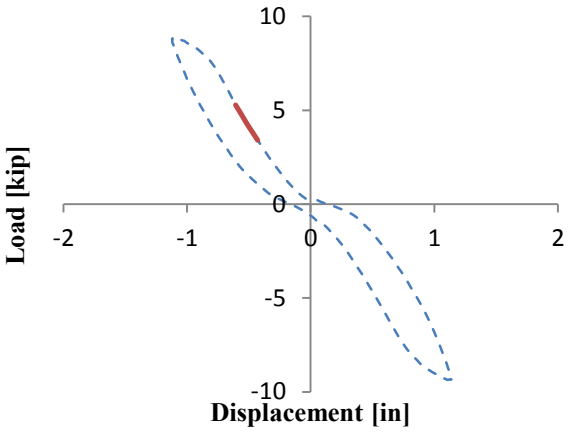

(e) 0.015 Drift Cycle

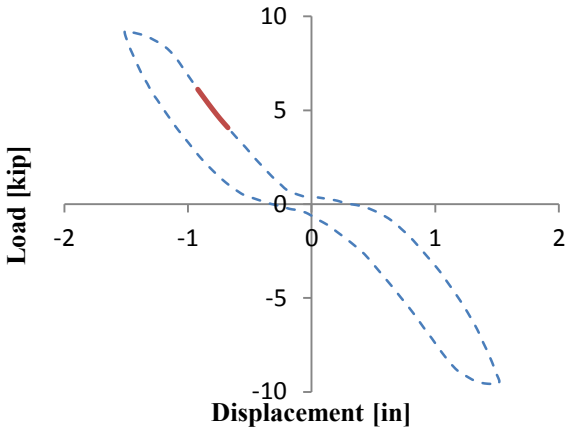

(f) 0.02 Drift Cycle

Figure 4-29: Hysteretic Progression of Specimen A2

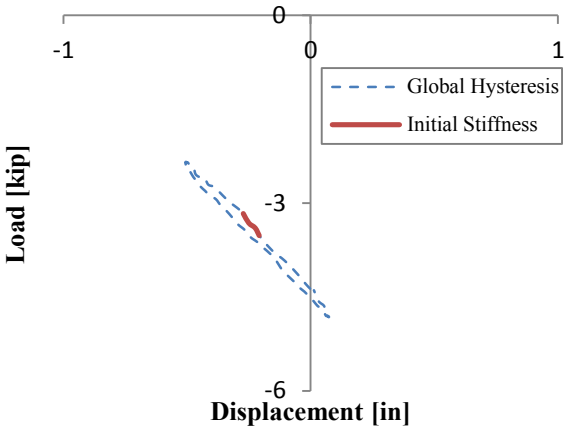

(a) 0.00375 Drift Cycle

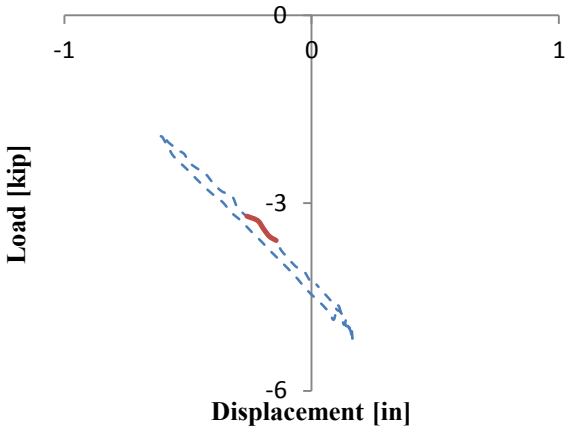

(b) 0.005 Drift Cycle

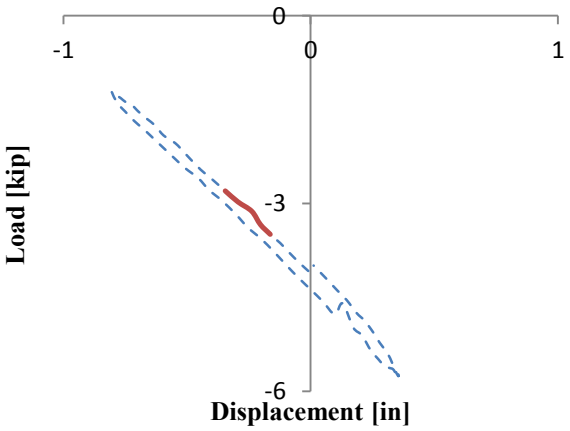

(c) 0.0075 Drift Cycle

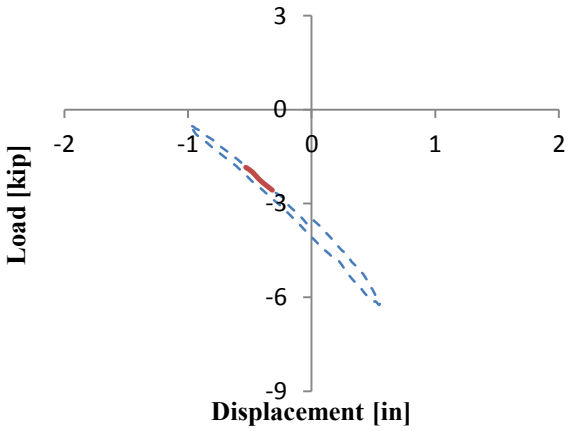

(d) 0.01 Drift Cycle

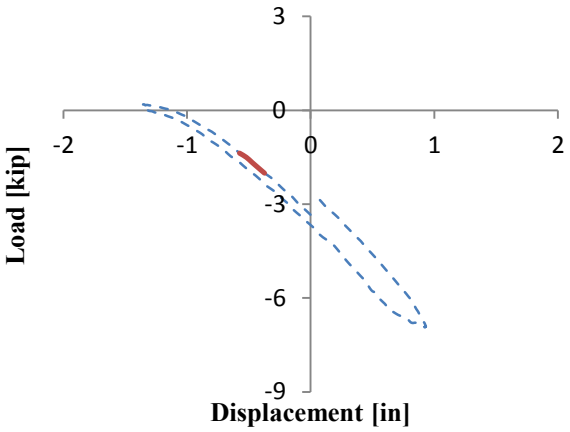

(e) 0.015 Drift Cycle

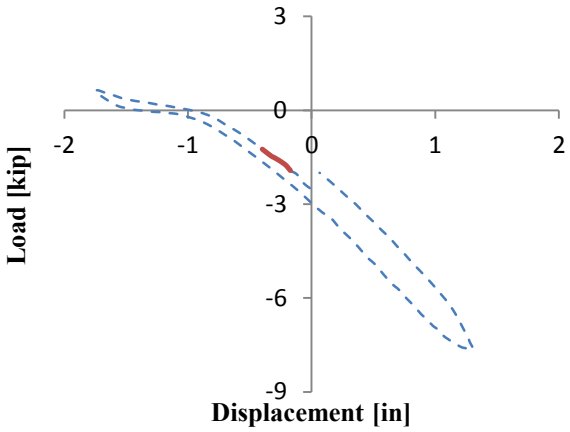

(f) 0.02 Drift Cycle

Figure 4-30: Hysteretic Progression of Specimen A3

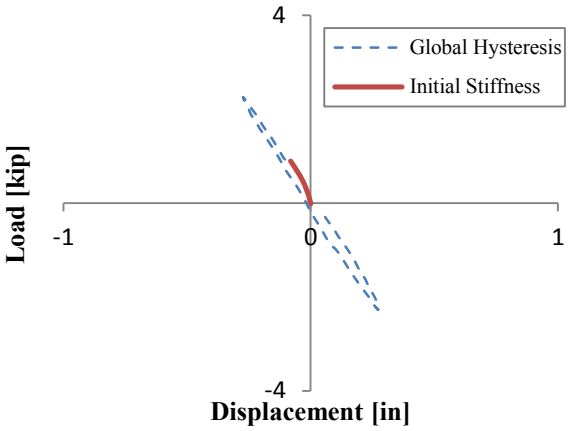

(a) 0.00375 Drift Cycle

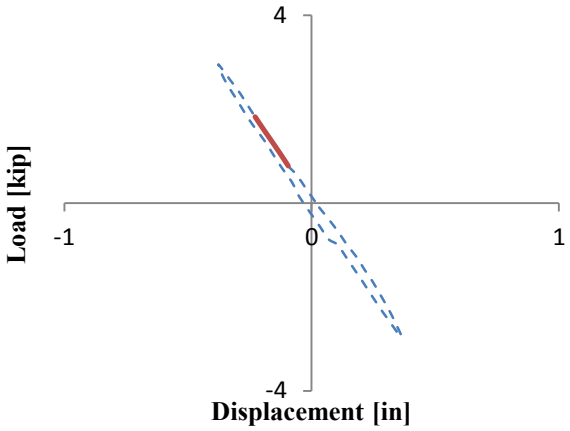

(b) 0.005 Drift Cycle

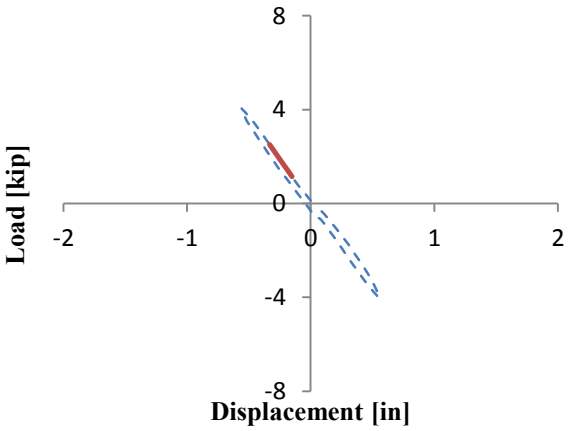

(c) 0.0075 Drift Cycle

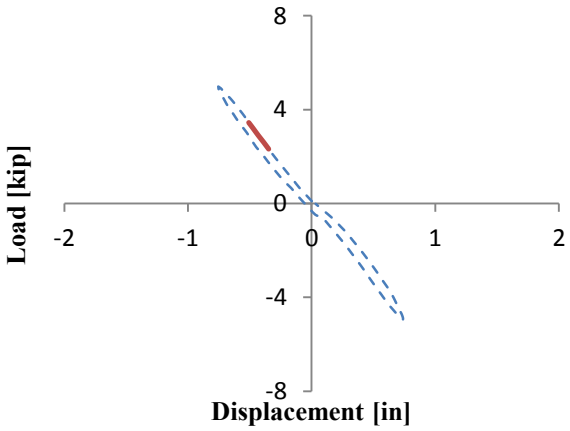

(d) 0.01 Drift Cycle

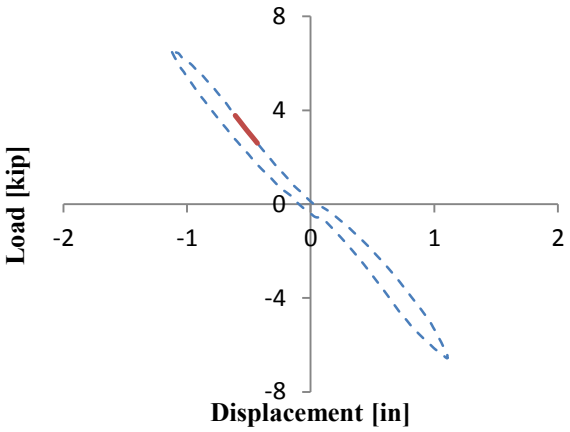

(e) 0.015 Drift Cycle

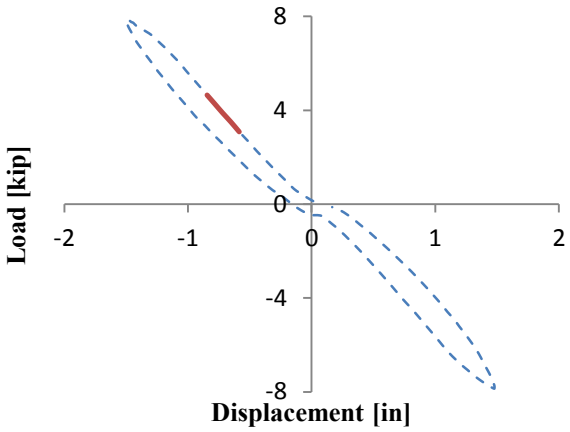

(f) 0.02 Drift Cycle

Figure 4-31: Hysteretic Progression of Specimen A4

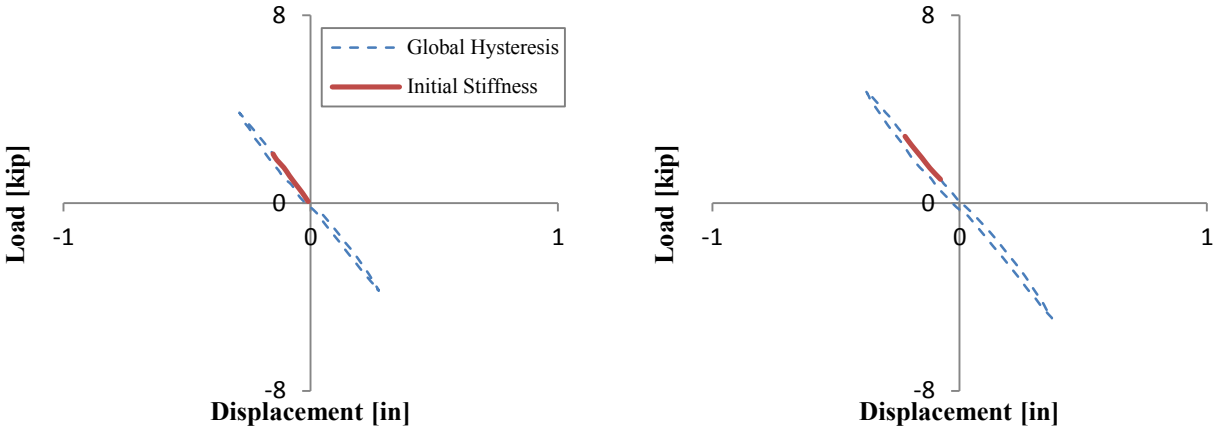

(a) 0.00375 Drift Cycle

(b) 0.005 Drift Cycle

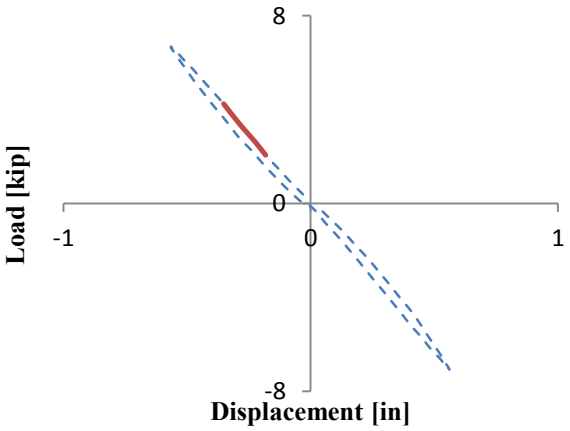

(c) 0.0075 Drift Cycle

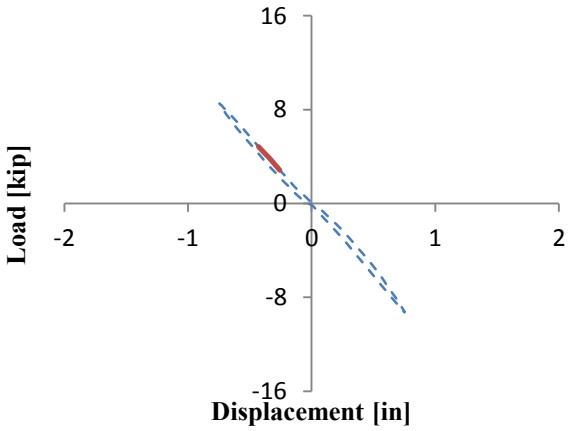

(d) 0.01 Drift Cycle

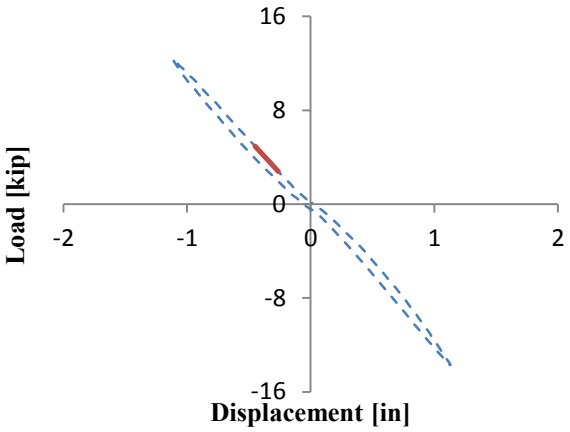

(e) 0.015 Drift Cycle

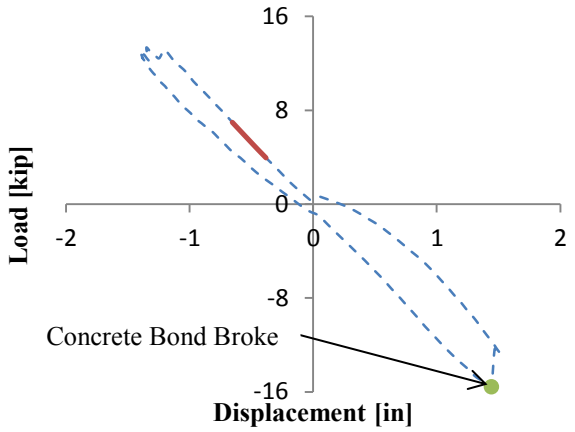

(f) 0.02 Drift Cycle

Figure 4-32: Hysteretic Progression of Specimen B1

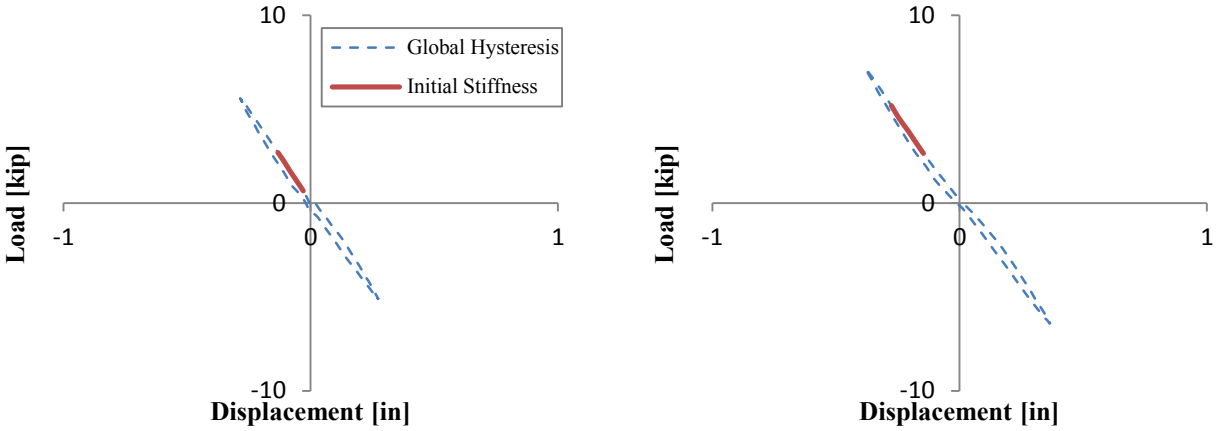

(a) 0.00375 Drift Cycle

(b) 0.005 Drift Cycle

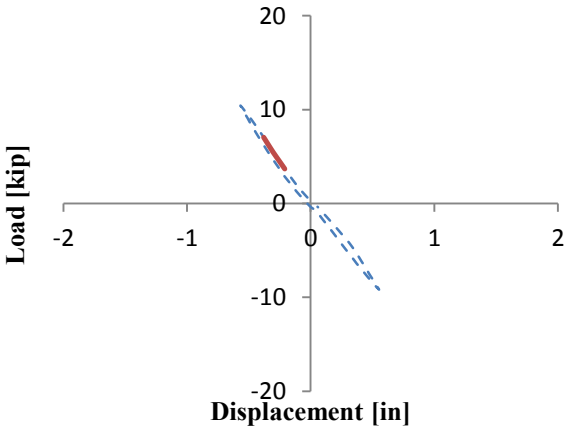

(c) 0.0075 Drift Cycle

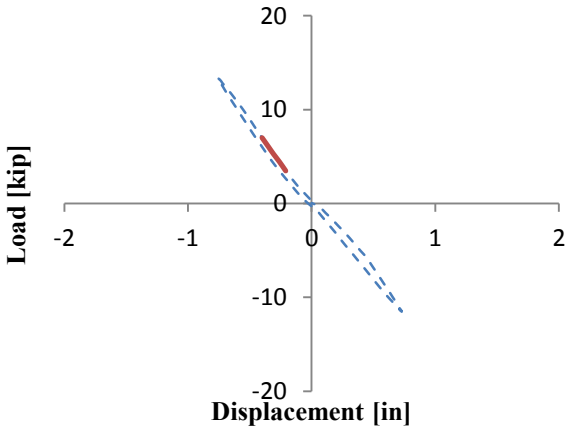

(d) 0.01 Drift Cycle

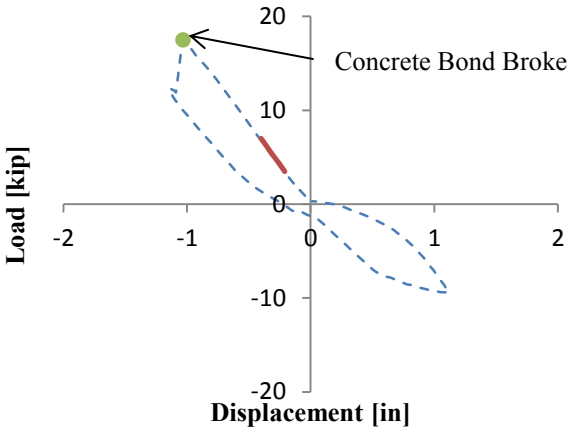

(e) 0.015 Drift Cycle

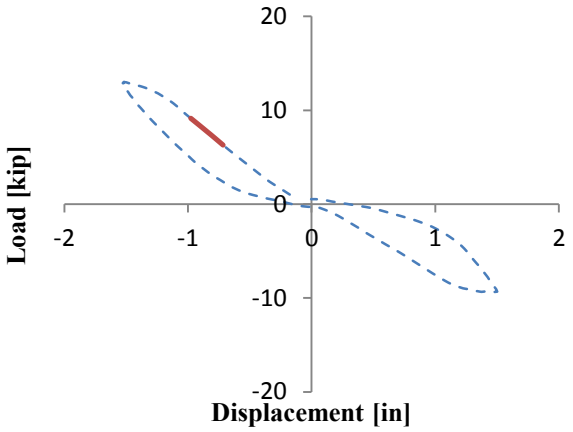

(f) 0.02 Drift Cycle

Figure 4-33: Hysteretic Progression of Specimen B2

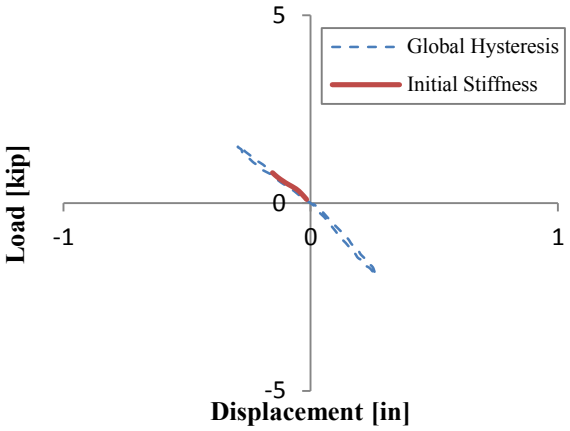

(a) 0.00375 Drift Cycle

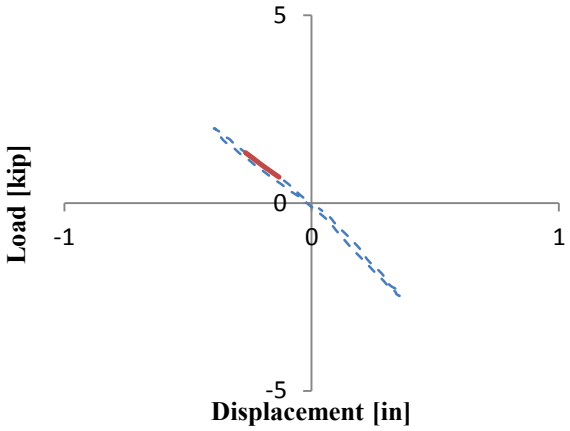

(b) 0.005 Drift Cycle

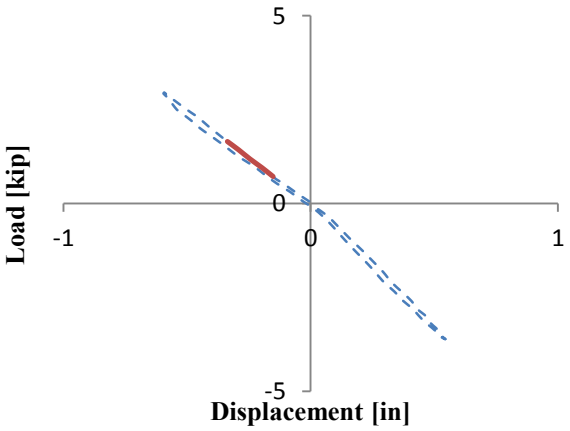

(c) 0.0075 Drift Cycle

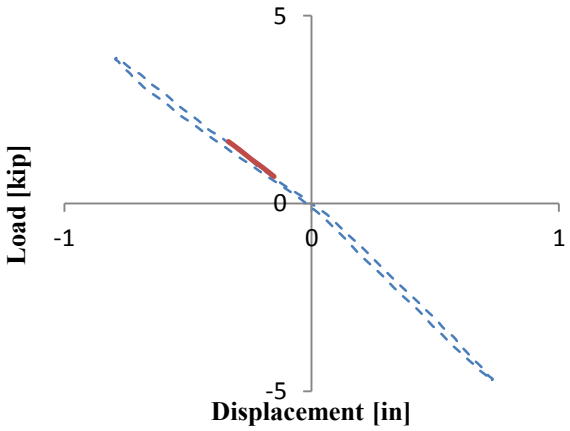

(d) 0.01 Drift Cycle

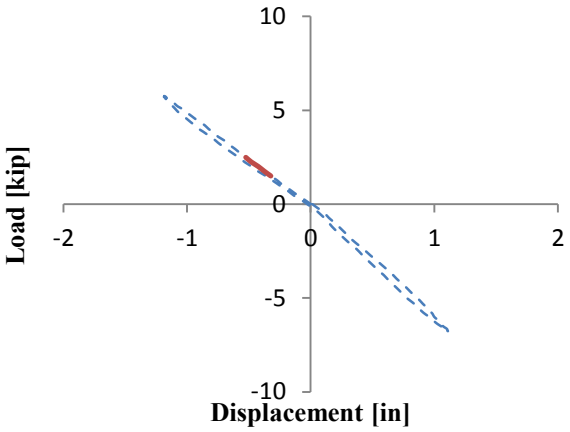

(e) 0.015 Drift Cycle

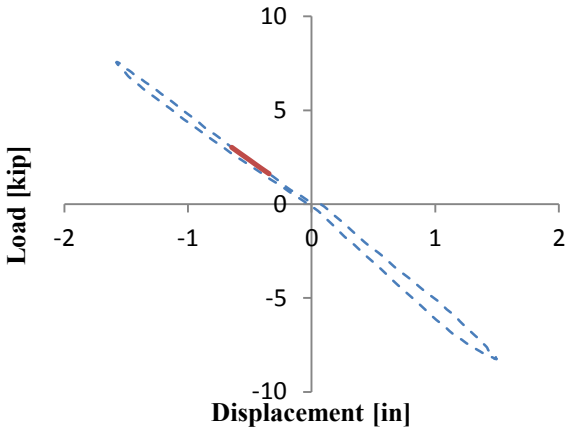

(f) 0.02 Drift Cycle

Figure 4-34: Hysteretic Progression of Specimen B3

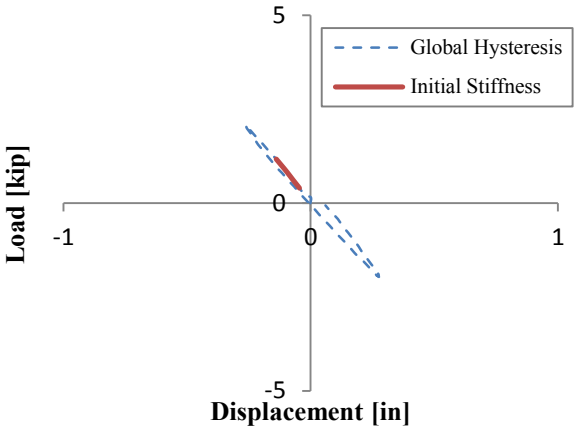

(a) 0.00375 Drift Cycle

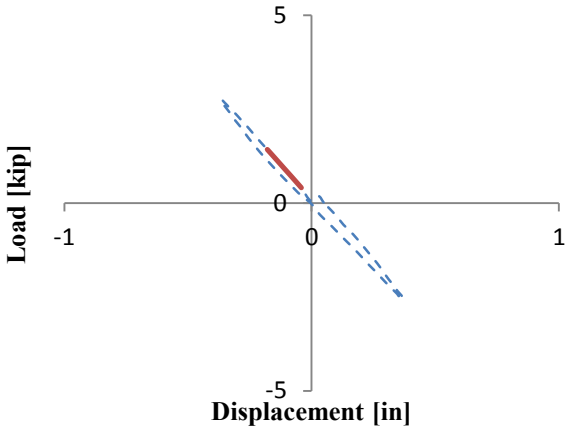

(b) 0.005 Drift Cycle

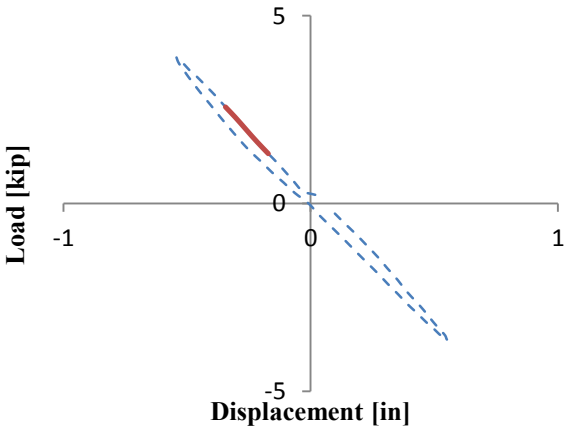

(c) 0.0075 Drift Cycle

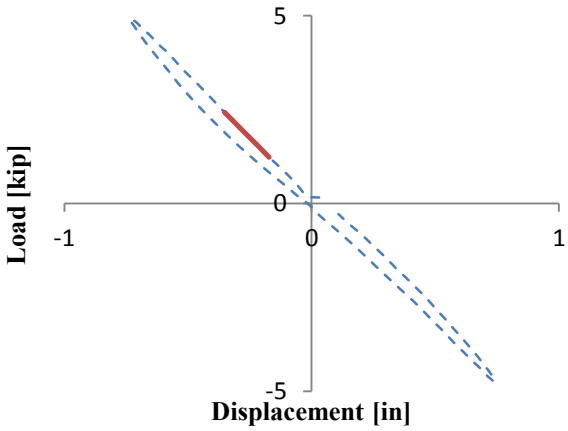

(d) 0.01 Drift Cycle

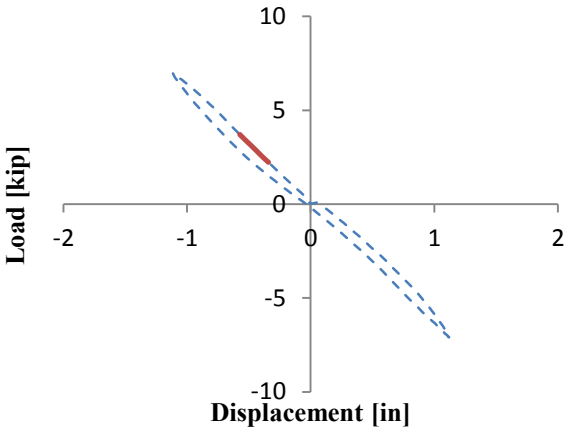

(e) 0.015 Drift Cycle

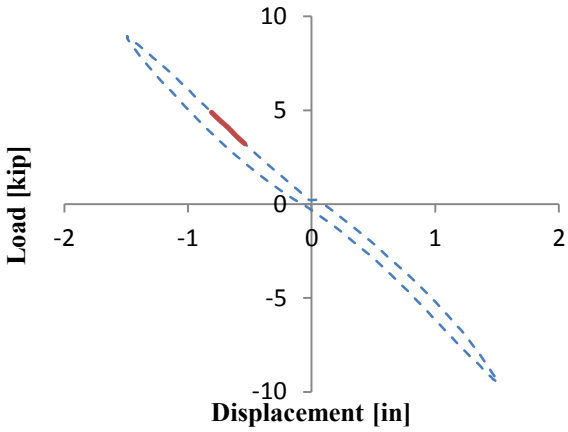

(f) 0.02 Drift Cycle

Figure 4-35: Hysteretic Progression of Specimen B4

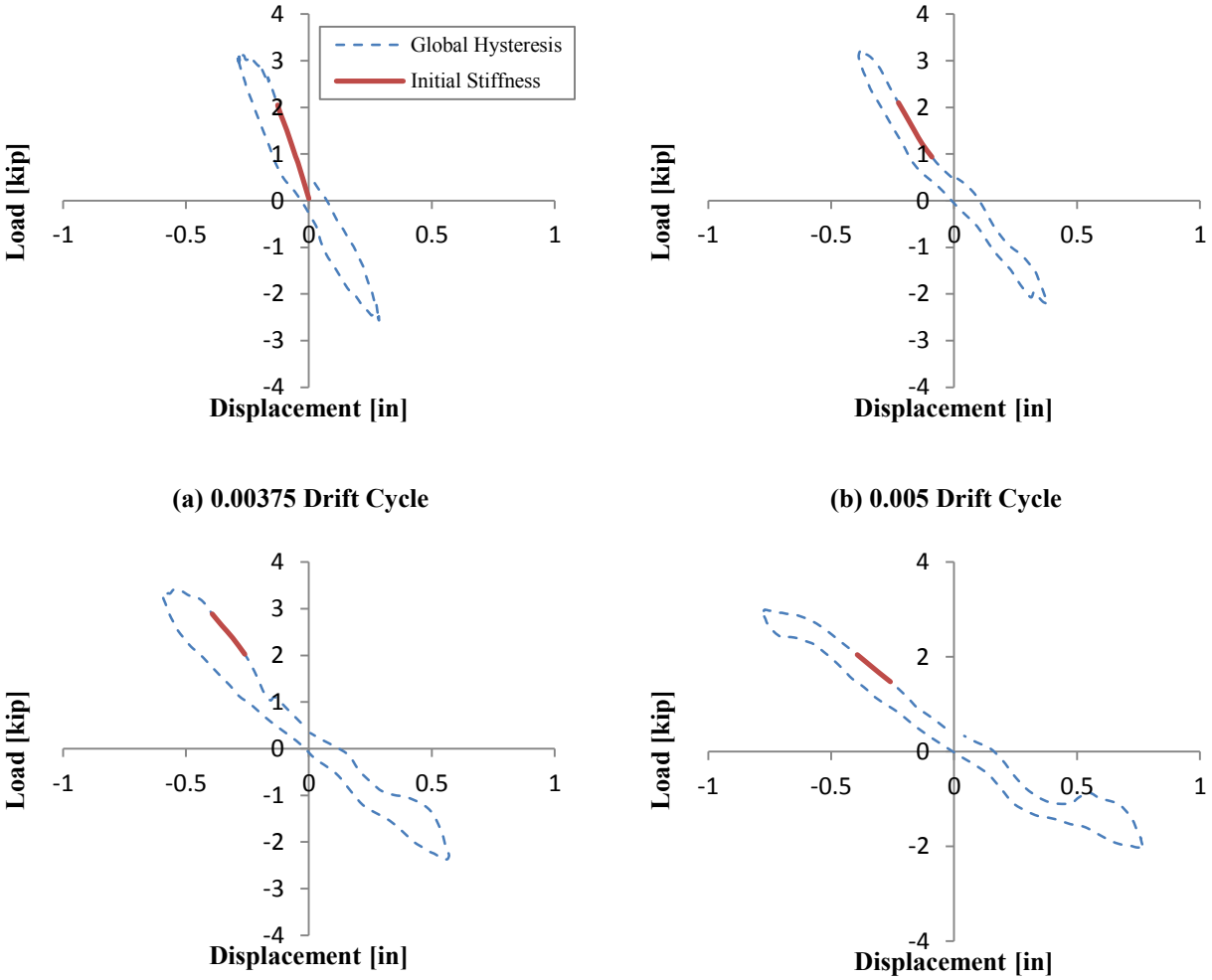

(a) 0.00375 Drift Cycle

(b) 0.005 Drift Cycle

(c) 0.0075 Drift Cycle

(d) 0.01 Drift Cycle

Figure 4-36: Hysteretic Progression of Specimen CA2

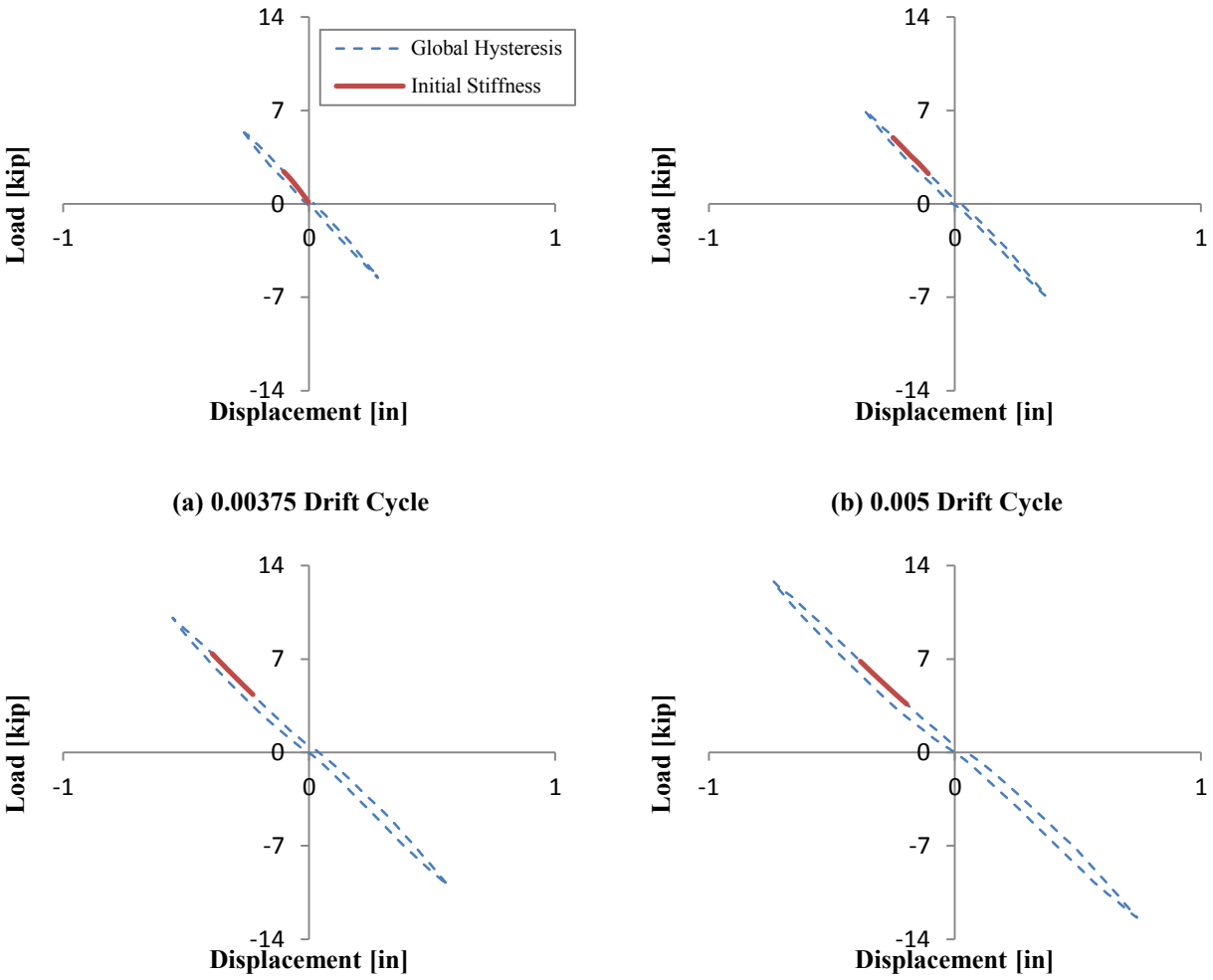

(a) 0.00375 Drift Cycle

(b) 0.005 Drift Cycle

(c) 0.0075 Drift Cycle

(d) 0.01 Drift Cycle

Figure 4-37: Hysteretic Progression of Specimen CB2

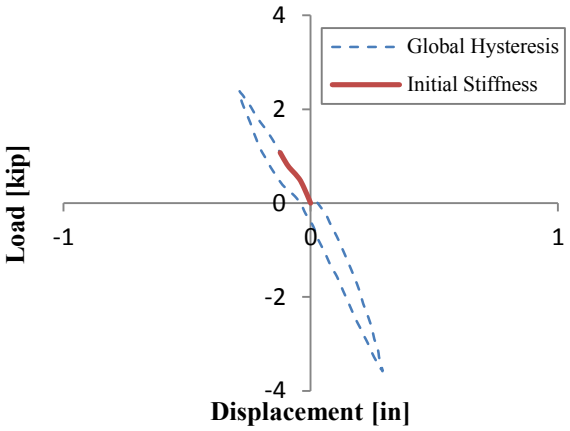

(a) 0.00375 Drift Cycle

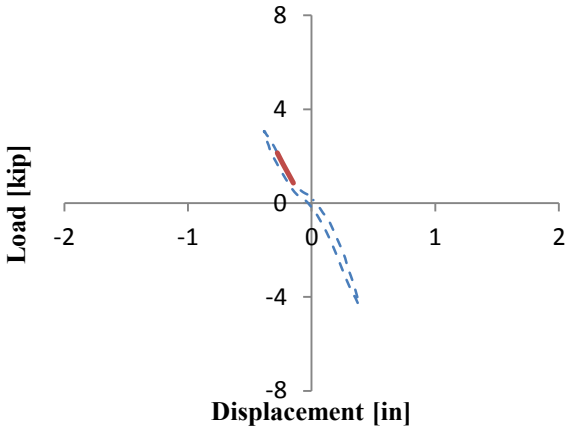

(b) 0.005 Drift Cycle

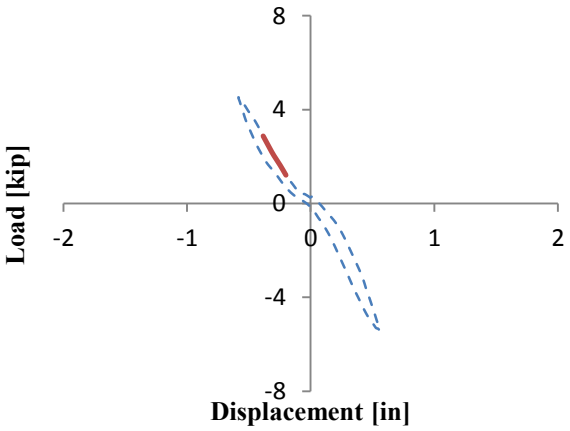

(c) 0.0075 Drift Cycle

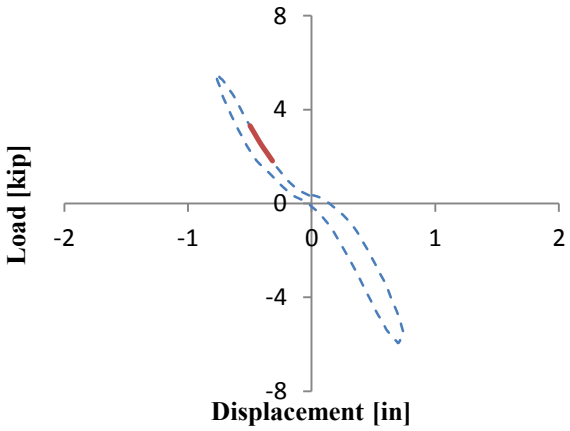

(d) 0.01 Drift Cycle

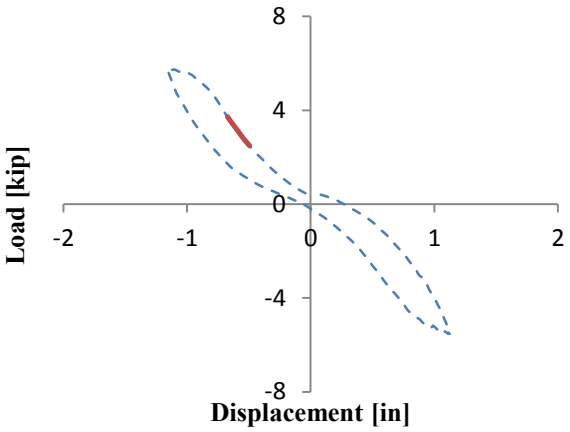

(e) 0.015 Drift Cycle

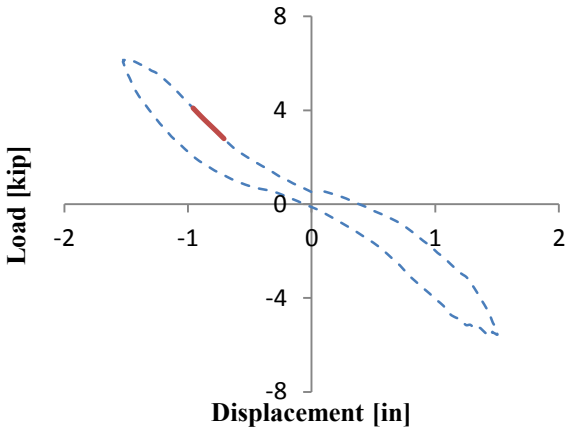

(f) 0.02 Drift Cycle

Figure 4-38: Hysteretic Progression of Specimen DA2

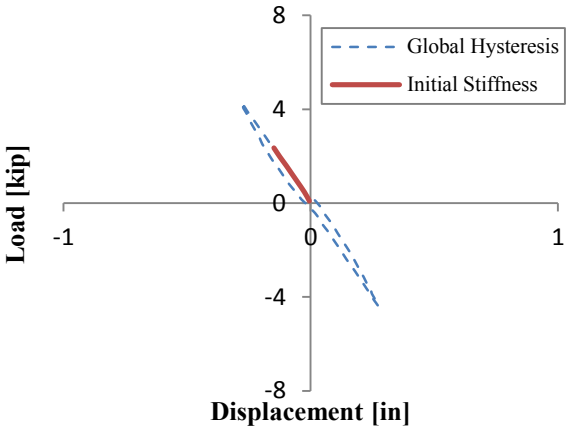

(a) 0.00375 Drift Cycle

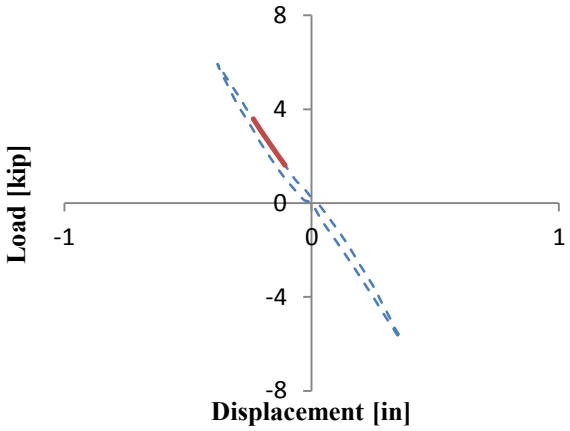

(b) 0.005 Drift Cycle

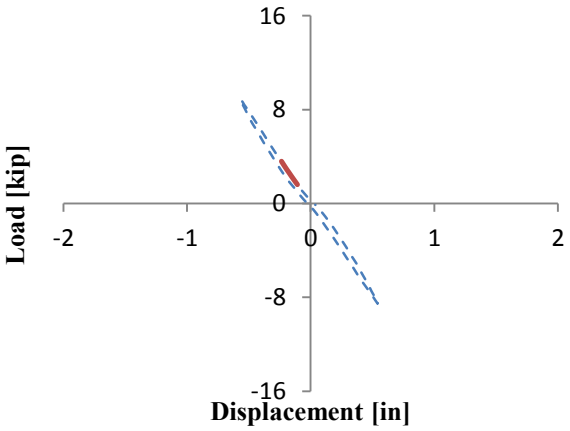

(c) 0.0075 Drift Cycle

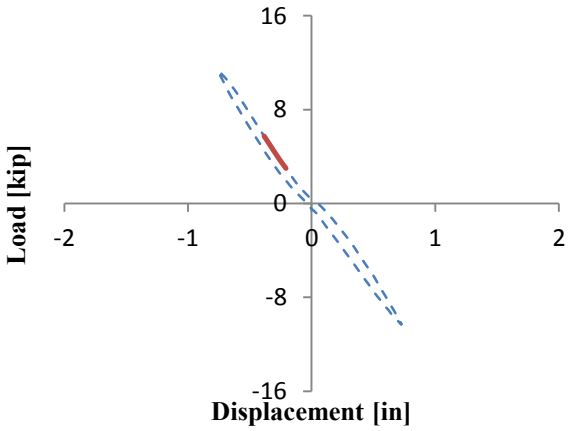

(d) 0.01 Drift Cycle

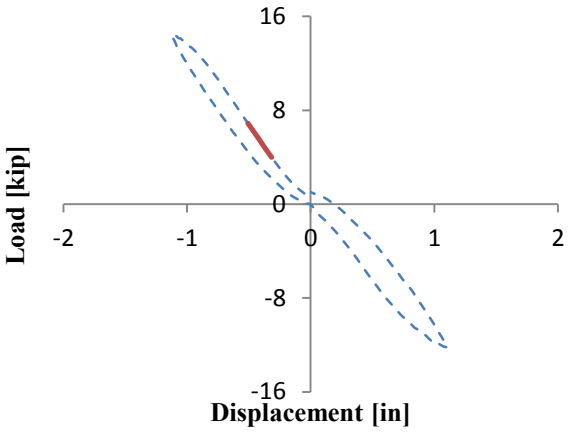

(e) 0.015 Drift Cycle

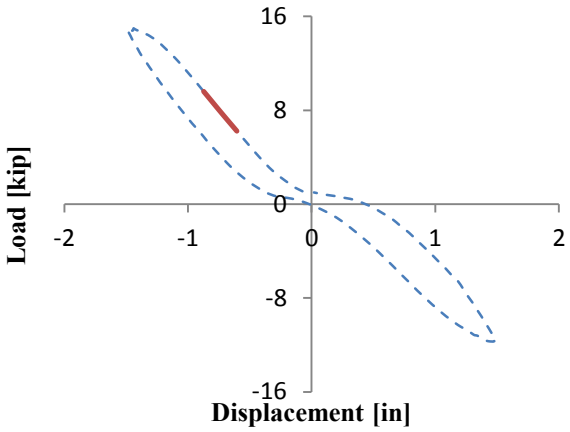

(f) 0.02 Drift Cycle

Figure 4-39: Hysteretic Progression of Specimen DB2

4.3.1 Individual Cycle Stiffness

From the hysteretic progression plots we took the initial stiffness from the first cycle at each displacement. These stiffnesses are shown in Table 4-1 up until the 0.02 drift cycle, and were plotted in Figure 5-3. These plots show the progression of the stiffness as the column progressed through the test. In the figure and table, specimens CB2, DB2, and B2 and specimens CA2, DA2, and A2 can be compared because they all have the same orientation, embedment depth, and are the same shape. The high initial stiffnesses in specimens B1, B2, CB2, and CA2 can be attributed to the strong concrete bond between the slab and the footing.

Table 4-1: Specimen Stiffness Progression

	$k_{initial}$ [kip/in]											
Cycle	A1	A2	A3[a]	A4	B1	B2	B3	B4	CA2	DA2	CB2	DB2
0.00375	13.03	14.96	5.22	10.89	14.09	20.01	4.87	8.25	15.61	8.98	22.90	15.54
0.00500	11.06	13.47	3.53	7.78	12.82	19.47	4.82	7.40	8.65	9.85	18.77	15.38
0.00750	10.99	13.10	3.80	7.52	12.77	19.68	5.05	7.23	6.47	8.97	18.52	15.38
0.01000	10.08	11.18	3.48	6.99	11.64	18.38	5.07	6.63	5.05	8.23	17.02	15.59
0.01500	10.07	10.54	3.22	6.59	11.47	18.38	4.85	6.41	-	6.95	-	15.18
0.02000	8.62	8.41	2.88	6.00	11.12	10.86	4.66	6.25	-	5.20	-	12.59

[a]Because the column yielded, these values are less than what the specimen would have exhibited

5 DISCUSSION

5.1 Elastic Stiffness

If these connections were pinned as is assumed in today's models there would be no stiffness, as the connections could not resist any moment. As was shown in the results, the connections actually had significant stiffness throughout the testing. When comparing specimens CA2, DA2, and A2 and CB2, DB2, and B2 it was evident that the specimens with the bolts engaged had higher strength and stiffness, however, the other specimens still had significant strength and stiffness. This shows that the connection is resisting the moment through the concrete embedment as well as through the strength in the bolt and bearing underneath the baseplate.

The stiffness of the connection itself can be determined using equations developed for springs in series. The total deflection of the column, Δ_t, can be broken down into two displacements; the deflection due to the column, Δ_c, and the deflection due to the rotation of the connection, Δ_{conn}. The relationship between these deflections is shown in Figure 5-1. From this deflection model and our knowledge of springs in series the stiffness of the connection can be determined. First the total stiffness, k_t, and the stiffness of the column, k_c, must be determined.

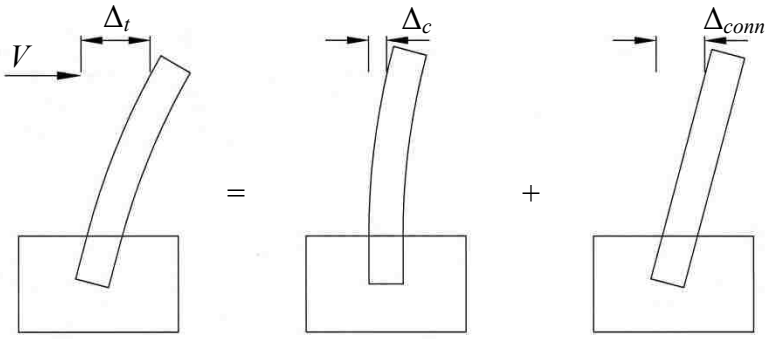

Figure 5-1: Stiffness Mechanism

The total stiffness, k_t, is given by equation 5-1.

$$k_t = \frac{V}{\Delta_t} \tag{5-1}$$

where:
V = lateral load, kip
Δ_t = total deflection, in

Both V and Δ_t can be obtained from experimental results for the specimens within the elastic range.

The stiffness due to the column, k_c, can be determined from the theoretical column stiffness of an embedded column given by equation 5-2.

$$k_c = \frac{3EI}{L^3} \tag{5-2}$$

where:
E = modulus of elasticity of column material, ksi
I = moment of inertia, in^4
L = length of column from line of action of actuator to top of slab, in

Once these two stiffnesses are known, the stiffness of the connection can be determined from equation 5-3, for springs in series.

$$\frac{1}{k_t} = \frac{1}{k_c} + \frac{1}{k_{conn}} \tag{5-3}$$

where:
k_{conn} = stiffness due to the connection, kip/in

The total stiffness was taken at three different linear portions of the first cycle of each specimen. Figure 5-2 shows these three linear segments. We chose to quantify the stiffness multiple times, using these three different segments to get an overall feel for the range of stiffness values that might be calculated; small changes in the total stiffness drastically change the connection stiffness. With these three different measures of the initial stiffness we could get a better picture of the range where the actual connection stiffness might fall.

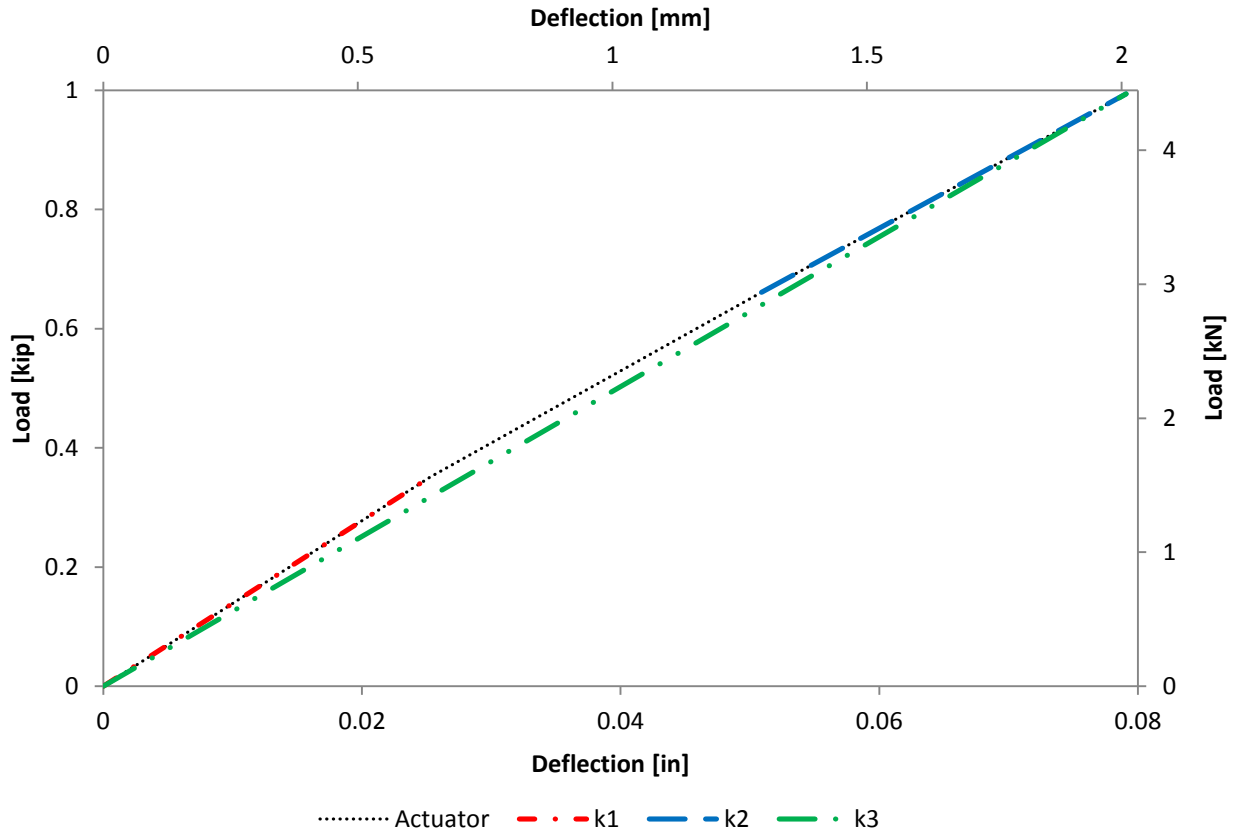

Figure 5-2: Total Stiffness

The first stiffness, k_1, is the slope of the line between the first and second data point of the first cycle of the test. The second stiffness, k_2, was taken as the slope of the line from the data point just before a deflection of 0.1 in, and the data point just before this one. The third stiffness, k_3, was taken as the slope of the line between the first data point in the series and the data point described above that falls just before a 0.1" drift. Using these stiffnesses, the connection stiffness was calculated for each k value and for each specimen, using equations 5-1 through 5-3. The displacements for these calculations were pulled from the uncorrected actuator displacement because at this point the drifts were so low that there was virtually no rotation in the actuator head. It should be noted that for specimen A3, only one stiffness was calculated, as the actuator control error limited the amount of data points before the column reached a drift of 0.1". We also did not include the data for specimens A4, B4, DA2, and DB2 because the bond between the slab and the footing had already broken from when the bases were tested previously. These changed the stiffness values significantly and they could not be compared to the other specimens. The stiffnesses are summarized in Table 5-1 through Table 5-3.

Table 5-1: Calculated Stiffnesses Based on k_1

Specimen	k_t	k_c	k_{conn}	k_t/k_c
A1	13.87	21.38	39.52	0.65
A2	17.27	30.97	39.05	0.56
A3	5.96	7.17	35.24	0.83
CA2	16.46	30.97	35.12	0.53
B1	15.64	19.15	85.26	0.82
B2	24.39	27.74	201.83	0.88
B3	5.63	6.42	45.55	0.88
CB2	23.49	30.97	97.23	0.76

Table 5-2: Calculated Stiffnesses Based on k_2

Specimen	k_t	k_c	k_{conn}	k_t/k_c
A1	11.81	21.38	26.38	0.55
A2	17.97	30.97	42.83	0.58
A3	5.96	7.17	35.24	0.83
CA2	16.21	30.97	33.99	0.52
B1	15.18	19.15	73.27	0.79
B2	19.48	27.74	65.39	0.70
B3	4.69	6.42	17.44	0.73
CB2	22.73	30.97	85.46	0.73

Table 5-3: Calculated Stiffnesses Based on k_3

Specimen	k_t	k_c	k_{conn}	k_t/k_c
A1	12.57	21.38	30.49	0.59
A2	16.65	30.97	36.02	0.54
A3	5.96	7.17	35.24	0.83
CA2	15.75	30.97	32.04	0.51
B1	14.66	19.15	62.52	0.77
B2	21.31	27.74	91.82	0.77
B3	5.17	6.42	26.60	0.81
CB2	23.20	30.97	92.42	0.75

It was determined that the stiffnesses based on k_3 were the most consistent. We would expect the stiffness of the connection to be the same for all the specimens at their respective embedment depths. This is because the stiffness of the connection only relies on factors that are consistent (embedment depth, anchor rod strength, base plate dimensions, etc.) in all the specimens and not the factors that change such as column shape and orientation. As can be seen from Table 5-3, the stiffness of the connection was very similar for the shallowly embedded columns, ranging from 30.49 – 36.02 kip/in. The deeper embedment stiffnesses had a wider variation but stayed within the same order of magnitude. These stiffnesses ranged from 26.60 – 92.42 kip/in. On specimen B3 the connection was strong enough to yield the column. We believe that the lower connection stiffness is due to increased deformation within the embedment. If this

value is omitted, the range of stiffnesses changes to 62.52-91.42 kip/in. We believe that this is a more accurate representation of the stiffness of the connection for the deeper embedded columns. Also, the total stiffness of the connection was not greatly affected by the embedment depth. For the strong axis specimens the shallow embedment total stiffness ranged from 12.57 – 16.65 kip/in, and for the deeper embedment it ranged from 14.66 – 23.20 kip/in. For the weak axis specimens with data that could be used, the stiffnesses for the different embeds were 5.96 kip/in and 5.17 kip/in respectively.

A ratio of the total stiffness to the expected stiffness of a fully embedded column can be used to compare the stiffnesses of the specimens. For the stiffness based on k_3, these ratios are shown in Table 5-3. Excluding the data for the weak axis specimens, the total stiffness of the shallow embedded columns was about 50%-60% the stiffness of a fully embedded column. The deeper embedded column stiffness was about 70%-80% the stiffness of a fully embedded column.

From the stiffness plots described in section 4.3.1 and the data summarized in Table 4-1 we created stiffness progression plots which are shown in Figure 5-3. These plots show the degradation of the total specimen stiffness as it progressed through the cycles. As can be seen, the specimens maintained stiffness up through the 0.02 drift cycle. For specimen A3, the values were lower than what would have been expected because the stiffnesses were taken after the actuator control error occurred. At this point the anchor rods yielded and strain hardened which would result in a lower total specimen stiffness.

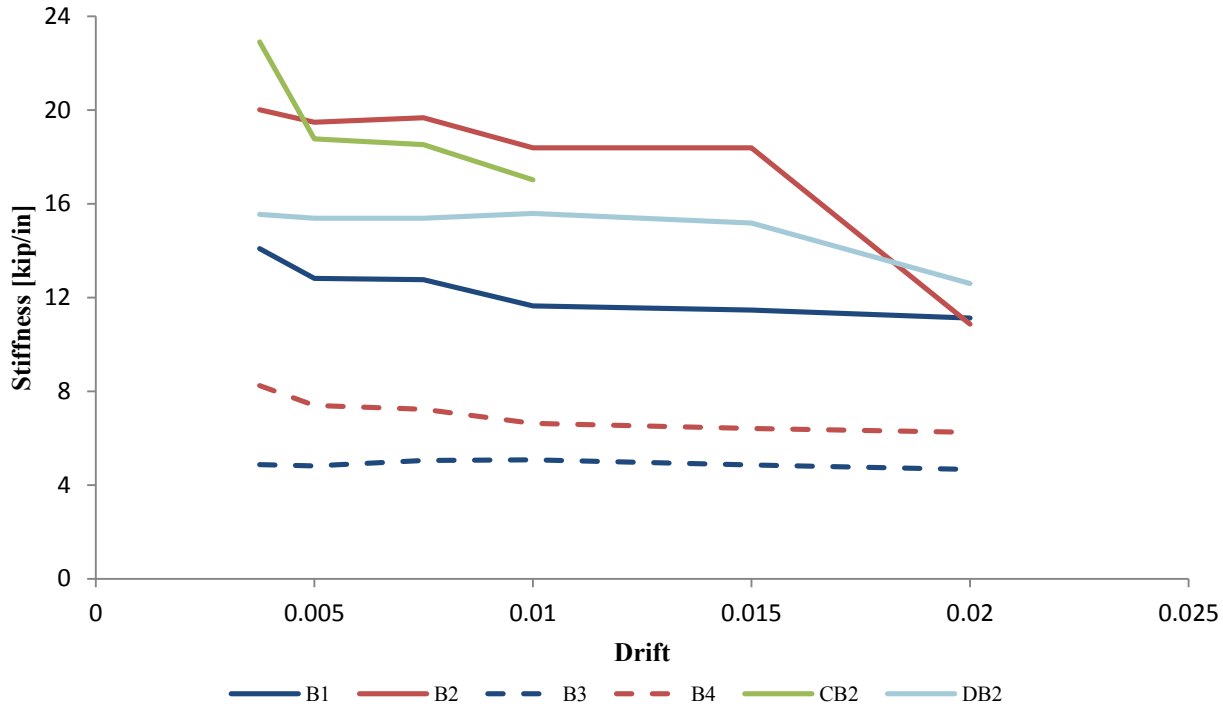

(a) Deep Embedment

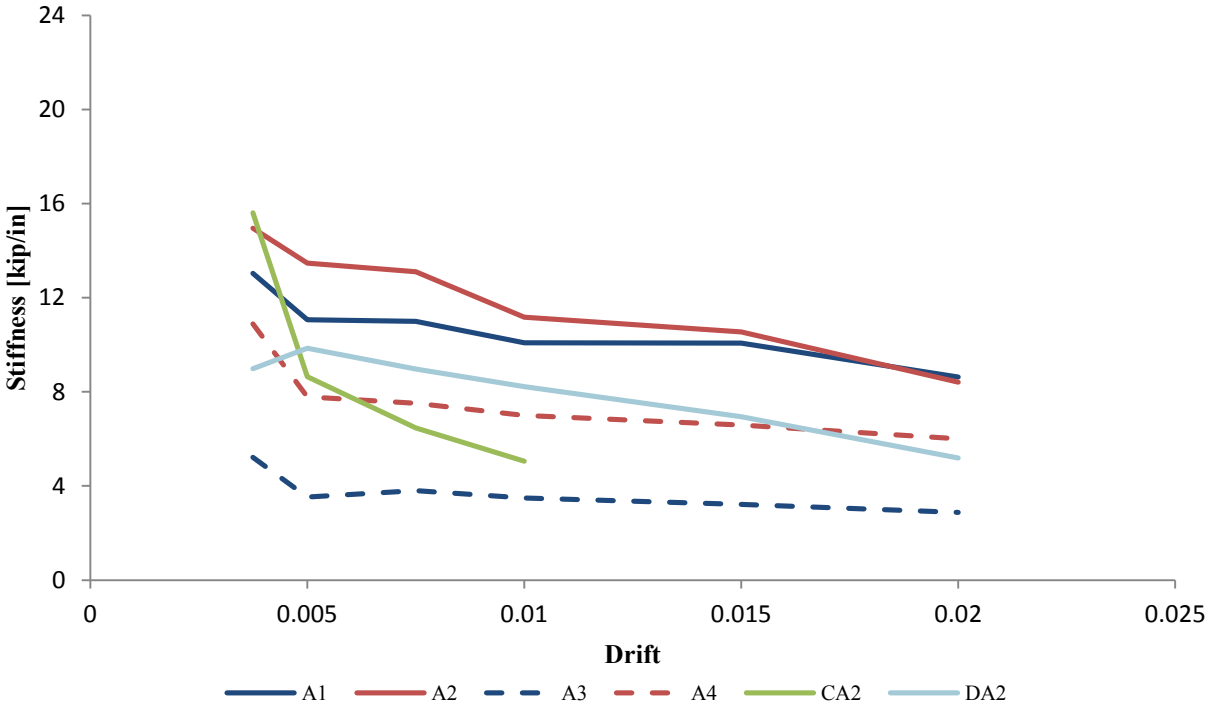

(b) Shallow Embedment

Figure 5-3: Specimen Stiffness Progression

5.2 Expected Strength

In order to understand the results, it was important that we found what the expected strength of these connections would be. Using the Baseplate Design Guide and following the steps for baseplates with large moments, we calculated the expected strength of our designed columns. Calculations for the expected strength are shown in Appendix B. For comparison these values were added to the backbone curves that were shown earlier. The new back bone curves are shown in Figure 5-4.

The expected ultimate strength was compared to the strengths of each of the specimens at 4% drift. By this point all of the specimens had yielded and were very close to, if not at their ultimate strength. For the shallow specimens the strength at 4% drift was 32% stronger on average than the expected ultimate strength and the deep specimens were 64% stronger. The average yield strength for both embedment depths was also compared to the expected yield strength. The average yield strength for the shallow specimens came out to be 86% stronger than the expected yield strength. For the deeper embedded columns the yield strength had to be estimated. When the bond broke the anchor bolts yielded rapidly and strain hardened at the same time so the load at yielding could not be precisely determined. To account for this it was estimated that for specimens B1 and B2 the yield load was 10% less than the load recorded just after the bond broke. For specimen B4 the bond had already partially broken from the earlier tests and the full bond break was not as drastic. The yield load was estimated as 5% less than the load just after the bond fully broke. The average yield strength of the deep specimens came out to be 144% stronger. It is also important to note that the yielding capacity of specimens A3 and B3 were governed by the yielding of the column. The strengths of each individual specimen are summed up in Table 5-4 for the shallow embeds and Table 5-4 for the deep embeds.

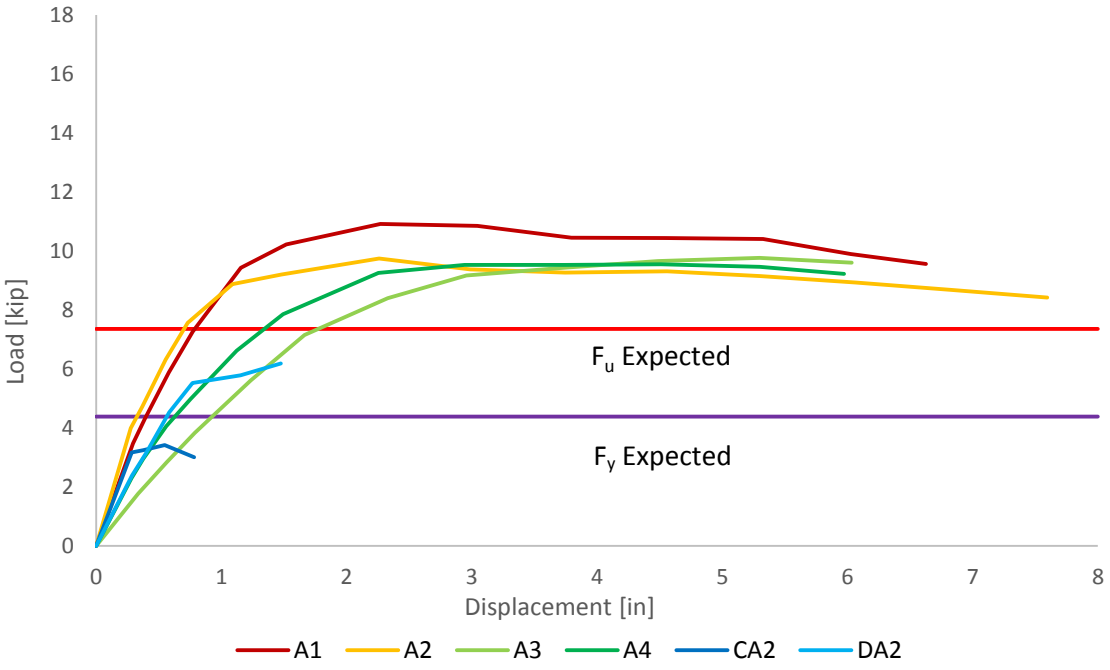

(a) Shallow Embedment

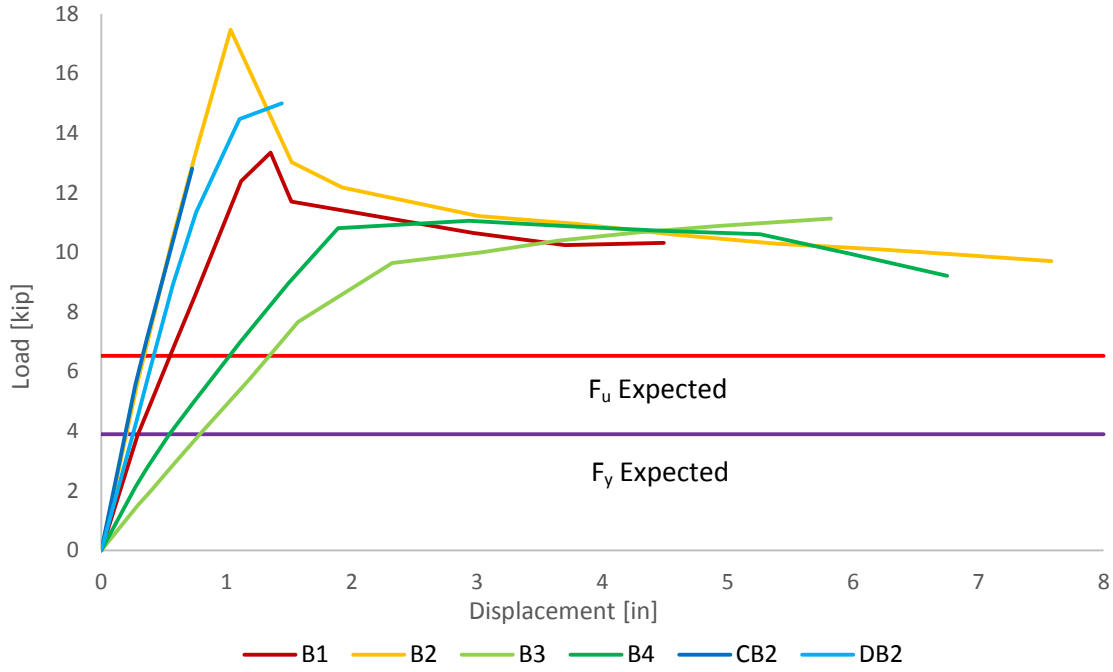

(b) Deep Embedment

Figure 5-4: Backbone Curves vs. Expected Strength

Table 5-4: Expected Strength vs. Actual Strength Shallow Embedment

Specimen	V_y [kip]	$V_{y,expected}$ [kip]	% Stronger	$V_{4\% Drift}$ [kip]	V_u [kip]	%Stronger
A1	8.48	4.38	94%	10.84	7.36	47%
A2	7.93	4.38	81%	9.37	7.36	27%
A3	8.08	4.38	84%	9.26	7.36	26%
A4	8.07	4.38	84%	9.52	7.36	29%
Average	8.14	4.38	86%	9.75	7.36	32%

Table 5-5: Expected Strength vs. Actual Strength Deep Embedment

Specimen	V_y [kip]	$V_{y,expected}$ [kip]	% Stronger	$V_{4\% Drift}$ [kip]	V_u [kip]	%Stronger
B1	9.85[a]	3.89	153%	10.64	6.53	63%
B2	10.73[a]	3.89	176%	11.21	6.53	72%
B3	8.69[b]	3.89	123%	10.00	6.53	53%
B4	8.71[a]	3.89	124%	11.06	6.53	69%
Average	9.49	3.89	144%	10.73	6.53	64%

[a]based on an estimated yield strength for the specimens that had a strong concrete bond
[b]column yielded before the specimen could break

5.3 Proposed Model

5.3.1 Bolt Forces

The forces in the anchor bolts were important to the overall strength of the connection. Material tests were performed on the anchor rods to determine the yield and ultimate strength and can be found in Appendix D. From these tests the yield strength and ultimate strength of the rods were determined (17.06 kips and 30.44 kips, respectively). Looking at the hysteretic plots of the specimens there was almost always (except for specimens with a strong concrete bond) an obvious initial yield point. We assumed that at this point one of the sets of the bolts began yielding.

5.3.2 Proposed Model

At this point we could create a model that would describe the unexplained strength that the specimen was able to resist [Figure 5-5]. From our observations we could tell that there was a section of the concrete that was resisting the applied force. It was also evident that the concrete in compression extended back underneath the baseplate and past the first set of bolts. This means that the first set of bolts were not resisting any load but rather the load was being resisted by the concrete underneath the set of bolts.

At this point we knew all of the forces acting to resist the load and we could begin to develop a model to explain the strength; the first force being the load in the yielded bolt and second force being the resultant force in the compression concrete. This resultant force was found by taking the sum of the forces in the y-direction. The only unknown that was left to solve for was the point at which the resultant was acting. Using statics this distance was determined for all the specimens that were limited by yielding in the anchor bolts and not in the column. For specimens B1, B2, and B4 the estimated yield loads were used to determine the resultant and location. B4 was most likely the best representation of the deep specimens because a small portion of elasticity was evident in the hysteretic plots after the bond broke. For columns A3 and B3 this model could not be developed because the ultimate strength was governed by yielding in the columns. For specimens CA2, DA2, BA2 and DB2 the model also could not be developed as the anchor bolts were not engaged. These calculations can be found in Appendix B and the location of the resulting force for each specimen is in Table 5-6.

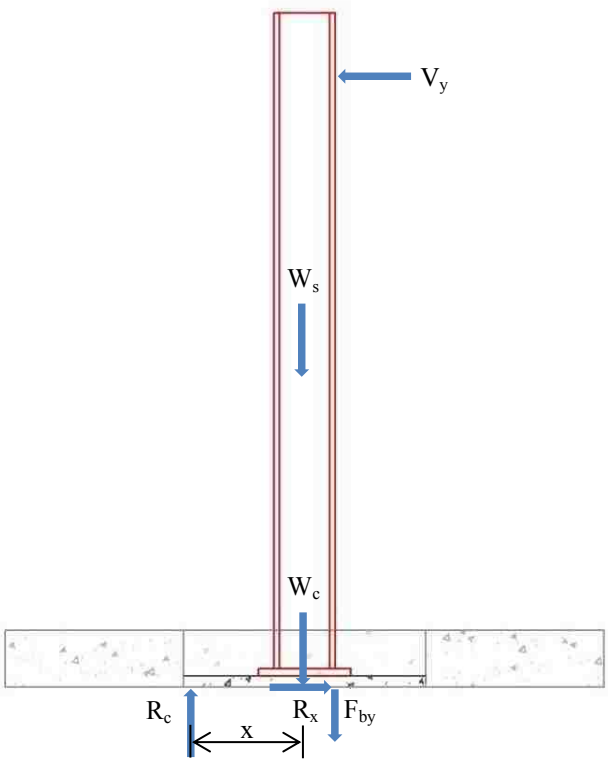

Figure 5-5: Resultant Force Distance

Table 5-6: Resultant Force Location

Specimen	V_y [kip]	x [in]
A1	8.48	15.16
A2	7.93	13.83
A4	7.34	12.44
B1[a]	10.94	22.77
B2[a]	11.92	25.14
B4[a,b]	9.17	18.32

[a] Lowest load after concrete break
[b] Most accurate of deep specimens

Using the locations of the resultant forces we developed a simplified model to quickly determine the strength of these specimens. From the locations of the resultants it could be seen that a 45º degree line from the face of the column drawn to the footing could roughly estimate the location of the resultant force. Figure 5-6 shows the locations of the resultants compared to

the 45º line drawn from the face of the column. For comparison the expected strength of each specimen was calculated using this method. The expected strengths based on the simplified model compared to the recorded strengths are shown in Table 5-7. All of the calculated strengths were within 20% of the actual strength. These calculations are found in Appendix B.

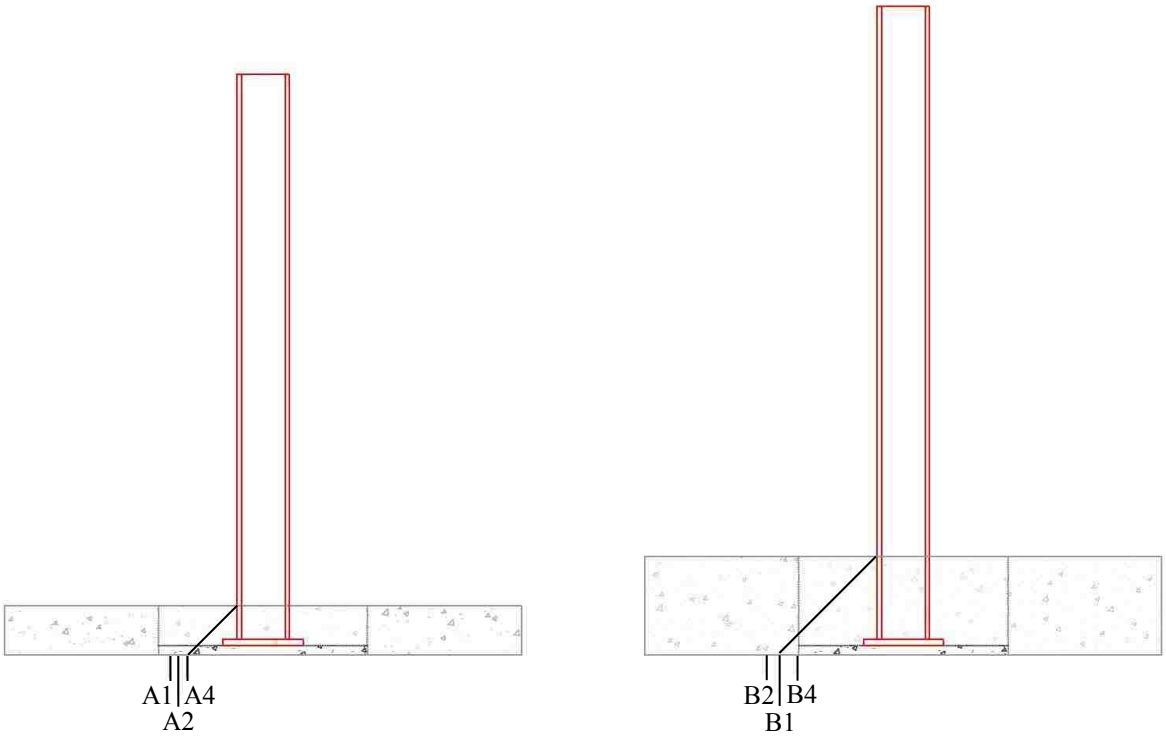

(a) Shallow Embedment **(a) Deep Embedment**

Figure 5-6: Resultant Force Locations

Table 5-7: Actual vs. Model Strength

Specimen	V_y [kip]	$V_{y,model}$ [kip]	Error
A1	8.48	7.16	18%
A2	7.93	7.26	9%
A4	7.34	7.18	2%
B1	9.85	9.85	0%
B2	10.73	9.95	8%
B4	8.71	9.87	-12%

The compression resultant force is the resultant of a distributed bearing force in the concrete. We only knew the overall resultant of the distributed load; there are many possibilities for the values of the distributed load, and corresponding extent, which give the same resultant and location of the resultant. If we assumed that the entire slab was effectively resisting the load the distributed load would extend past the bolt that is in tension. This is unfeasible as it would say that the bolt was in tension while the baseplate around it was in compression. The only explanation is that the entire slab was not contributing to resisting the forces. From the pictures at the yield point we could see that the bearing area of the concrete extended to some point in the baseplate. Figure 5-7 shows the model with the distributed load.

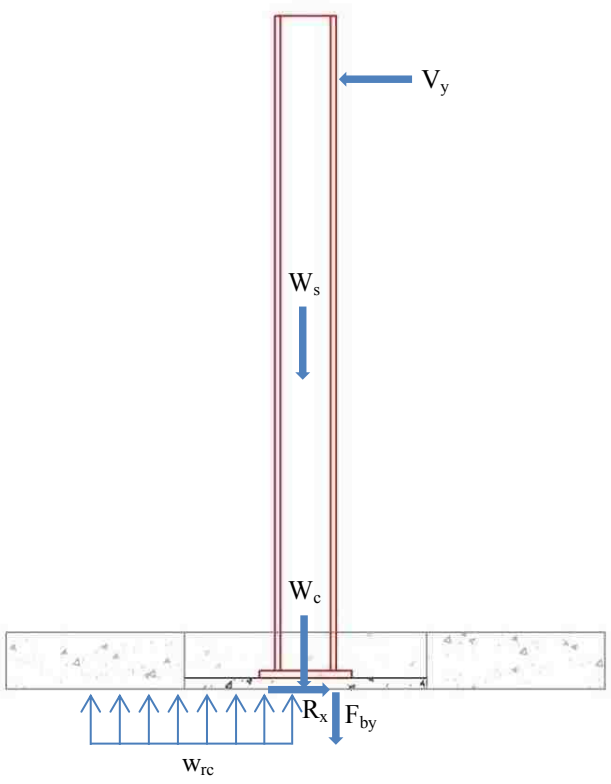

Figure 5-7: Proposed Model

5.4 **Further Research**

There were many useful results from the tests we carried out but further research could be done to understand these connections better. These tests helped us to know modifications that could be done to the specimens to be able to create a more accurate model. Below are some modifications that could be made in further research.

First, the model that was developed worked very well as long as there was a definitive yield point in the specimen. This was no available for the specimens that had high concrete bond. For future tests, if the bond between the concrete was limited as much as possible, a definitive yield point could most likely be observed in both the shallow and deep specimens. This could be achieved by applying form release between the footing and the slab.

Second, the specimens with high concrete bond exhibited very large strength resistance. Once the bond broke this load dropped significantly. In future specimens the bond between the footing and slab could be made stronger to allow the specimen to gain strength past the point the bond would have typically broke. This could be accomplished by placing dowels from the footing to the slab. This would keep the footing from separating from the slab.

6 CONCLUSION

An experimental study was performed on shallow embedded gravity column steel base connections to determine the strength and stiffness of the connections. There were eight standard specimens and four modified specimens tested. Of the standard specimens, four were W8×48 columns and four were W8×35 columns, each of them were tested in the strong and weak axis and each of them were tested with an embedment depth of eight and sixteen inches. The modified specimens were W8×48 columns tested at both embedment depths, and all four of them did not have the anchor bolts engaged while two of them had the slab braced to prevent it from moving up and down.

Based on the results from our research the following conclusions can be made.

1. All of the specimens exhibited higher strength than was predicted from the base plate design guide. The shallow specimens had a yield strength 86% stronger than the expected strength and the deeper specimens had a yield strength 144% stronger. The ultimate strengths for the specimens were 32% and 64% stronger than the expected strengths, respectively. In turn, the existing models for predicting the strength of these connections are not sufficient.
2. The total stiffness of the shallow connections tested in the strong axis ranged from 12.57 -16.65 kip/in while the total stiffness of the deeper connections tested in the strong axis ranged from 14.66-21.31 kip/in. For the weak axis specimens with valid data, the total

stiffness for the shallowly embedded column was 5.96 kip/in, while the total stiffness for the deep specimen was 5.17 kip/in. The shallow embedment was able to provide stiffness that was very close to the stiffness of the deeper embeds, suggesting that the shallow embedment was approaching a fixed connection.

3. The resultant compressive block was not located under the base plate as is suggested by the base plate design guide. Rather the resultant is located under the slab-one-grade concrete at a distance father from the center of the column than the edge of the base plate.
4. An approximate model can be used to predict the strength of these connections. In the model, a 45° line drawn from the face of the column down to the interface between the slab-on-grade and the footing will give an approximate location for the resultant of the compression block in the concrete. This approximate model was able to predict the strength of the specimens to within 20%.

REFERENCES

[1] Xiao, Y., Wu, H., Yaprak, T. T., Martin, G. R., and Mander, J. B. (2006). "Experimental studies on seismic behavior of steel pile-to-pile-cap connections." *Journal of Bridge Engineering*, 11(2), 151-159.

[2] Fisher, M. F., and Kloiber L. A. (2006). *Base Plate and Anchor Rod Design,* 2nd Ed., American Institute of Steel Construction.

[3] PCI Industry Handbook Committee. (1999). *PCI Design Handbook,*5th Edition, Precast/Prestressed Concrete Intitute, Chicago, IL.

[4] Marcakis, K., and Mitchell, D. (1980). "Precast concrete connections with embedded steel members." *PCI Journal,* 25, 88-116.

[5] Cui, Y., Nagae, T., and Nakashima, M. (2009). "Hysteretic behavior and strength capacity of shallowly embedded steel column bases." *Journal of Structural Engineering*, 135(10), 1231-1238.

[6] Shama, A. A., Mander, J. B., and Aref, A. J. (2002). "Seismic performance and retrofit of steel pile to concrete cap connections." *ACI structural journal*, *99*(1).

[7] Richards, P. W., Rollins, K. M., and Stenlund, T. E. (2010). Experimental Testing of Pile-to-Cap Connections for Embedded Pipe Piles. *Journal of Bridge Engineering*, 16(2), 286-294.

[8] Eastman, R. S. (2011). "Experimental Investigation of Steel Pipe Pile to Concrete Cap Connections." Master's thesis, Brigham Young University, Provo, UT.

[9] Kanvinde, A. M., and Deierlein, G. G. (2011). "Recent Research on Column Base Connections." *Modern Steel Construction*, 51(4), 42-44.

[10] Thambiratnam, D. P., and Paramasivam, P. (1986). "Base plates under axial loads and moments." *Journal of Structural Engineering*, 112(5), 1166-1181.

[11] AISC. (2012). *Steel Construction Manual,* 14th Edition, American Institute of Steel Construction, Chicago, IL.

[12] Pertold, J., Xiao, R. Y., and Wald, F. (2000). "Embedded steel column bases: II. Design model proposal." *Journal of Constructional Steel Research*, 56(3), 271-286.

[13] Brady, M. D., and Schwinger, C. (2014). "Tips to take your team to the top." *Modern Steel Construction,* 54(2), 17-23.

[14] Standard, A.S.T.M. (2013). "Annual Book of ASTM Standards." *American Society for Testing and Materials Annual,* West Conshohocken, PA, USA, 1(01.03).

APPENDIX A. DESIGN JUSTIFICATION

Prototype Column Designs

The prototype columns represent typical gravity columns that would commonly be found in steel buildings. For this experiment the two model columns will represent typical interior and exterior gravity columns. The bigger W12 and W14 columns represent interior columns for a typical steel structure that ranges from 9-17 stories tall. The smaller W12 and W14 columns represent exterior columns for a structure that ranges from 7-11 stories tall. These columns were assumed to support a tributary area of $900ft^2$ and $450ft^2$ respectively. For the design of these columns the floor dead load was assumed to be 80psf, the roof dead load was assumed to be 40psf, the floor live load was assumed to be 50psf which resulted in a reduced floor live load of 20psf for both the interior and exterior columns, the roof live load was assumed to be 25psf which resulted in a reduced roof live load of 15psf for both the interior and exterior columns, and the wall weight was assumed to be 25psf. The calculations that accompany these findings can be found in the appendix.

Justification for Column/Baseplate Geometry

The prototype column selection was based on a scale factor between the prototype shapes and the model shapes. While a general scale factor of ⅔ could be used to scale W12 shapes to W8 shapes, shapes that had similar depth to width, d/b_f, and width to flange, $b_f/2t_f$, ratios were chosen. For the two model shapes a W8×48 and a W8×35 were selected. For the W8×48 it was

determined that a W12×106 and a W14×176 had the most similar properties. For the W8×35 it was found that a W12×79 and a W14×61 had the most similar properties. The calculations for these findings can be found in the appendix.

Once the prototype columns had been selected the design of the base plates for the prototype columns could be determined. For each prototype the maximum compressive capacity for the column, ϕP_n, was used as the maximum axial load, P_u [11]. Next the required base plate area was calculated as outlined in in the guide. Using this area the dimensions of a square base plate were determined and then optimized using the procedures outlined in the base plate design guide. After the base plate had been optimized the required thickness of the baseplate was calculated following the procedures outlined in the design guide [2]. This procedure was repeated for each prototype column. These calculations can be found in the appendix.

After the finalized dimensions of the baseplates were determined, they were scaled down to find the potential dimensions of the model baseplates. A scale factor of the depth of the model to the depth of the prototype was used to scale down the dimensions as well as the size of the welds that would be used to connect the column to the base plate. The guide states that for most columns subjected to axial compression a $\frac{5}{16}$" weld is sufficient [2]. The same scale factor was used to reduce the size of the weld, since W8 shapes are not typical for gravity columns and would not need as much weld as is specified in the guide.

Next baseplates were design for the model columns as if they were to actually be used in practice. To determine the sizes of the baseplates for the models, the same procedures that are outlined in the explanation of the design of the prototype baseplates were used. Later on these various designs were compared to find the most suitable design for the specimen columns.

Before the baseplate dimensions could be finalized it had to be verified that the baseplate had the necessary clearance distances for the anchor rod holes. In the base plate and anchor rod design guide it states that whenever possible, a ¾" anchor rod should be used [2]. This suggestion was followed in the design process because the model columns will be much smaller than typical columns and therefore the ¾" rods will have sufficient capacity. The guide specifies that an oversized hole with a diameter of 1 $^{5}/_{16}$" be used with a ¾" anchor rod [2]. It also states that the clear dimension from the edge of the hole to the edge of the plate be no less than ½" [2]. To find the required clear dimension between the hole and the weld on the column table 7-15 from the Steel Construction Manual was referenced. For a ¾" bolt the manual requires that there be ¾" spacing between the center of the bolt to the edge of the fillet weld [11]. Now since oversized holes are being used in the design a 2" diameter washer must be used, so the clear spacing must also allow room for this washer [2]. Thus the clear spacing from the center of the bolt to the edge of the fillet weld was limited to no less than 1".

After determining the necessary clear spacings, the base plate design could be finalized. The first design that met all of the requirements was a PL 1" × 14" × 0' 10". Although this baseplate would work a square base plate would make the construction process much easier [13]. To find a square design that would work a plate with square dimensions was designed that would provide the required clearances. The dimensions came out to be 13" × 13". Next the plate thickness was determined based on the new plate dimensions. To obtain this thickness the steps outlined in the guide were followed based on the new dimensions, although in this case the only unknown was the required thickness. For both columns the required thicknesses came out to be slightly over 1" but since using the maximum compressive strength for the axial load of the column was a very conservative assumption, it was decided that a 1" thick plate would be

sufficient and would simplify the fabrication process. These calculations can be found in Appendix B. Design Calculations.

Justification for Concrete Design

The bottom layer of reinforcement was designed for temperature and shrinkage and then checked to see if it had the capacity to be lifted. Since the same reinforcement would be used for both designs, the larger slab was used for these calculations to assure that the design would be suitable for both cases. It is also important to note a concrete compressive strength of 750psi was used for all the calculations. This represents the 3-day strength of a 3000psi concrete because the slabs needed to be moved three days after being poured. For footings the required temperature and shrinkage was determined by the following equation, As = 0.0018bh. Since this is a slab b was based on the desired spacing of the bars for the slab. This was an iterative process because the spacing was unknown at the beginning of the process. So to start out the process a spacing of 14" was assumed. This resulted in requiring an area of .31in^2 per 14". Using this spacing different layouts were determined knowing that the outside bars would have to be placed to guide the PVC and the inside bars to guide the anchor rods. After this process the maximum spacing in the footing came out to be 14 ⅜". This spacing was then checked to see if #5 bars were still sufficient for temperature and shrinkage. Next the moment capacity of a 14 ⅜" wide by 12" tall slab was determined and compared with the maximum moment demand on the slab. To be conservative the weight of a 7' × 7' × 2' 4" slab was used as the total weight. Since the bottom layer of reinforcement will be the same for both embeds this moment demand represents the maximum moment demand that will be placed on either slab.

Next the block-out dimensions were determined for the placement of the column. The only limiting factor for this part of the design was that there be enough space for workability.

Since the corners of the baseplate would be closest to the edge of the block-out, there first needed to be ample space for the baseplate to fit in the block-out. With block-out dimensions of 24" × 24" there is a clear dimension of about 3" between the corner of the baseplate and the block-out. Next a life-size print out of the block-out was made to determine if there was enough room for tools and workability. These dimensions provided sufficient space for constructability.

Next the upper layer of reinforcement was designed. Once again this rebar was designed for temperature and shrinkage but it did not need to be checked for capacity because the bottom reinforcement will provide sufficient capacity to lift the specimen. It was assumed that the slab would be 8" thick even though the top layer of concrete is 12" thick. This more closely represents the concrete slab-on-grade and the other 4" represents the soil above the footing. So for one layer of 8" slab-on-grade concrete, five #4 bars were used in both directions. The outside bars were placed to guide the PVC as was done in the bottom layer of reinforcement. The next bars were placed as close to the block-out as possible to provide reinforcing strength to the block-out. The inside bars, totaling four in all for each layer were interrupted by the block-out and were placed with a clear cover of 1 ½" from the block-out. The edges of these bars also acted as guides for the reinforcement placed between the center bars and the outside bars. For the deeper slab a second layer identical to the layer designed in this step was placed a foot lower because it was design for 12" of concrete. These calculations can be found in the appendix.

Lastly the bars needed to pick up the slab were designed. Since #4 bars were already being used, they were checked to see if they had the capacity to lift the slab. Four #4 bars with a 180-degree loop were used to pick up the slab. The loops at the top had to have a diameter of 4" to accommodate for the lifting strap. One of the legs of each bar would go all the way to the bottom layer of reinforcement. This leg will act as a guide for the outside bars of each mat of

reinforcement. The other leg of the bar will have an embedment depth of 12". This is the minimum required embedment depth because the required depth is less. Therefore the bars used to pick up the slab will be more than sufficient to ensure that it can be moved safely.

APPENDIX B. DESIGN CALCULATIONS

This appendix will detail the calculations used throughout the research explained in this document.

Column Proportion Calculations

The following spreadsheet shows the design steps followed scale the model columns up to prototype columns with similar scaled properties.

W8×48

$b_{f48} := 8.11 \quad t_{f48} := .685 \quad d_{48} := 8.5$

1. Determine depth to width and width to flange thickness ratios

$$\frac{b_{f48}}{2t_{f48}} = 5.92$$

$$\frac{d_{48}}{b_{f48}} = 1.048$$

2. Select possible prototype shapes and find the same ratios.

W12×120

$b_{f120} := 12.3 \quad t_{f120} := 1.11 \quad d_{120} := 13.1$

$$\frac{b_{f120}}{2t_{f120}} = 5.541$$

$$\frac{d_{120}}{b_{f120}} = 1.065$$

W12×106

$b_{f106} := 12.2 \quad t_{f106} := .990 \quad d_{106} := 12.9$

$$\frac{b_{f106}}{2t_{f106}} = 6.162$$

$$\frac{d_{106}}{b_{f106}} = 1.057$$

W14×193

$b_{f193} := 15.7 \quad t_{f193} := 1.44 \quad d_{193} := 15.5$

$$\frac{b_{f193}}{2t_{f193}} = 5.451$$

$$\frac{d_{193}}{b_{f193}} = 0.987$$

W14×176

$b_{f176} := 15.7 \quad t_{f176} := 1.31 \quad d_{176} := 15.2$

$$\frac{b_{fl76}}{2t_{fl76}} = 5.992$$

$$\frac{d_{176}}{b_{fl76}} = 0.968$$

3. Select prototype shapes that work best

*Use W12×106 and W14×176 as prototype column shapes

W8×35

$b_{f35} := 8.02 \quad t_{f35} := .495 \quad d_{35} := 8.12$

1. Determine depth to width and width to flange thickness ratios

$$\frac{b_{f35}}{2t_{f35}} = 8.101$$

$$\frac{d_{35}}{b_{f35}} = 1.012$$

2. Select possible prototype shapes and find the same ratios.

W12×79

$b_{f79} := 12.1 \quad t_{f79} := .735 \quad d_{79} := 12.4$

$$\frac{b_{f79}}{2t_{f79}} = 8.231$$

$$\frac{d_{79}}{b_{f79}} = 1.025$$

W12×87

$b_{f87} := 12.1 \quad t_{f87} := .810 \quad d_{87} := 12.5$

$$\frac{b_{f87}}{2t_{f87}} = 7.469$$

$$\frac{d_{87}}{b_{f87}} = 1.033$$

W14×53

$b_{f53} := 8.06 \quad t_{f53} := .660 \quad d_{53} := 13.9$

$$\frac{b_{f53}}{2t_{f53}} = 6.106$$

$$\frac{d_{53}}{b_{f53}} = 1.725$$

W14×61

$b_{f61} := 10 \qquad t_{f61} := .645 \qquad d_{61} := 13.9$

$$\frac{b_{f61}}{2t_{f61}} = 7.752$$

$$\frac{d_{61}}{b_{f61}} = 1.39$$

3. Select prototype shapes that work best

*Use W12×79 and W14×61 as prototype column shapes

Base Plate Size Calculations

The following spreadsheet shows the design steps follow to find the baseplate design for the model columns used in the testing

Base Plate Calculations - Prototype

W12×106 - f'_c = 3000 psi

Given:

$f_{c3} := 3000\text{psi}$ $d_{106} := 12.9\text{in}$ $b_{fl06} := 12.2\text{in}$ $\phi P_n := 1100\text{kip}$

1. Determine the required axial compressive strength.

$P_u := \phi P_n = 1100\text{kip}$

2. Determine the required base plate area.

$$A_{1req} := \frac{P_u}{2 \cdot .65 \cdot .85 f_{c3}} = 331.825\text{in}^2$$

3. Optimize the base plate dimensions, N and B.

$$\Delta := \frac{.95 d_{106} - .8 \cdot b_{fl06}}{2} = 1.247\text{in}$$

$$N_1 := \sqrt{A_{1req}} + \Delta = 19.464\text{in}$$

$N_2 := 20\text{in}$

$$B_1 := \frac{A_{1req}}{N_2} = 16.591\text{in}$$

$B_2 := 17\text{in}$

4. Calculate the required base plate thickness.

$$m_1 := \frac{N_2 - .95 d_{106}}{2} = 3.873\text{in}$$

$$n_1 := \frac{B_2 - .8 \cdot b_{fl06}}{2} = 3.62\text{in}$$

$\phi P_p := .65 \cdot f_{c3} \cdot 2 \cdot B_2 \cdot N_2 = 1326\text{kip}$

$$X := \frac{4 \cdot d_{106} \cdot b_{fl06}}{(d_{106} + b_{fl06})^2} \cdot \frac{P_u}{\phi P_p} = 0.829$$

$$\lambda_1 := \frac{2\sqrt{X}}{1 + \sqrt{1 - X}} = 1.288$$

$\lambda := 1$

$$\lambda n := \lambda \cdot \frac{\sqrt{d_{106} \cdot b_{fl106}}}{4} = 3.136\,in$$

$$l_1 := \max(\lambda n, m_1, n_1) = 3.873\,in$$

$$t_{min} := l_1 \cdot \sqrt{\frac{2 \cdot P_u}{.9 \cdot 36\,ksi \cdot B_2 \cdot N_2}} = 1.731\,in$$

$$t := 1.75\,in$$

5. Scale down the base plate dimensions.

$$N_s := N_1 \cdot \frac{8.5}{12.9} = 12.825\,in$$

$$N_s := 13\,in$$

$$B_s := B_1 \cdot \frac{8.5}{12.9} = 10.932\,in$$

$$B_s := 11\,in$$

$$t_s := t_{min} \cdot \frac{8.5}{12.9} = 1.14\,in$$

$$t_s := 1.5\,in$$

6. Scale down the weld size.

$$w := \frac{5}{16} \cdot \frac{8.5}{12.9} = 0.206$$

$$w_s := \frac{1}{4}\,in$$

W14×176 - f'_c = 3000 psi

Given:

$$f_{c3} := 3000\,psi \qquad d_{176} := 15.2\,in \qquad b_{fl176} := 15.7\,in \qquad \phi P_n := 2010\,kip$$

1. Determine the required axial compressive strength.

$$P_u := \phi P_n = 2.01 \times 10^3 \cdot kip$$

2. Determine the required base plate area.

$$A_{1req} := \frac{P_u}{2 \cdot .65 \cdot .85 f_{c3}} = 606.335\,in^2$$

3. Optimize the base plate dimensions, N and B.

$$\Delta := \frac{.95 d_{176} - .8 \cdot b_{fl176}}{2} = 0.94\,in$$

$$N_1 := \sqrt{A_{1req}} + \Delta = 25.564\,in$$

$$N_2 := 26in$$

$$B_1 := \frac{A_{1req}}{N_2} = 23.321in$$

$$B_2 := 23.5in$$

4. Calculate the required base plate thickness.

$$m_1 := \frac{N_2 - .95 \cdot d_{176}}{2} = 5.78 \cdot in$$

$$n_1 := \frac{B_2 - .8 \cdot b_{fl176}}{2} = 5.47 \cdot in$$

$$\phi P_p := .65 \cdot f_{c3} \cdot 2 \cdot B_2 \cdot N_2 = 2382.9 \cdot kip$$

$$X := \frac{4 \cdot d_{176} \cdot b_{fl176}}{\left(d_{176} + b_{fl176}\right)^2} \cdot \frac{P_u}{\phi P_p} = 0.843$$

$$\lambda_1 := \frac{2\sqrt{X}}{1 + \sqrt{1 - X}} = 1.316$$

$$\lambda := 1$$

$$\lambda n := \lambda \cdot \frac{\sqrt{d_{176} \cdot b_{fl176}}}{4} = 3.862in$$

$$l_1 := max\left(\lambda n, m_1, n_1\right) = 5.78 \cdot in$$

$$t_{min} := l_1 \cdot \sqrt{\frac{2 \cdot P_u}{.9 \cdot 36ksi \cdot B_2 \cdot N_2}} = 2.605in$$

$$t := 2.75in$$

5. Scale down the base plate dimensions.

$$N_s := N_1 \cdot \frac{8.5}{15.2} = 14.296in$$

$$N_s := 14.5in$$

$$B_s := B_1 \cdot \frac{8.5}{15.2} = 13.041in$$

$$B_s := 13in$$

$$t_s := t_{min} \cdot \frac{8.5}{15.2} = 1.457in$$

$$t_s := 1.5in$$

6. Scale down the weld size.

$$w := \frac{5}{16} \cdot \frac{8.5}{15.2} = 0.175$$

$$w_s := \frac{3}{16}in$$

W12×79 - $f'_c = 3000$ psi

Given:

$$f_{c3} := 3000psi \qquad d_{79} := 12.4in \qquad b_{f79} := 12.1in \qquad \phi P_n := 809kip$$

1. Determine the required axial compressive strength.

$$P_u := \phi P_n = 809 \cdot kip$$

2. Determine the required base plate area.

$$A_{1req} := \frac{P_u}{2 \cdot .65 \cdot .85 f_{c3}} = 244.042in^2$$

3. Optimize the base plate dimensions, N and B.

$$\Delta := \frac{.95 d_{79} - .8 \cdot b_{f79}}{2} = 1.05 \cdot in$$

$$N_1 := \sqrt{A_{1req}} + \Delta = 16.672in$$

$$N_2 := 17in$$

$$B_1 := \frac{A_{1req}}{N_2} = 14.355in$$

$$B_2 := 14.5in$$

4. Calculate the required base plate thickness.

$$m_1 := \frac{N_2 - .95 d_{79}}{2} = 2.61 \cdot in$$

$$n_1 := \frac{B_2 - .8 \cdot b_{f79}}{2} = 2.41 \cdot in$$

$$\phi P_p := .65 \cdot f_{c3} \cdot 2 \cdot B_2 \cdot N_2 = 961.35kip$$

$$X := \frac{4 \cdot d_{79} \cdot b_{f79}}{\left(d_{79} + b_{f79}\right)^2} \cdot \frac{P_u}{\phi P_p} = 0.841$$

$$\lambda_1 := \frac{2\sqrt{X}}{1 + \sqrt{1 - X}} = 1.312$$

$$\lambda := 1$$

$$\lambda n := \lambda \cdot \frac{\sqrt{d_{79} \cdot b_{f79}}}{4} = 3.062in$$

$$l_1 := \max\left(\lambda n, m_1, n_1\right) = 3.062 \cdot in$$

$$t_{min} := l_1 \cdot \sqrt{\frac{2 \cdot P_u}{.9 \cdot 36 ksi \cdot B_2 \cdot N_2}} = 1.378 in$$

$$t := 2.5 in$$

5. Scale down the base plate dimensions.

$$N_s := N_1 \cdot \frac{8.12}{12.4} = 10.917 in$$

$$N_s := 11 in$$

$$B_s := B_1 \cdot \frac{8.12}{12.4} = 9.4 in$$

$$B_1 := 9.5 in$$

$$t_s := t_{min} \cdot \frac{8.12}{12.4} = 0.903 in$$

$$t_s := 1 in$$

6. Scale down the weld size.

$$w := \frac{5}{16} \cdot \frac{8.12}{12.4} = 0.205$$

$$w_s := \frac{1}{4} in$$

W14×61 - $f'_c = 3000$ psi

Given:

$$f_{c3} := 3000 psi \qquad d_{61} := 13.9 in \qquad b_{f61} := 10 in \qquad \phi P_n := 543 kip$$

1. Determine the required axial compressive strength.

$$P_u := \phi P_n = 543 \cdot kip$$

2. Determine the required base plate area.

$$A_{1req} := \frac{P_u}{2 \cdot .65 \cdot .85 f_{c3}} = 163.801 in^2$$

3. Optimize the base plate dimensions, N and B.

$$\Delta := \frac{.95 d_{61} - .8 \cdot b_{f61}}{2} = 2.602 in$$

$$N_1 := \sqrt{A_{1req}} + \Delta = 15.401 in$$

$$N_2 := 15.5 in$$

$$B_1 := \frac{A_{1req}}{N_2} = 10.568 in$$

$$B_2 := 11 in$$

4. Calculate the required base plate thickness.

$$m_1 := \frac{N_2 - .95 d_{61}}{2} = 1.148\,in$$

$$n_1 := \frac{B_2 - .8 b_{fb1}}{2} = 1.5\,in$$

$$\phi P_p := .65 \cdot f_{c3} \cdot 2 \cdot B_2 \cdot N_2 = 664.95\,kip$$

$$X := \frac{4 \cdot d_{61} \cdot b_{fb1}}{(d_{61} + b_{fb1})^2} \cdot \frac{P_u}{\phi P_p} = 0.795$$

$$\lambda_1 := \frac{2\sqrt{X}}{1 + \sqrt{1 - X}} = 1.227$$

$$\lambda := 1$$

$$\lambda n := \lambda \cdot \frac{\sqrt{d_{61} \cdot b_{fb1}}}{4} = 2.947\,in$$

$$l_1 := \max(\lambda n, m_1, n_1) = 2.947\,in$$

$$t_{min} := l_1 \cdot \sqrt{\frac{2 \cdot P_u}{.9 \cdot 36\,ksi \cdot B_2 \cdot N_2}} = 1.307\,in$$

$$t := 1.5\,in$$

5. Scale down the base plate dimensions.

$$N_s := N_1 \cdot \frac{8.12}{13.9} = 8.997\,in$$

$$N_s := 9$$

$$B_s := B_1 \cdot \frac{8.12}{13.9} = 6.173\,in$$

$$B_s := 6.5\,in$$

$$t_s := t_{min} \cdot \frac{8.12}{13.9} = 0.763\,in$$

$$t_s := 1\,in$$

6. Scale down the weld size.

$$w := \frac{5}{16} \cdot \frac{8.12}{13.9} = 0.183$$

$$w_s := \frac{3}{16}\,in$$

Base Plate Calculations - Model Columns

W8×48 - f'_c = 3000 psi

Given:

$f_{c3} := 3000\,psi \qquad d_{48} := 8.5\,in \qquad b_{f48} := 8.1\,in \qquad \phi P_n := 367\,kip$

1. Determine the required axial compressive strength.

$P_u := \phi P_n = 367\,kip$

2. Determine the required base plate area.

$$A_{1req} := \frac{P_u}{2 \cdot .65 \cdot .85 f_{c3}} = 110.709\,in^2$$

3. Optimize the base plate dimensions, N and B.

$$\Delta := \frac{.95 d_{48} - .8 \cdot b_{f48}}{2} = 0.793\,in$$

$$N_1 := \sqrt{A_{1req}} + \Delta = 11.315\,in$$

$N_2 := 11.5\,in$

$$B_1 := \frac{A_{1req}}{N_2} = 9.627\,in$$

$B_2 := 10\,in$

4. Calculate the required base plate thickness.

$$m_1 := \frac{N_2 - .95 d_{48}}{2} = 1.712\,in$$

$$n_1 := \frac{B_2 - .8 \cdot b_{f48}}{2} = 1.756\,in$$

$\phi P_p := .65 \cdot f_{c3} \cdot 2 \cdot B_2 \cdot N_2 = 448.5\,kip$

$$X := \frac{4 \cdot d_{48} \cdot b_{f48}}{\left(d_{48} + b_{f48}\right)^2} \cdot \frac{P_u}{\phi P_p} = 0.818$$

$$\lambda_1 := \frac{2\sqrt{X}}{1 + \sqrt{1 - X}} = 1.268$$

$\lambda := 1$

$$\lambda n := \lambda \cdot \frac{\sqrt{d_{48} \cdot b_{f48}}}{4} = 2.076\,in$$

$l_1 := \max\left(\lambda n, m_1, n_1\right) = 2.076\,in$

$$t_{min} := l_1 \cdot \sqrt{\frac{2 \cdot P_u}{.9 \cdot 36 ksi \cdot B_2 \cdot N_2}} = 0.921 in$$

$$t := 1in$$

W8×35 - $f'_c = 3000$ psi

Given:

$$f_{c3} := 3000psi \qquad d_{35} := 8.12in \qquad b_{f35} := 8.02in \qquad \phi P_n := 261kip$$

1. Determine the required axial compressive strength.

$$P_u := \phi P_n = 261 \cdot kip$$

2. Determine the required base plate area.

$$A_{1req} := \frac{P_u}{2 \cdot .65 \cdot .85 f_{c3}} = 78.733 in^2$$

3. Optimize the base plate dimensions, N and B.

$$\Delta := \frac{.95 d_{35} - .8 \cdot b_{f35}}{2} = 0.649 in$$

$$N_1 := \sqrt{A_{1req}} + \Delta = 9.522 in$$

$$N_2 := 10in$$

$$B_1 := \frac{A_{1req}}{N_2} = 7.873 in$$

$$B_2 := 8in$$

4. Calculate the required base plate thickness.

$$m_1 := \frac{N_2 - .95 d_{35}}{2} = 1.143 in$$

$$n_1 := \frac{B_2 - .8 \cdot b_{f35}}{2} = 0.792 in$$

$$\phi P_p := .65 \cdot f_{c3} \cdot 2 \cdot B_2 \cdot N_2 = 312 \cdot kip$$

$$X := \frac{4 \cdot d_{35} \cdot b_{f35}}{(d_{35} + b_{f35})^2} \cdot \frac{P_u}{\phi P_p} = 0.837$$

$$\lambda_1 := \frac{2\sqrt{X}}{1 + \sqrt{1 - X}} = 1.303$$

$$\lambda := 1$$

$$\lambda n := \lambda \cdot \frac{\sqrt{d_{35} \cdot b_{f35}}}{4} = 2.017\,in$$

$$l_1 := \max\left(\lambda n, m_1, n_1\right) = 2.017\,in$$

$$t_{min} := l_1 \cdot \sqrt{\frac{2 \cdot P_u}{.9 \cdot 36\,ksi \cdot B_2 \cdot N_2}} = 0.905\,in$$

$$t := 1\,in$$

**After doing the initial design, we decided to modify the baseplate to be square, as baseplates for gravity columns are typically square for ease of construction.*

Base Plate Checks - Final Model Columns

W8×48 - f'_c = 3000 psi

Given:

$$f_{c4} := 3000\,psi \qquad d_{48} := 8.5\,in \qquad b_{f48} := 8.11\,in \qquad \phi P_n := 367\,kip$$

1. Determine the required axial compressive strength.

$$P_u := \phi P_n = 367\,kip$$

2. Determine the required base plate area.

$$A_{1req} := \frac{P_u}{2 \cdot .65 \cdot .85 f_{c4}} = 110.709\,in^2$$

$$N_2 := 13\,in$$

$$B_2 := 13\,in$$

$$A_{1prov} := N_2 \cdot B_2 = 169\,in^2$$

3. Calculate the required base plate thickness.

$$m_1 := \frac{N_2 - .95 d_{48}}{2} = 2.463\,in$$

$$n_1 := \frac{B_2 - .8 \cdot b_{f48}}{2} = 3.256\,in$$

$$\phi P_p := .65 \cdot f_{c4} \cdot 2 \cdot B_2 \cdot N_2 = 659.1\,kip$$

$$X := \frac{4 \cdot d_{48} \cdot b_{f48}}{\left(d_{48} + b_{f48}\right)^2} \cdot \frac{P_u}{\phi P_p} = 0.557$$

$$\lambda_1 := \frac{2\sqrt{X}}{1 + \sqrt{1 - X}} = 0.896$$

$$\lambda n := \lambda \cdot \frac{\sqrt{d_{48} \cdot b_{f48}}}{4} = 2.076\,in$$

$$l_1 := \max\left(m_1, n_1, \lambda n\right) = 3.256\,in$$

$$t_{min} := l_1 \cdot \sqrt{\frac{2 \cdot P_u}{.9 \cdot 36\,ksi \cdot B_2 \cdot N_2}} = 1.192\,in$$

$$t := 1.25\,in$$

W8×35 - $f'_c = 3000$ psi

Given:

$$f_{c4} := 3000\,psi \qquad d_{35} := 8.12\,in \qquad b_{f35} := 8.02\,in \qquad \phi P_n := 261\,kip$$

1. Determine the required axial compressive strength.

$$P_u := \phi P_n = 261 \cdot kip$$

2. Determine the required base plate area.

$$A_{1req} := \frac{P_u}{2 \cdot .65 \cdot .85 f_{c4}} = 78.733\,in^2$$

$$N_2 := 13\,in$$

$$B_2 := 13\,in$$

$$A_{1prov} := N_2 \cdot B_2 = 169 \cdot in^2$$

3. Calculate the required base plate thickness.

$$m_1 := \frac{N_2 - .95 d_{35}}{2} = 2.643\,in$$

$$n_1 := \frac{B_2 - .8 \cdot b_{f35}}{2} = 3.292\,in$$

$$\phi P_p := .65 \cdot f_{c4} \cdot 2 \cdot B_2 \cdot N_2 = 659.1 \cdot kip$$

$$X := \frac{4 \cdot d_{35} \cdot b_{f35}}{\left(d_{35} + b_{f35}\right)^2} \cdot \frac{P_u}{\phi P_p} = 0.396$$

$$\lambda_1 := \frac{2\sqrt{X}}{1 + \sqrt{1 - X}} = 0.708$$

$$\lambda := 1$$

$$\lambda n := \lambda \cdot \frac{\sqrt{d_{35} \cdot b_{f35}}}{4} = 2.017\,in$$

$$l_1 := \max\left(m_1, n_1, \lambda n\right) = 3.292\,in$$

$$t_{min} := l_1 \cdot \sqrt{\frac{2 \cdot P_u}{.9 \cdot 36\,ksi \cdot B_2 \cdot N_2}} = 1.016\,in$$

$$t := 1.25\,in$$

**After deciding on the final dimensions of 13" × 13", we decided to use a thickness of 1", which is closer to the scaled down dimensions, but still close enough to the actual design.*

4. Final Dimensions

13"×13"×1"

Concrete Calculations

The following spreadsheet shows the design steps followed in the design of the footing and slab.

*The compressive strength of the concrete was taken as 25% of the normal compressive strength due to a 3-day curing period before the concrete needs to be used.

Bottom Reinforcement

1. Determine Temperature and Shrinkage Reinforcement Requirements

$$A_{sb} := .0018\left(14 + \frac{3}{8}\right)in \cdot 12in = 0.31 \cdot in^2$$

*Use #5 bars

$$A_{sb} := .31in^2$$

2. Determine the moment capacity of bottom slab

*The bottom slab is assumed to be simply supported at the pickup points

$$w := 1.4 \cdot 150pcf \cdot \left(14 + \frac{3}{8}\right)in \cdot 2.5ft = 0.6289\frac{kip}{ft}$$

$$M_u := \frac{w \cdot (7ft)^2}{8} = 3.8521kip \cdot ft$$

Given

$$3.852112 = .9 \cdot A_{sb} \cdot 60 \cdot \left(9.063 - \frac{A_{sb} \cdot 60}{1.7 \cdot \frac{3}{4} \cdot 14.5}\right)$$

$$\text{Find}\left(A_{sb}\right) \rightarrow (2.6946534737417418064 \quad 0.09788340125825819361)16$$

$$.0979in^2 < .31in^2 \qquad \text{[Good]}$$

$$a := \frac{A_{sb} \cdot 60ksi}{.85\frac{3}{4}ksi \cdot 14.5in} = 2.0122in$$

$$c := \frac{a}{.8} = 2.5152in$$

$$\varepsilon := \frac{9.063in - c}{c} \cdot .003 = 0.0078$$

$$\varepsilon > .005 \qquad \text{[Good]}$$

3. Check if Shear Reinforcement is Required

$$V_u := \frac{w \cdot 7ft}{2} = 2.2012kip$$

$$\phi V_c := \frac{2\cdot\sqrt{750}\cdot 14.5\cdot 9.063.75}{1000}\cdot kip = 5.3984kip$$

$$\frac{1}{2}\cdot\phi V_c = 2.6992kip$$

$V_u < \frac{1}{2}\cdot\phi V_c$ [Good - No shear reinforcing required]

4. Check if provided reinforcement is sufficient for the negative moment

*After one iteration it was determined that this element is compression controlled so $\phi = .65$

$$M_{un} := \frac{w\cdot[(2)ft]^2}{2} = 1.2578kip\cdot ft$$

Given

$$1.257812 = .65A_{sb}\cdot 60\cdot\left[2.3125 - \frac{A_{sb}\cdot 60}{1.7\cdot\frac{3}{4}\cdot(14.5)}\right]$$

$$Find(A_{sb}) \rightarrow (0.26864040645419171762\ 0.44389865604580828238$$

$.269in^2 < .3lin^2$ [Good]

$$a := \frac{A_{sb}\cdot 60ksi}{.851ksi\cdot 14.5in} = 1.5091in$$

$$c := \frac{a}{.8} = 1.8864in$$

$$\varepsilon := \frac{2.25in - c}{c}\cdot .003 = 0.0006$$

$\varepsilon < .0021$ [Beam is compression controlled - this was accounted for with a lower ϕ factor]

Top Reinforcement

1. Determine Temperature and Shrinkage Reinforcement Requirements

$$A_{st} := .00188in\cdot 12in = 0.1728in^2$$

*Use #4 bars

Pickup Bars

1. Determine the capacity of #5 bars

$$P_b := 60ksi\cdot .3lin^2 = 18.6kip$$

$$P_u := 1.4\cdot 150pcf\cdot 2.5ft\cdot 7ft\cdot 7ft = 25.725kip$$

$$A_{sreq} := \frac{P_u}{8\cdot 60ksi} = 0.0536in^2$$

$A_{sprov} := .3\,in^2$

#5 bars sufficient

2. Determine the required development length

$$l_d := \frac{60000 \cdot 1.1}{25 \cdot \sqrt{1000}} \cdot \frac{A_{sreq}}{A_{sprov}} \frac{A_{sprov}}{in} = 4.0675in$$

*must use minimum development length or hook

$l_{dmin} := 12in$

*must use hook since 12" is not available

3. Determine the dimensions of the hook

$r := \frac{5}{8}in \cdot 3 = 1.875in$

$l_{dhook} := 12 \cdot \frac{5}{8}in = 7.5in$

$$l_{dh} := \frac{.02 \cdot 60000 \frac{5}{8}}{\sqrt{1000}} \cdot \left(\frac{A_{sreq}}{A_{sprov}} \frac{A_{sprov}}{in} \right) = 1.2711in$$

$l_{dprov} > l_{dh}$ [Good]

Expected Strength Calculations

The following spreadsheet shows the steps followed to determine the expected strength for all of the specimens.

Given

$B := 13in \quad N := B = 13in \quad f_{pmax} := .65 \cdot 3000psi \cdot .85 = 1.657ksi$

$T_{ue} := 30.42684kip + 30.44773kip = 60.875kip \quad T_{ye} := 17158.53lbf + 16956.37lbf = 34.115kip$

$L_s := 7ft + 8in - \left(4in + \frac{4.5in}{2}\right) = 7.146ft \quad H_s := 7ft + 8in = 7.667ft \quad W_{48} := 48\frac{lbf}{ft} \quad W_{35} := 35\frac{lbf}{ft}$

$L_d := 8ft + 7in - \left(4in + \frac{4.5in}{2}\right) = 8.063ft \quad H_d := 8ft + 7in = 8.583ft$

$d_{35} := 8.12in \quad b_{f35} := 8.02in \quad d_{48} := 8.5in \quad b_{f48} := 8.11in \quad t_{f48} := .685in \quad t_{f35} := .495in$

$q_{max} := f_{pmax} \cdot B = 21.547\frac{kip}{in} \quad f := \frac{N}{2} - 1.25in = 5.25in \quad m_{48} := \frac{N - .95d_{48}}{2} = 2.463in$

$n_{48} := \frac{B - .8 \cdot b_{f48}}{2} = 3.256in \quad x_{48} := f - \frac{d_{48}}{2} - \frac{t_{f48}}{2} = 0.055ft \quad x_{35} := f - \frac{d_{35}}{2} - \frac{t_{f35}}{2} = 0.079ft$

$m_{35} := \frac{N - .95d_{35}}{2} = 2.643in \quad n_{35} := \frac{B - .8 \cdot b_{f35}}{2} = 3.292in$

W8×48 Shallow - Fy

1. Determine e and compare it to e_{crit}

$P := 4.3869kip$

$M_r := L_s \cdot P = 31.348kip \cdot ft$

$P_r := H_s \cdot W_{48} + (13in)^2 \cdot (8in - .75in) \cdot 150pcf = 0.474kip$

$f_p := \frac{P_r}{B \cdot N} = 2.807psi$

$e := \frac{M_r}{P_r} = 793.022in$

$e_{crit} := \frac{N}{2} - \frac{P_r}{2 \cdot q_{max}} = 6.489in$

2. Determine the bearing length

$Y := \left(f + \frac{N}{2}\right) + \sqrt{\left(f + \frac{N}{2}\right)^2 - \frac{2 \cdot P_r \cdot (e + f)}{q_{max}}} = 21.895in$

$$Y := \left(f + \frac{N}{2}\right) - \sqrt{\left(f + \frac{N}{2}\right)^2 - \frac{2 \cdot P_r \cdot (e + f)}{q_{max}}} = 1.605\,in$$

3. Determine the Force in the bolts and compare it to the known force

$$T_y := q_{max} \cdot Y - P_r = 34.115\,kip$$

$$T_{ye} = 34.115\,kip$$

4. Determine Base Plate Yielding at Bearing Interface

$$t_{p11} := 1.5 m_{48} \cdot \sqrt{\frac{f_{pmax}}{36\,ksi}} = 0.793\,in$$

$$t_{p12} := 2.11 \cdot \sqrt{\frac{f_{pmax} \cdot Y \cdot \left(m_{48} - \frac{Y}{2}\right)}{36\,ksi}} = 0.739\,in \quad < 1\,in \quad \text{<=== OK since Y < m}$$

$$t_{p21} := 1.5 n_{48} \cdot \sqrt{\frac{f_{pmax}}{36\,ksi}} = 1.048\,in$$

$$t_{p22} := 2.11 \cdot \sqrt{\frac{f_{pmax} \cdot Y \cdot \left(n_{48} - \frac{Y}{2}\right)}{36\,ksi}} = 0.898\,in \quad < 1\,in \quad \text{<=== OK since Y < n}$$

5. Determine Base Plate Yielding at Tension Interface

$$T_u := q_{max} \cdot Y - P_r = 34.115\,kip$$

$$t_p := 2.11 \cdot \sqrt{\frac{T_u \cdot x_{48}}{B \cdot 36\,ksi}} = 0.462\,in \quad < 1\,in \quad \text{<=== OK}$$

$$P_{sy1} := P = 4.387\,kip$$

W8×48 Shallow - Fu

1. Determine e and compare it to e_{crit}

$$P := 7.3589\,kip$$

$$M_r := L_s \cdot P = 52.585\,kip \cdot ft$$

$$P_r := H_s \cdot W_{48} + (13in)^2 \cdot (8in - .75in) \cdot 150pcf = 0.474\,kip$$

$$f_p := \frac{P_r}{B \cdot N} = 2.807\,psi$$

$$e := \frac{M_r}{P_r} = 110.856\,\text{in}$$

$$e_{crit} := \frac{N}{2} - \frac{P_r}{2 \cdot q_{max}} = 0.541\,\text{in}$$

2. Determine the bearing length

$$Y := \left(f + \frac{N}{2}\right) + \sqrt{\left(f + \frac{N}{2}\right)^2 - \frac{2 \cdot P_r \cdot (e + f)}{q_{max}}} = 20.653\,\text{in}$$

$$Y := \left(f + \frac{N}{2}\right) - \sqrt{\left(f + \frac{N}{2}\right)^2 - \frac{2 \cdot P_r \cdot (e + f)}{q_{max}}} = 2.847\,\text{in}$$

3. Determine the Force in the bolts and compare it to the known force

$$T_u := q_{max} \cdot Y - P_r = 60.875\,\text{kip}$$

$$T_{ue} = 60.875\,\text{kip}$$

4. Determine Base Plate Yielding at Bearing Interface

$$t_{p11} := 1.5 m_{48} \cdot \sqrt{\frac{f_{pmax}}{36\,\text{ksi}}} = 0.793\,\text{in}$$

$$t_{p12} := 2.11 \cdot \sqrt{\frac{f_{pmax} \cdot Y \cdot \left(m_{48} - \frac{Y}{2}\right)}{36\,\text{ksi}}} = 0.779\,\text{in} \quad < 1\,\text{in} \quad \text{<=== OK since Y < m}$$

$$t_{p21} := 1.5 n_{48} \cdot \sqrt{\frac{f_{pmax}}{36\,\text{ksi}}} = 1.048\,\text{in}$$

$$t_{p22} := 2.11 \cdot \sqrt{\frac{f_{pmax} \cdot Y \cdot \left(n_{48} - \frac{Y}{2}\right)}{36\,\text{ksi}}} = 1.034\,\text{in} \quad < 1\,\text{in} \quad \text{<=== since Y < n}$$

*Although the plate will yield before the bolt reaches its ultimate strength, the bolt will break before the plate reaches its ultimate strength

5. Determine Base Plate Yielding at Tension Interface

$$T_u := q_{max} \cdot Y - P_r = 60.875\,\text{kip}$$

$$t_p := 2.11 \cdot \sqrt{\frac{T_u \cdot x_{48}}{B \cdot 36\,\text{ksi}}} = 0.617\,\text{in} \quad < 1\,\text{in} \quad \text{<=== OK}$$

$$P_{su1} := P = 7.359\,\text{kip}$$

W8×35 Shallow - Fy

1. Determine e and compare it to e_{crit}

$P := 4.381\,kip$

$M_r := L_s \cdot P = 31.307\,kip \cdot ft$

$P_r := H_s \cdot W_{35} + (13in)^2 \cdot (8in - .75in) \cdot 150pcf = 0.375\,kip$

$f_p := \frac{P_r}{B \cdot N} = 2.217\,psi$

$e := \frac{M_r}{P_r} = 83.553\,ft$

$e_{crit} := \frac{N}{2} - \frac{P_r}{2 \cdot q_{max}} = 0.541\,ft$

2. Determine the bearing length

$Y := \left(f + \frac{N}{2}\right) + \sqrt{\left(f + \frac{N}{2}\right)^2 - \frac{2 \cdot P_r \cdot (e + f)}{q_{max}}} = 21.899\,in$

$Y := \left(f + \frac{N}{2}\right) - \sqrt{\left(f + \frac{N}{2}\right)^2 - \frac{2 \cdot P_r \cdot (e + f)}{q_{max}}} = 1.601\,in$

3. Determine the Force in the bolts and compare it to the known force

$T_y := q_{max} \cdot Y - P_r = 34.115\,kip$

$T_{ye} = 34.115\,kip$

4. Determine Base Plate Yielding at Bearing Interface

$t_{p11} := 1.5 m_{35} \cdot \sqrt{\frac{f_{pmax}}{36ksi}} = 0.851\,in$

$t_{p12} := 2.11 \cdot \sqrt{\frac{f_{pmax} \cdot Y \cdot \left(m_{35} - \frac{Y}{2}\right)}{36ksi}} = 0.778\,in \quad < 1in \quad$ <=== OK since Y < m

$t_{p21} := 1.5 n_{35} \cdot \sqrt{\frac{f_{pmax}}{36ksi}} = 1.06\,in$

$t_{p22} := 2.11 \cdot \sqrt{\frac{f_{pmax} \cdot Y \cdot \left(n_{35} - \frac{Y}{2}\right)}{36ksi}} = 0.904\,in \quad < 1in \quad$ <=== OK since Y < n

5. Determine Base Plate Yielding at Tension Interface

$T_u := q_{max} \cdot Y - P_r = 34.115\,kip$

$t_p := 2.11 \cdot \sqrt{\frac{T_u \cdot x_{35}}{B \cdot 36\,ksi}} = 0.553\,in \quad < 1in \quad$ <=== OK

$P_{sy2} := P = 4.381\,kip$

W8×35 Shallow - Fu

1. Determine e and compare it to e_{crit}

$P := 7.354\,kip$

$M_r := L_s \cdot P = 52.555\,kip \cdot ft$

$P_r := H_s \cdot W_{35} + (13in)^2 \cdot (8in - .75in) \cdot 150pcf = 0.375\,kip$

$f_p := \frac{P_r}{B \cdot N} = 2.217\,psi$

$e := \frac{M_r}{P_r} = 140.263\,ft$

$e_{crit} := \frac{N}{2} - \frac{P_r}{2 \cdot q_{max}} = 0.541\,ft$

2. Determine the bearing length

$Y := \left(f + \frac{N}{2}\right) + \sqrt{\left(f + \frac{N}{2}\right)^2 - \frac{2 \cdot P_r \cdot (e + f)}{q_{max}}} = 20.657\,in$

$Y := \left(f + \frac{N}{2}\right) - \sqrt{\left(f + \frac{N}{2}\right)^2 - \frac{2 \cdot P_r \cdot (e + f)}{q_{max}}} = 2.843\,in$

3. Determine the Force in the bolts and compare it to the known force

$T_u := q_{max} \cdot Y - P_r = 60.875\,kip$

$T_{ue} = 60.875\,kip$

4. Determine Base Plate Yielding at Bearing Interface

$t_{p11} := 1.5 m_{35} \cdot \sqrt{\frac{f_{pmax}}{36ksi}} = 0.851\,in$

$t_{p12} := 2.11 \cdot \sqrt{\frac{f_{pmax} \cdot Y \cdot \left(m_{35} - \frac{Y}{2}\right)}{36ksi}} = 0.844\,in \quad < 1in \quad$ <=== OK since Y < m

$$t_{p21} := 1.5 n_{35} \sqrt{\frac{f_{pmax}}{36ksi}} = 1.06in$$

$$t_{p22} := 2.11 \sqrt{\frac{f_{pmax} \cdot Y \cdot \left(n_{35} - \frac{Y}{2}\right)}{36ksi}} = 1.044in \quad < 1in \quad <=== \text{since } Y < n$$

*Although the plate will yield before the bolt reaches its ultimate strength, the bolt will break before the plate reaches its ultimate strength

5. Determine Base Plate Yielding at Tension Interface

$$T_u := q_{max} \cdot Y - P_r = 60.875kip$$

$$t_p := 2.11 \sqrt{\frac{T_u \cdot x_{35}}{B \cdot 36ksi}} = 0.739in \quad < 1in \quad <=== OK$$

$$P_{su2} := P = 7.355kip$$

W8×48 Deep - Fy

1. Determine e and compare it to e_{crit}

$$P := 3.8962kip$$

$$M_r := L_d \cdot P = 31.413kip \cdot ft$$

$$P_r := H_d \cdot W_{48} + (13in)^2 \cdot (16in - .75in) \cdot 150pcf = 0.636kip$$

$$f_p := \frac{P_r}{B \cdot N} = 3.762psi$$

$$e := \frac{M_r}{P_r} = 592.962in$$

$$e_{crit} := \frac{N}{2} - \frac{P_r}{2 \cdot q_{max}} = 6.485in$$

2. Determine the bearing length

$$Y := \left(f + \frac{N}{2}\right) + \sqrt{\left(f + \frac{N}{2}\right)^2 - \frac{2 \cdot P_r \cdot (e + f)}{q_{max}}} = 21.887in$$

$$Y := \left(f + \frac{N}{2}\right) - \sqrt{\left(f + \frac{N}{2}\right)^2 - \frac{2 \cdot P_r \cdot (e + f)}{q_{max}}} = 1.613in$$

3. Determine the Force in the bolts and compare it to the known force

$$T_y := q_{max} \cdot Y - P_r = 34.115kip$$

$T_{ye} = 34.115\,kip$

4. Determine Base Plate Yielding at Bearing Interface

$$t_{p11} := 1.5\,m_{48}\cdot\sqrt{\frac{f_{pmax}}{36\,ksi}} = 0.793\,in$$

$$t_{p12} := 2.11\cdot\sqrt{\frac{f_{pmax}\cdot Y\cdot\left(m_{48}-\frac{Y}{2}\right)}{36\,ksi}} = 0.74\,in \qquad < 1\,in \qquad \text{<=== OK since Y < m}$$

$$t_{p21} := 1.5\,n_{48}\cdot\sqrt{\frac{f_{pmax}}{36\,ksi}} = 1.048\,in$$

$$t_{p22} := 2.11\cdot\sqrt{\frac{f_{pmax}\cdot Y\cdot\left(n_{48}-\frac{Y}{2}\right)}{36\,ksi}} = 0.9\,in \qquad < 1\,in \qquad \text{<=== OK since Y < n}$$

5. Determine Base Plate Yielding at Tension Interface

$$T_u := q_{max}\cdot Y - P_r = 34.115\,kip$$

$$t_p := 2.11\cdot\sqrt{\frac{T_u\cdot x_{48}}{B\cdot 36\,ksi}} = 0.462\,in \qquad < 1\,in \qquad \text{<=== OK}$$

$$P_{dy1} := P = 3.896\,kip$$

W8×48 Deep - Fu

1. Determine e and compare it to e_{crit}

$$P := 6.528\,kip$$

$$M_r := L_d\cdot P = 52.634\,kip\cdot ft$$

$$P_r := H_d\cdot W_{48} + (13\,in)^2\cdot(16\,in - .75\,in)\cdot 150\,pcf = 0.636\,kip$$

$$f_p := \frac{P_r}{B\cdot N} = 3.762\,psi$$

$$e := \frac{M_r}{P_r} = 82.795\,ft$$

$$e_{crit} := \frac{N}{2} - \frac{P_r}{2\cdot q_{max}} = 0.54\,ft$$

2. Determine the bearing length

$$Y := \left(f + \frac{N}{2}\right) + \sqrt{\left(f + \frac{N}{2}\right)^2 - \frac{2\cdot P_r\cdot(e + f)}{q_{max}}} = 20.645\,in$$

$$Y := \left(f + \frac{N}{2}\right) - \sqrt{\left(f + \frac{N}{2}\right)^2 - \frac{2 \cdot P_r \cdot (e + f)}{q_{max}}} = 2.855\,in$$

3. Determine the Force in the bolts and compare it to the known force

$$T_u := q_{max} \cdot Y - P_r = 60.875\,kip$$

$$T_{ue} = 60.875\,kip$$

4. Determine Base Plate Yielding at Bearing Interface

$$t_{p11} := 1.5 m_{48} \cdot \sqrt{\frac{f_{pmax}}{36\,ksi}} = 0.793\,in \quad < 1\,in \quad \text{<=== OK since Y > m}$$

$$t_{p12} := 2.11 \cdot \sqrt{\frac{f_{pmax} \cdot Y \cdot \left(m_{48} - \frac{Y}{2}\right)}{36\,ksi}} = 0.778\,in$$

$$t_{p21} := 1.5 n_{48} \cdot \sqrt{\frac{f_{pmax}}{36\,ksi}} = 1.048\,in$$

$$t_{p22} := 2.11 \cdot \sqrt{\frac{f_{pmax} \cdot Y \cdot \left(n_{48} - \frac{Y}{2}\right)}{36\,ksi}} = 1.034\,in \quad < 1\,in \quad \text{<=== since Y < n}$$

*Although the plate will yield before the bolt reaches its ultimate strength, the bolt will break before the plate reaches its ultimate strength

5. Determine Base Plate Yielding at Tension Interface

$$T_u := q_{max} \cdot Y - P_r = 60.875\,kip$$

$$t_p := 2.11 \cdot \sqrt{\frac{T_u \cdot x_{48}}{B \cdot 36\,ksi}} = 0.617\,in \quad < 1\,in \quad \text{<=== OK}$$

$$P_{du1} := P = 6.528\,kip$$

W8×35 Deep - Fy

1. Determine e and compare it to e_{crit}

$$P := 3.8906\,kip$$

$$M_r := L_d \cdot P = 31.368\,kip \cdot ft$$

$$P_r := H_d \cdot W_{35} + (13\,in)^2 \cdot (16\,in - .75\,in) \cdot 150\,pcf = 0.524\,kip$$

$$f_p := \frac{P_r}{B \cdot N} = 3.101\,psi$$

$$e := \frac{M_r}{P_r} = 59.847\,in$$

$$e_{crit} := \frac{N}{2} - \frac{P_r}{2 \cdot q_{max}} = 0.541\,in$$

2. Determine the bearing length

$$Y := \left(f + \frac{N}{2}\right) + \sqrt{\left(f + \frac{N}{2}\right)^2 - \frac{2 \cdot P_r \cdot (e + f)}{q_{max}}} = 21.892\,in$$

$$Y := \left(f + \frac{N}{2}\right) - \sqrt{\left(f + \frac{N}{2}\right)^2 - \frac{2 \cdot P_r \cdot (e + f)}{q_{max}}} = 1.608\,in$$

3. Determine the Force in the bolts and compare it to the known force

$$T_y := q_{max} \cdot Y - P_r = 34.115\,kip$$

$$T_{ye} = 34.115\,kip$$

4. Determine Base Plate Yielding at Bearing Interface

$$t_{p11} := 1.5 m_{35} \cdot \sqrt{\frac{f_{pmax}}{36\,ksi}} = 0.851\,in$$

$$t_{p12} := 2.11 \cdot \sqrt{\frac{f_{pmax} \cdot Y \cdot \left(m_{35} - \frac{Y}{2}\right)}{36\,ksi}} = 0.779\,in \quad < 1\,in \quad \text{<=== OK since Y < m}$$

$$t_{p21} := 1.5 n_{35} \cdot \sqrt{\frac{f_{pmax}}{36\,ksi}} = 1.06\,in$$

$$t_{p22} := 2.11 \cdot \sqrt{\frac{f_{pmax} \cdot Y \cdot \left(n_{35} - \frac{Y}{2}\right)}{36\,ksi}} = 0.905\,in \quad < 1\,in \quad \text{<=== OK since Y < n}$$

5. Determine Base Plate Yielding at Tension Interface

$$T_u := q_{max} \cdot Y - P_r = 34.115\,kip$$

$$t_p := 2.11 \cdot \sqrt{\frac{T_u \cdot x_{35}}{B \cdot 36\,ksi}} = 0.553\,in \quad < 1\,in \quad \text{<=== OK}$$

$$P_{dy2} := P = 3.891\,kip$$

W8×35 Deep - Fu

1. Determine e and compare it to e_{crit}

$$P := 6.524\,kip$$

$$M_r := L_d \cdot P = 52.601\,kip\cdot ft$$

$$P_r := H_d \cdot W_{35} + (13in)^2 \cdot (16in - .75in) \cdot 150pcf = 0.524kip$$

$$f_p := \frac{P_r}{B \cdot N} = 3.101psi$$

$$e := \frac{M_r}{P_r} = 100.357ft$$

$$e_{crit} := \frac{N}{2} - \frac{P_r}{2 \cdot q_{max}} = 0.541ft$$

2. Determine the bearing length

$$Y := \left(f + \frac{N}{2}\right) + \sqrt{\left(f + \frac{N}{2}\right)^2 - \frac{2 \cdot P_r \cdot (e + f)}{q_{max}}} = 20.651in$$

$$Y := \left(f + \frac{N}{2}\right) - \sqrt{\left(f + \frac{N}{2}\right)^2 - \frac{2 \cdot P_r \cdot (e + f)}{q_{max}}} = 2.849in$$

3. Determine the Force in the bolts and compare it to the known force

$$T_u := q_{max} \cdot Y - P_r = 60.875kip$$

$$T_{ue} = 60.875kip$$

4. Determine Base Plate Yielding at Bearing Interface

$$t_{p11} := 1.5 m_{35} \cdot \sqrt{\frac{f_{pmax}}{36ksi}} = 0.851in \quad < 1in \quad \text{<=== OK since Y > m}$$

$$t_{p12} := 2.11 \cdot \sqrt{\frac{f_{pmax} \cdot Y \cdot \left(m_{35} - \frac{Y}{2}\right)}{36ksi}} = 0.844in$$

$$t_{p21} := 1.5 n_{35} \cdot \sqrt{\frac{f_{pmax}}{36ksi}} = 1.06in$$

$$t_{p22} := 2.11 \cdot \sqrt{\frac{f_{pmax} \cdot Y \cdot \left(n_{35} - \frac{Y}{2}\right)}{36ksi}} = 1.044in \quad < 1in \quad \text{<=== since Y < n}$$

*Although the plate will yield before the bolt reaches its ultimate strength, the bolt will break before the plate reaches its ultimate strength

5. Determine Base Plate Yielding at Tension Interface

$$T_u := q_{max} \cdot Y - P_r = 60.875\,kip$$

$$t_p := 2.11 \cdot \sqrt{\frac{T_u \cdot x_{35}}{B \cdot 36\,ksi}} = 0.739\,in \quad < 1\,in \quad <=== OK$$

$$P_{du2} := P = 6.524\,kip$$

Since the expected strength was almost identical for the different shapes, an average was taken that could be compared to the actual strengths for both.

$$P_{yshallow} := \frac{P_{sy1} + P_{sy2}}{2} = 4.384\,kip$$

$$P_{ushallow} := \frac{P_{su1} + P_{su2}}{2} = 7.357\,kip$$

$$P_{ydeep} := \frac{P_{dy1} + P_{dy2}}{2} = 3.893\,kip$$

$$P_{udeep} := \frac{P_{du1} + P_{du2}}{2} = 6.526\,kip$$

Force Equilibrium Calculations

The following calculations show the steps followed to determine the location of the resultant resisting force in the concrete.

A1

Given

$P := 8483.4312$

$h := 7 \cdot 12 + 4.25 = 88.25$

$W_s := 35 \cdot \frac{h + 6.25 - 1.5}{12} = 271.25$

$s_b := 10.5$

$T_{b2} := 17060$

$w_c := \frac{136.15}{12^3}$

$w_s := 5(12)$

$h_s := 8$

$l := 7(12)$

$P \cdot h - 2T_{b2} \cdot \frac{s_b}{2} - \left(W_s + w_c \cdot h_s \cdot w_s \cdot l + 2 \cdot T_{b2}\right) \cdot x = 0$

$\text{Find}(x) \rightarrow 15.160017569878686917$

A2

Given

$P := 7934.4392$

$h := 7 \cdot 12 + 4.25 = 88.25$

$W_s := 48 \cdot \frac{h + 6.25 - 1.55}{12} = 371.8$

$s_b := 10.5$

$T_{b2} := 17060$

$w_c := \frac{136.15}{12^3}$

$w_s := 5(12)$

$h_s := 8$

$l := 7(12)$

$P \cdot h - 2T_{b2} \cdot \frac{s_b}{2} - \left(W_s + w_c \cdot h_s \cdot w_s \cdot l + 2 \cdot T_{b2}\right) \cdot x = 0$

$\text{Find}(x) \rightarrow 13.833373108837680157$

A4

Given

$P := 7339.537037$

$h := 7 \cdot 12 + 4.25 = 88.25$

$W_s := 48 \cdot \frac{h + 6.25 - 1.5}{12} = 372$

$s_b := 10.5$

$T_{b2} := 17060$

$w_c := \frac{136.15}{12^3}$

$w_s := 5(12)$

$h_s := 8$

$l := 7(12)$

$P \cdot h - 2T_{b2} \cdot \frac{s_b}{2} - \left(W_s + w_c \cdot h_s \cdot w_s \cdot l + 2 \cdot T_{b2}\right) \cdot x = 0$

$\text{Find}(x) \rightarrow 12.439571445410219766$

B1

Given

$P := 9850 = 9.85 \times 10^3$

$h := 7 \cdot 12 + 4.25 + 13 = 101.25$

$W_s := 35 \cdot \frac{h + 6.25}{12} = 313.542$

$s_b := 10.5$

$T_{b2} := 17060$

$w_c := \frac{136.15}{12^3}$

$w_s := 5(12)$

$h_s := 16$

$l := 7(12)$

$P \cdot h - 2T_{b2} \cdot \frac{s_b}{2} - \left(W_s + w_c \cdot h_s \cdot w_s \cdot l + 2 \cdot T_{b2}\right) \cdot x = 0$

$\text{Find}(x) \rightarrow 20.059781814764228561$

B2

Given

$P := 10730 = 1.073 \times 10^4$

$h := 7 \cdot 12 + 4.25 + 13 = 101.25$

$W_s := 48 \cdot \frac{h + 6.25}{12} = 430$

$s_b := 10.5$

$T_{b2} := 17060$

$w_c := \frac{136.15}{12^3}$

$w_s := 5(12)$

$h_s := 16$

$l := 7(12)$

$P \cdot h - 2T_{b2} \cdot \frac{s_b}{2} - \left(W_s + w_c \cdot h_s \cdot w_s \cdot l + 2 \cdot T_{b2}\right) \cdot x = 0$

$\text{Find}(x) \rightarrow 22.180957697353945449$

B4

Given

$P := 8710$

$h := 7 \cdot 12 + 4.25 + 13 = 101.25$

$W_s := 48 \cdot \frac{h + 6.25}{12} = 430$

$s_b := 10.5$

$T_{b2} := 17060$

$w_c := \frac{136.15}{12^3}$

$w_s := 5(12)$

$h_s := 16$

$l := 7(12)$

$P \cdot h - 2T_{b2} \cdot \frac{s_b}{2} - \left(W_s + w_c \cdot h_s \cdot w_s \cdot l + 2 \cdot T_{b2}\right) \cdot x = 0$

$\text{Find}(x) \rightarrow 17.180794712780435332$

APPENDIX C. STRAIN DATA

This appendix will present the strain gauge data that was recorded during the tests. This data was not used in this research but will be used in future research. For each specimen the strain gauge data is plotted for the maximum load during each cycle in both the positive and negative directions. Only the first few cycles were recorded because in many cases the strain gauges failed after getting to large displacements. For specimen A3 the strain was taken at displacements that matched those of the other specimens from the large initial push. In turn specimen A3 only had strains plotted from the positive direction push.

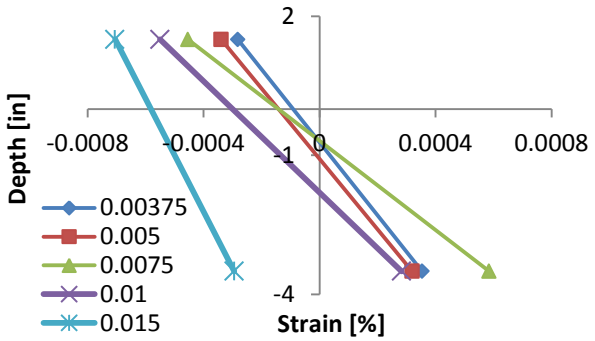

a) South East Flange Positive Maximum

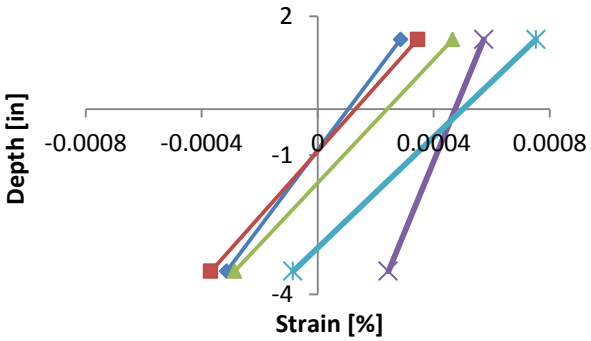

b) South West Flange Positive Maximum

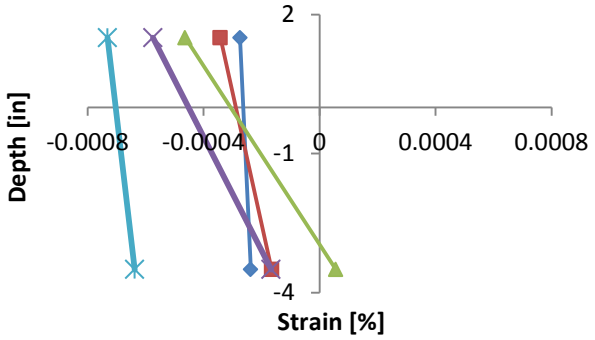

c) North East Flange Positive Maximum

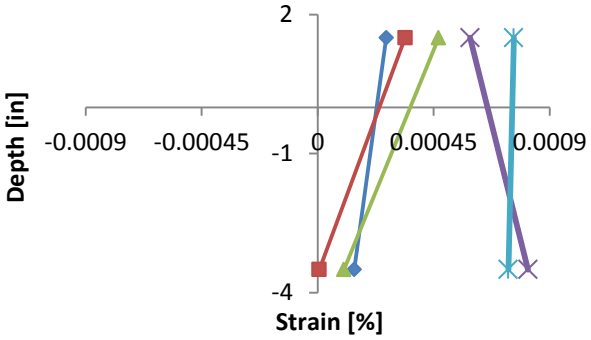

d) North West Flange Positive Maximum

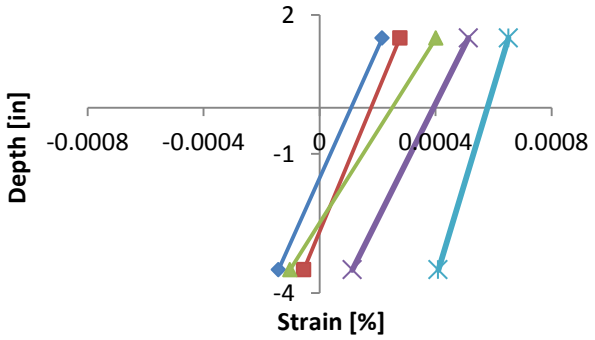

e) South East Flange Negative Maximum

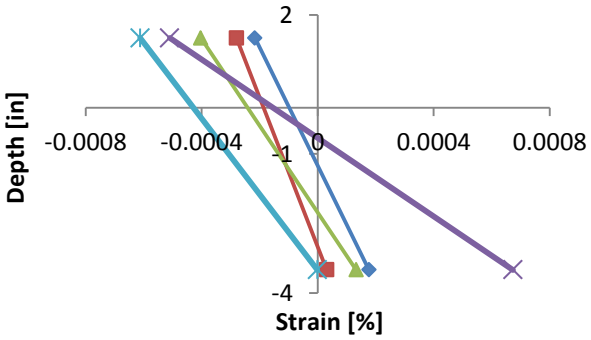

f) South West Flange Negative Maximum

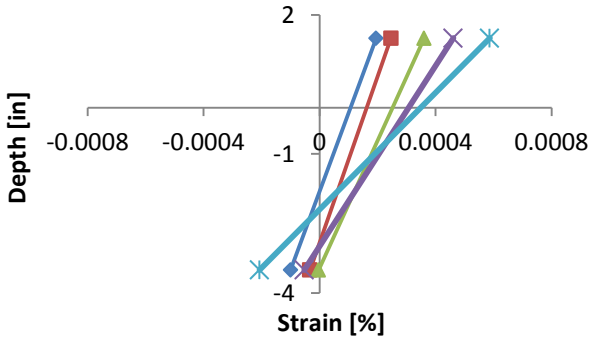

g) North East Flange Negative Maximum

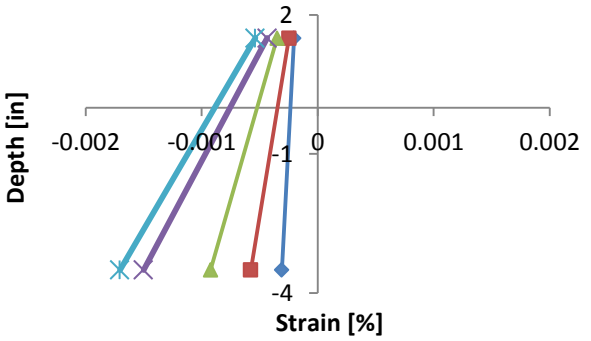

h) North West Flange Negative Maximum

Figure C-1: Strain Gauge Data for Specimen A1

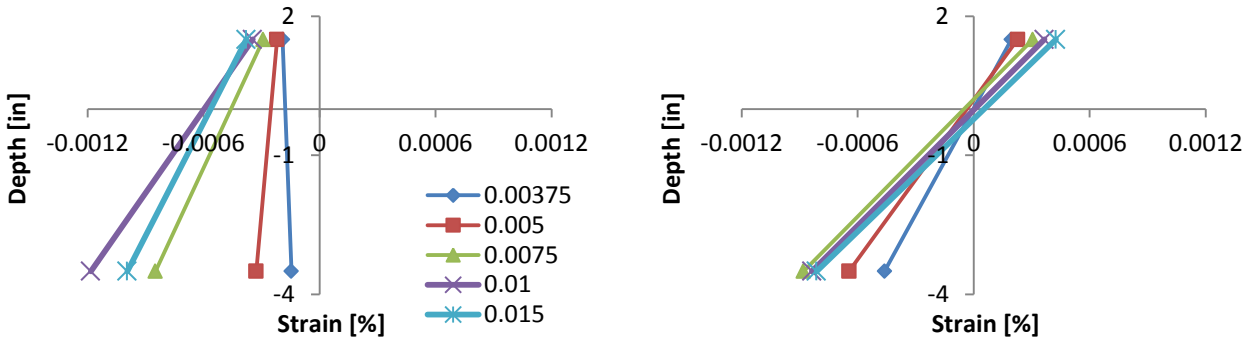

a) South East Flange Positive Maximum

b) South West Flange Positive Maximum

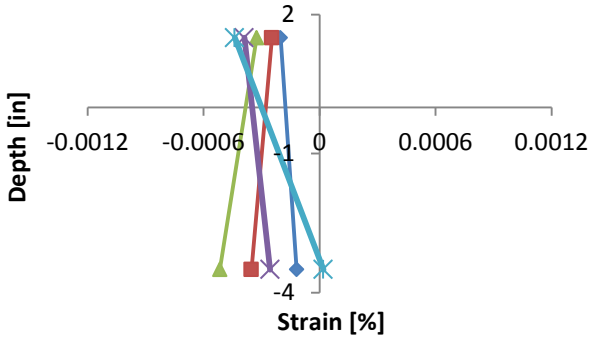

c) North East Flange Positive Maximum

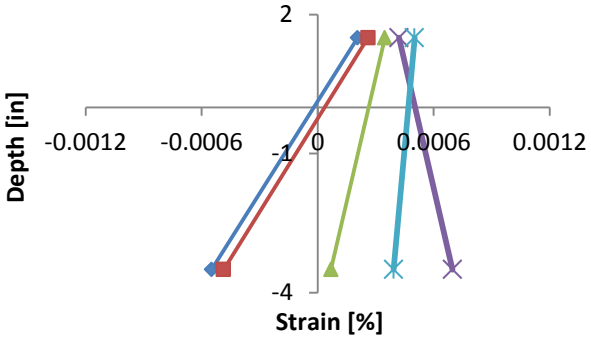

d) North West Flange Positive Maximum

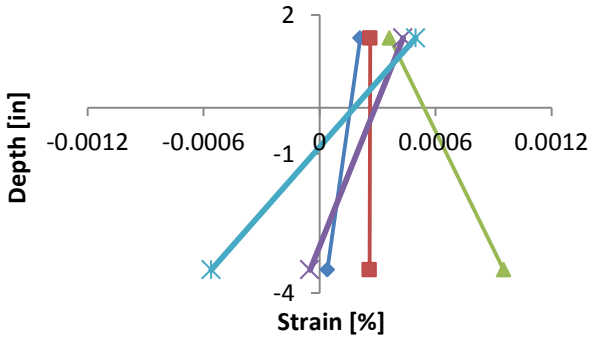

e) South East Flange Negative Maximum

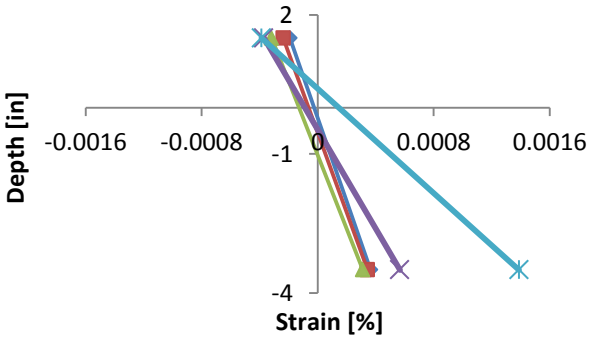

f) South West Flange Negative Maximum

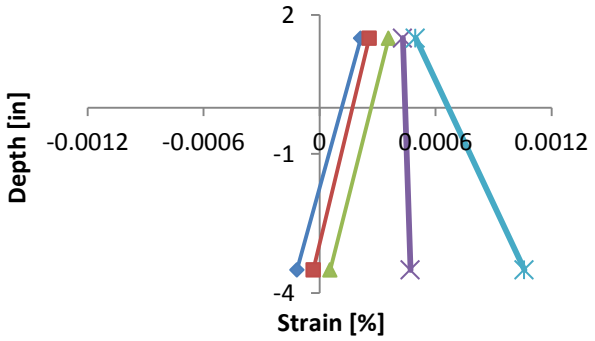

g) North East Flange Negative Maximum

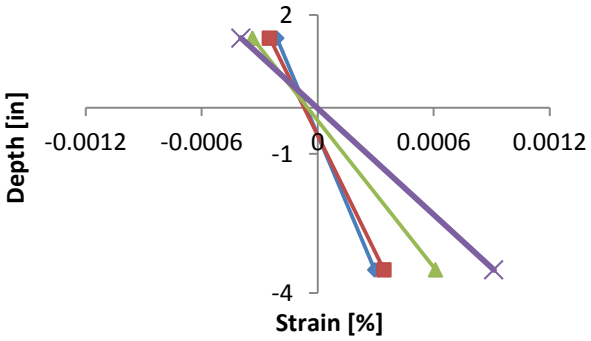

h) North West Flange Negative Maximum

Figure C-2: Strain Gauge Data for Specimen A2

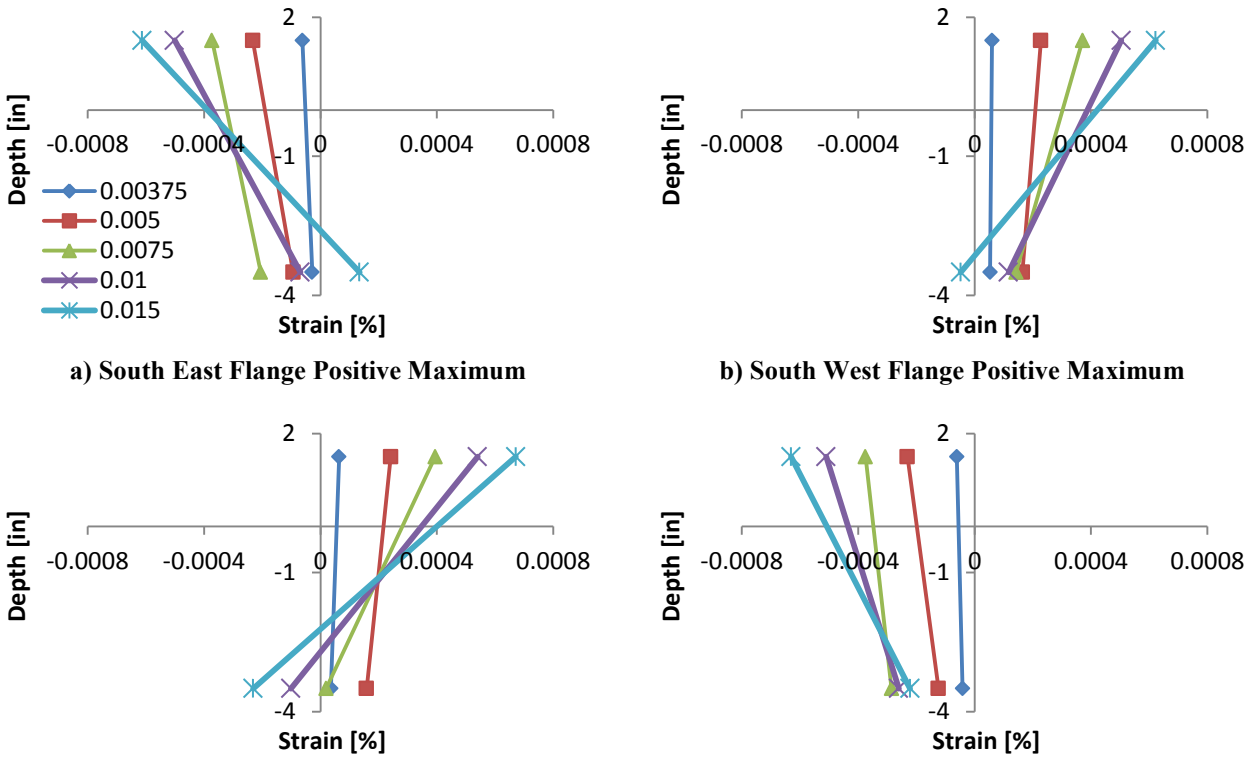

a) South East Flange Positive Maximum

b) South West Flange Positive Maximum

c) North East Flange Positive Maximum

d) North West Flange Positive Maximum

Figure C-3: Strain Gauge Data for Specimen A3

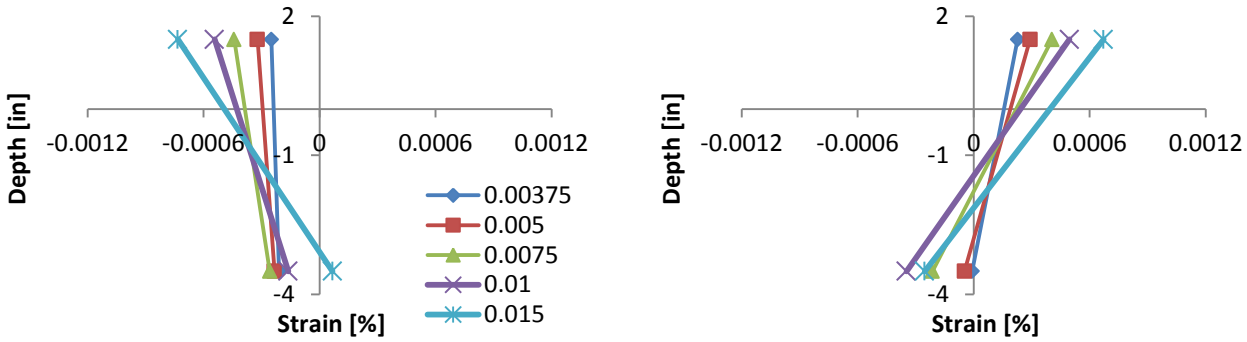

a) South East Flange Positive Maximum

b) South West Flange Positive Maximum

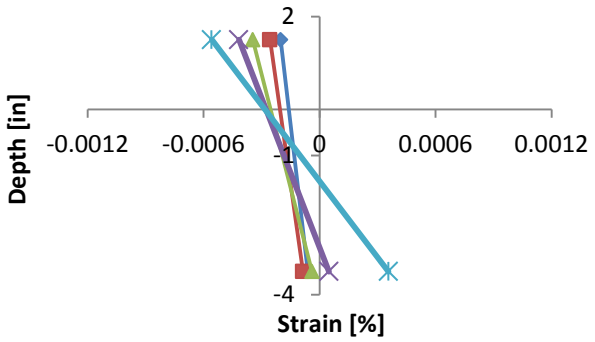

c) North East Flange Positive Maximum

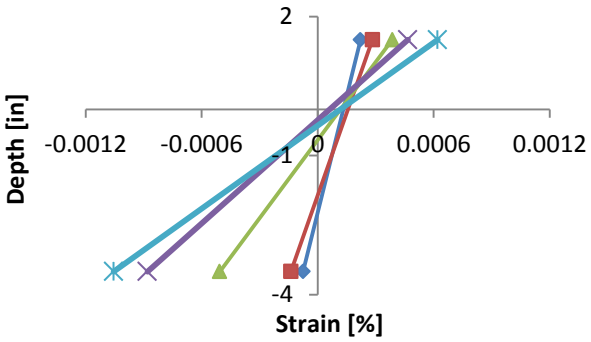

d) North West Flange Positive Maximum

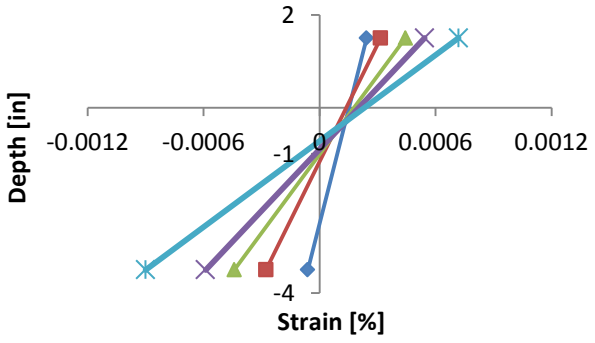

e) South East Flange Negative Maximum

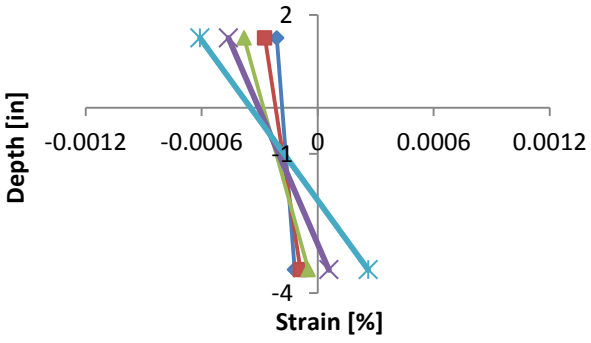

f) South West Flange Negative Maximum

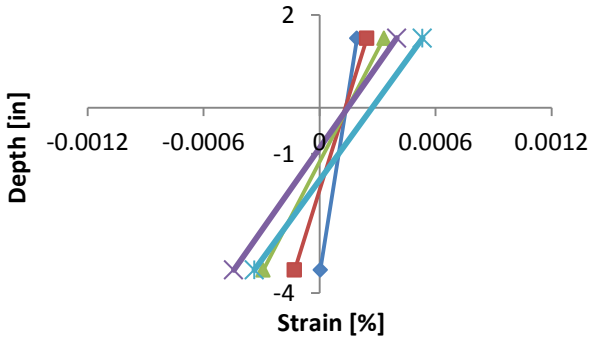

g) North East Flange Negative Maximum

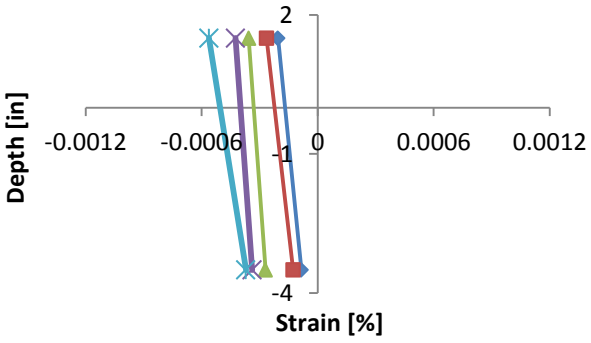

h) North West Flange Negative Maximum

Figure C-4: Strain Gauge Data for Specimen A4

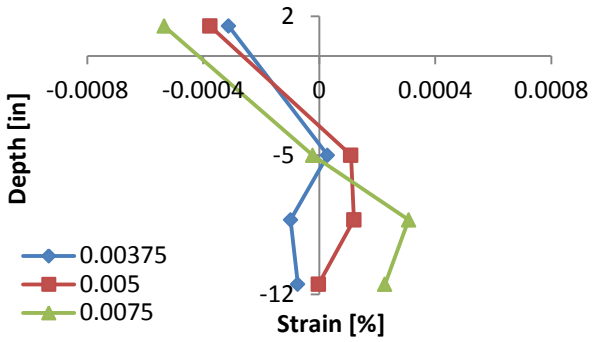

a) South East Flange Positive Maximum

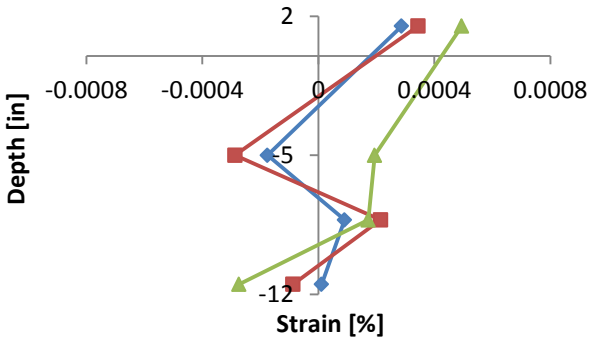

b) South West Flange Positive Maximum

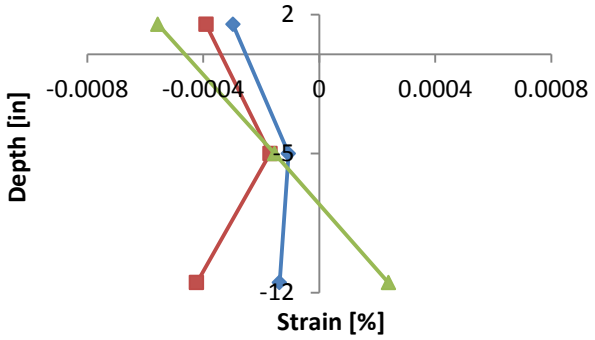

c) North East Flange Positive Maximum

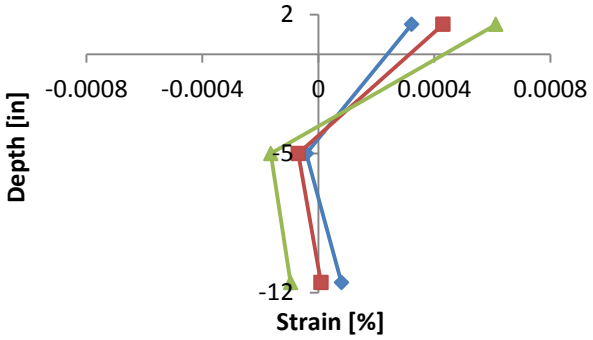

d) North West Flange Positive Maximum

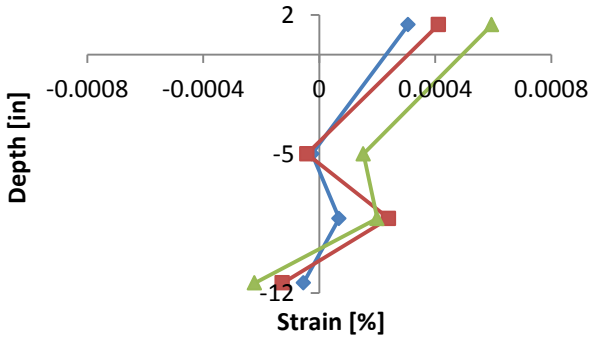

e) South East Flange Negative Maximum

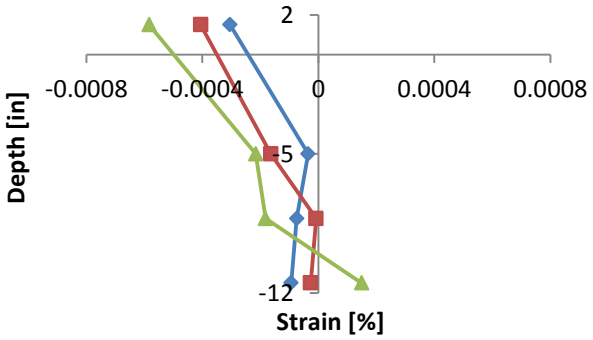

f) South West Flange Negative Maximum

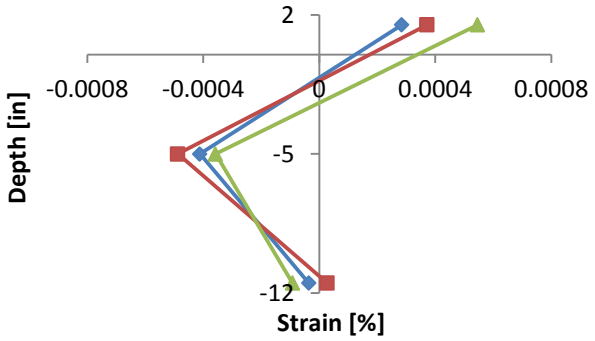

g) North East Flange Negative Maximum

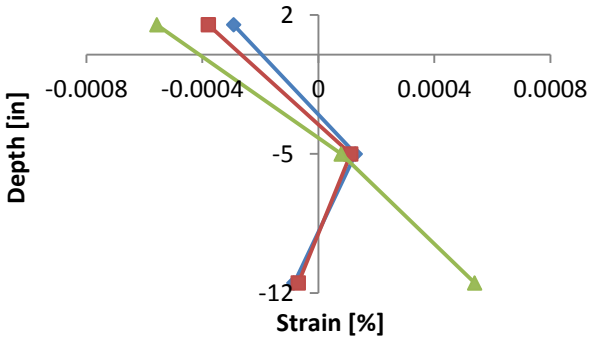

h) North West Flange Negative Maximum

Figure C-5: Strain Gauge Data for Specimen B1

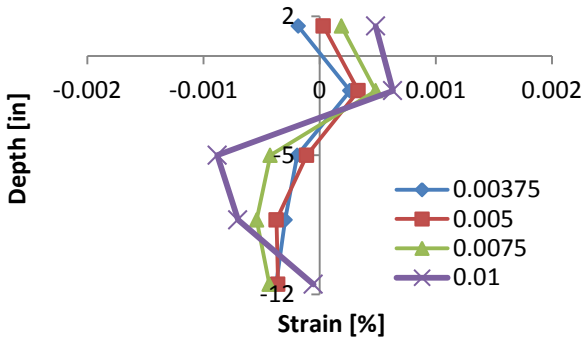

a) South East Flange Positive Maximum

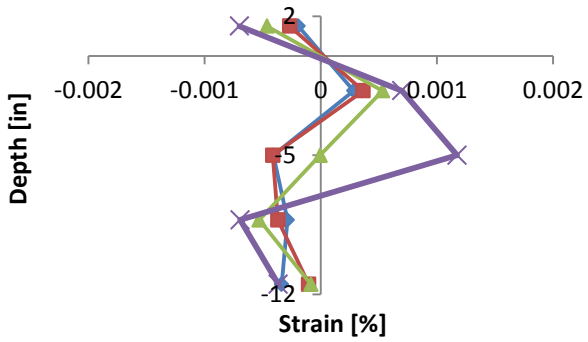

b) South West Flange Positive Maximum

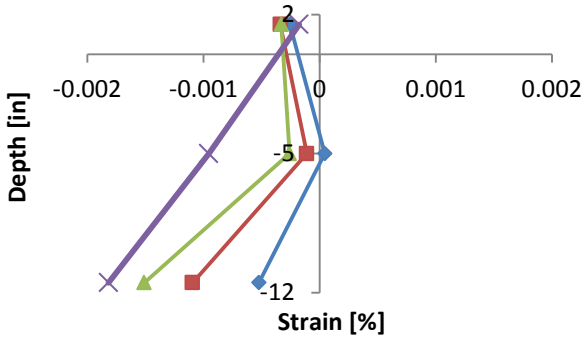

c) North East Flange Positive Maximum

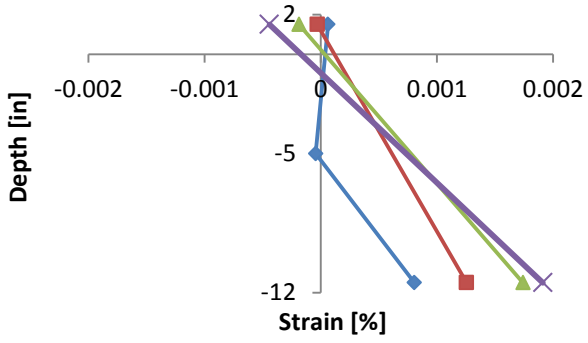

d) North West Flange Positive Maximum

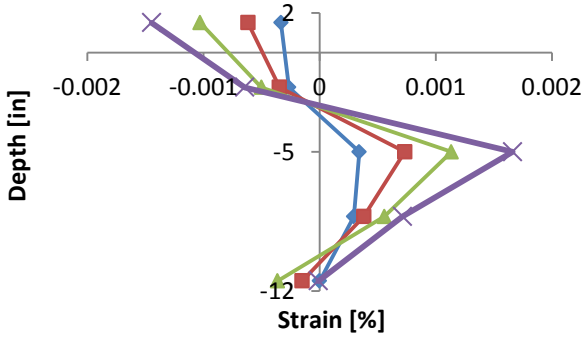

e) South East Flange Negative Maximum

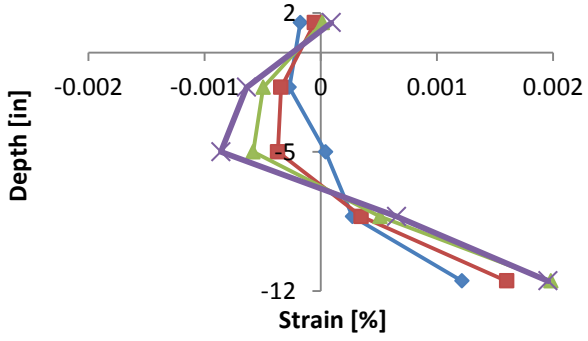

f) South West Flange Negative Maximum

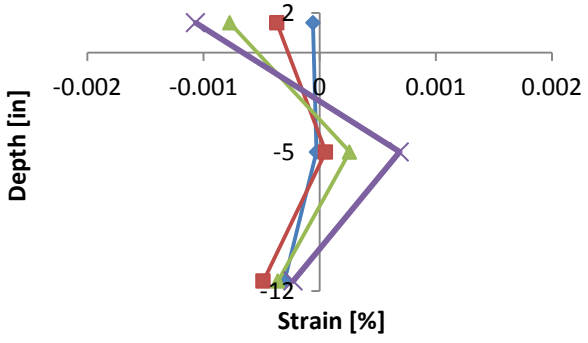

g) North East Flange Negative Maximum

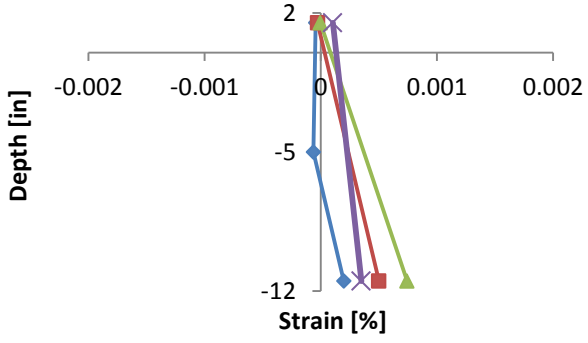

h) North West Flange Negative Maximum

Figure C-6: Strain Gauge Data for Specimen B2

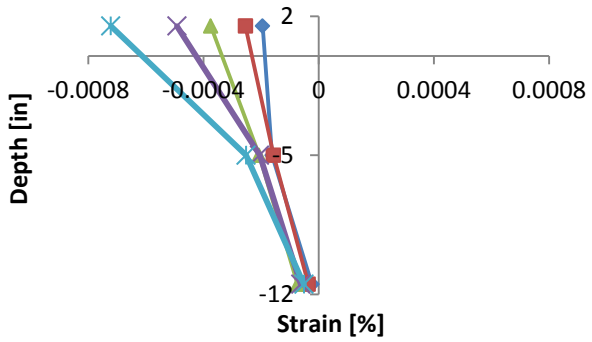

a) South East Flange Positive Maximum

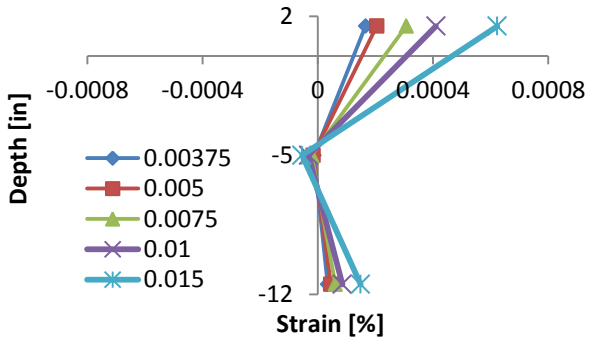

b) South West Flange Positive Maximum

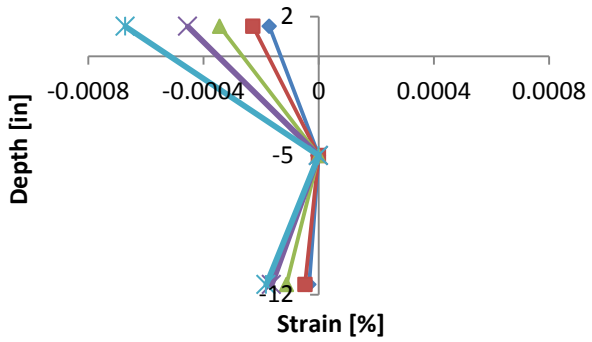

c) North East Flange Positive Maximum

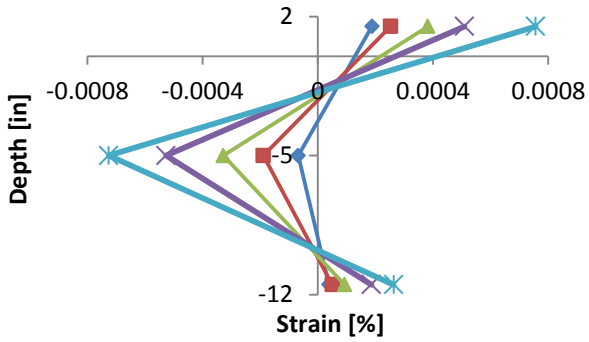

d) North West Flange Positive Maximum

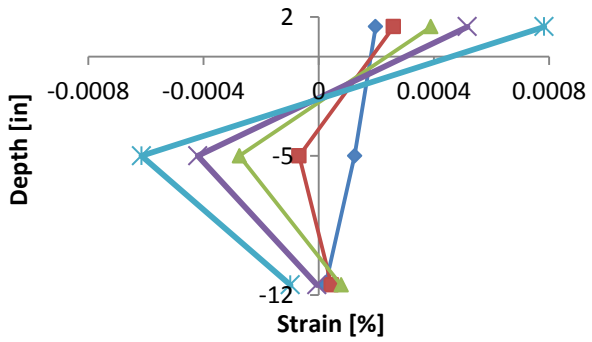

e) South East Flange Negative Maximum

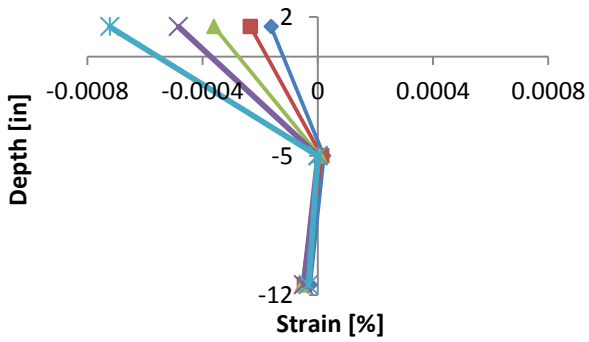

f) South West Flange Negative Maximum

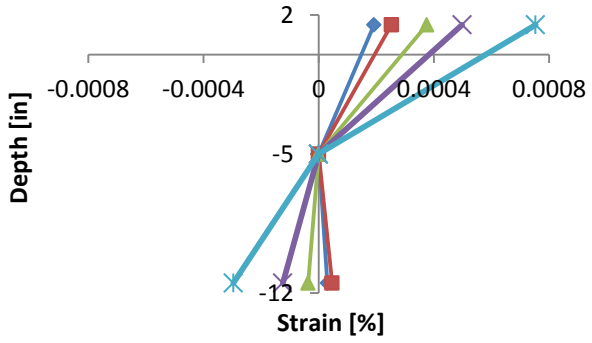

g) North East Flange Negative Maximum

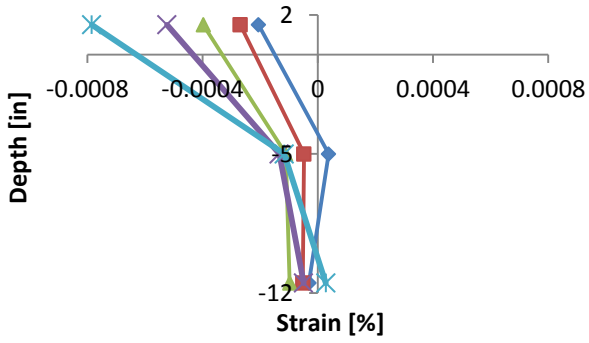

h) North West Flange Negative Maximum

Figure C-7: Strain Gauge Data for Specimen B3

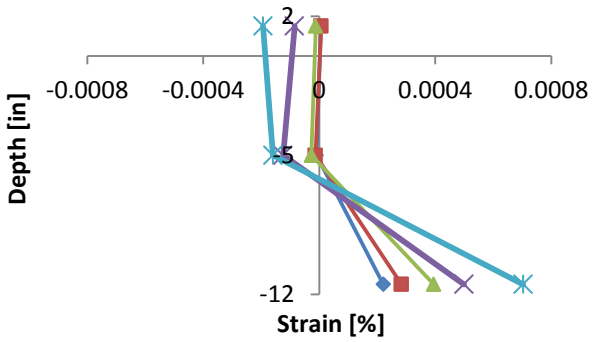

a) South East Flange Positive Maximum

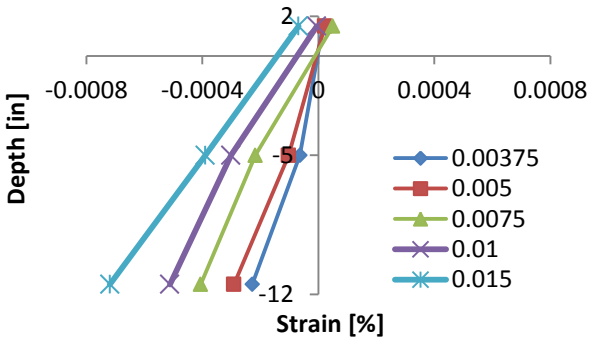

b) South West Flange Positive Maximum

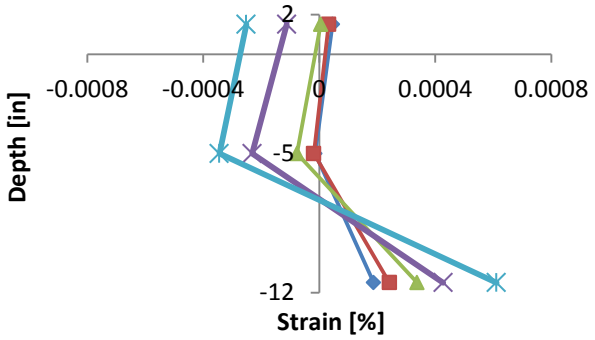

c) North East Flange Positive Maximum

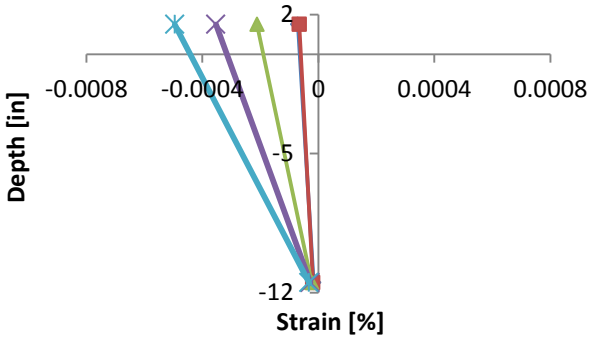

d) North West Flange Positive Maximum

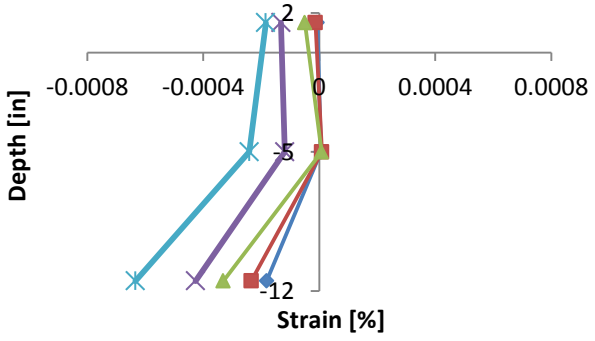

e) South East Flange Negative Maximum

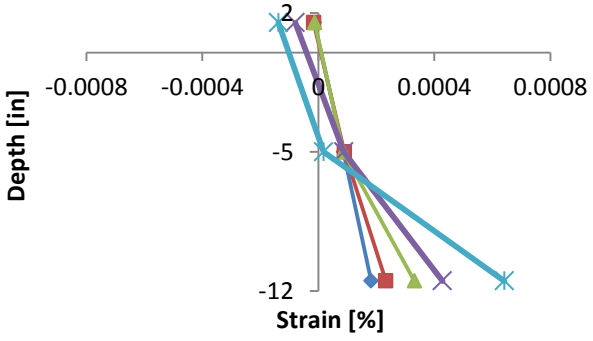

f) South West Flange Negative Maximum

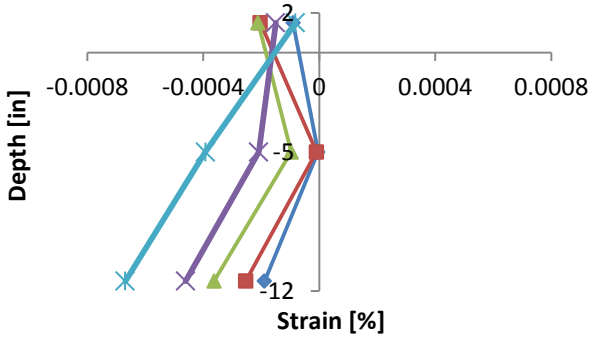

g) North East Flange Negative Maximum

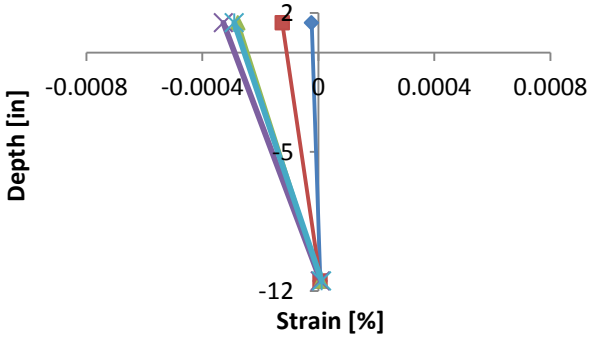

h) North West Flange Negative Maximum

Figure C-8: Strain Gauge Data for Specimen B4

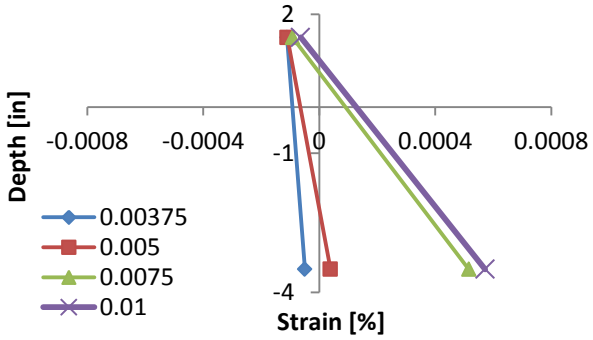

a) South East Flange Positive Maximum

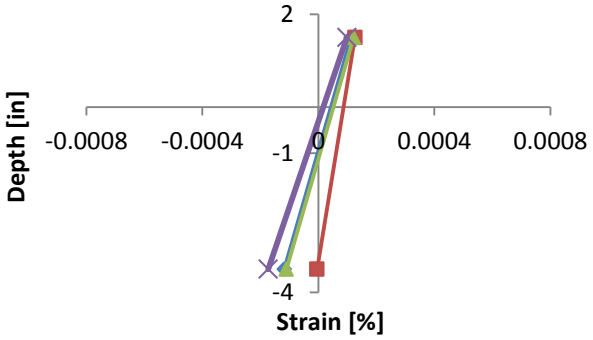

b) South West Flange Positive Maximum

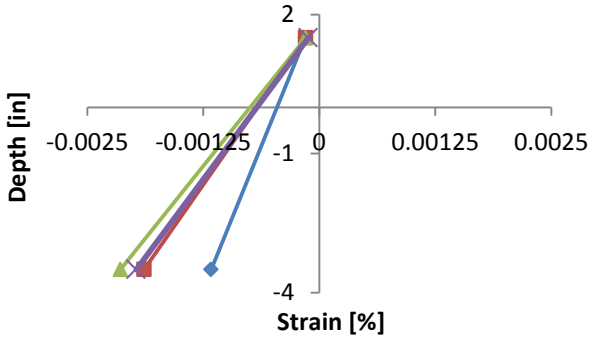

c) North East Flange Positive Maximum

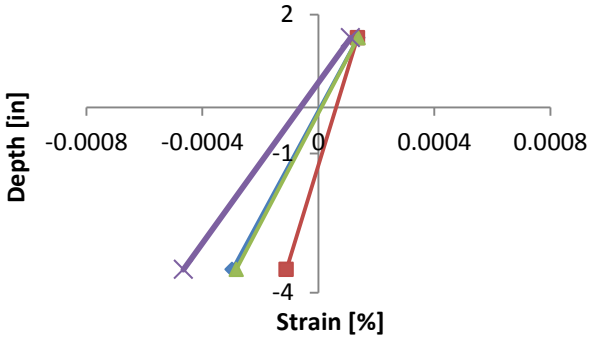

d) North West Flange Positive Maximum

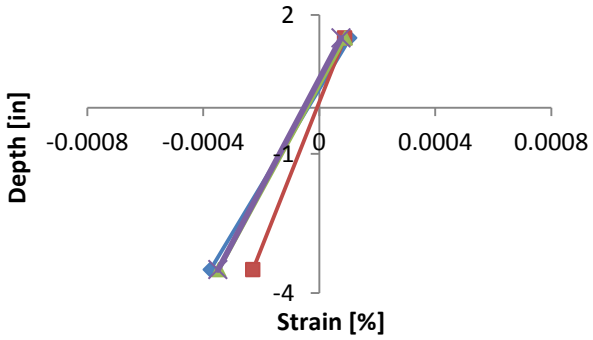

e) South East Flange Negative Maximum

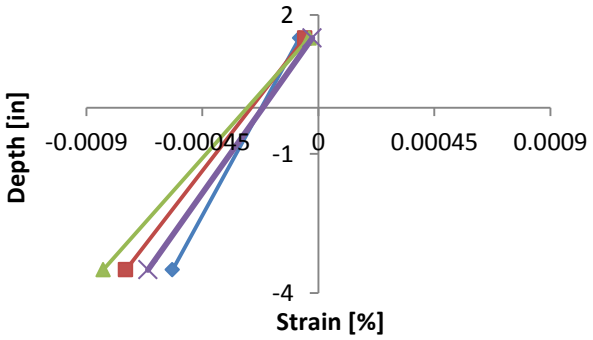

f) South West Flange Negative Maximum

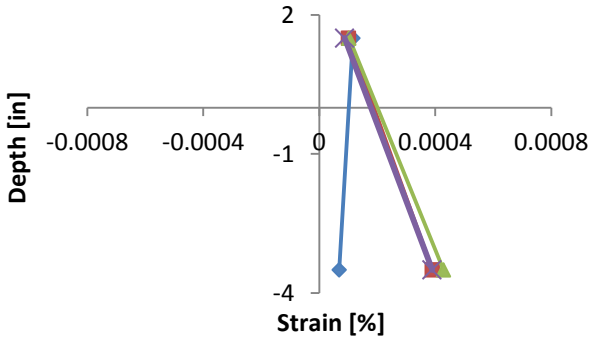

g) North East Flange Negative Maximum

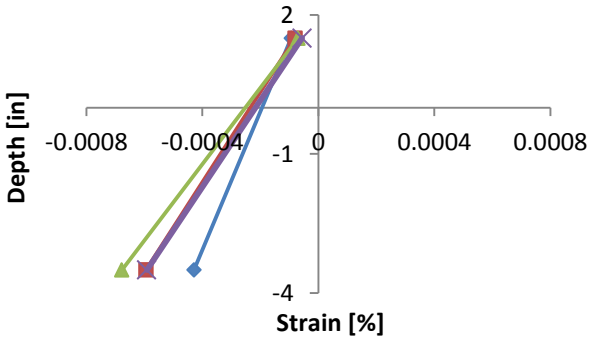

h) North West Flange Negative Maximum

Figure C-9: Strain Gauge Data for Specimen CA2

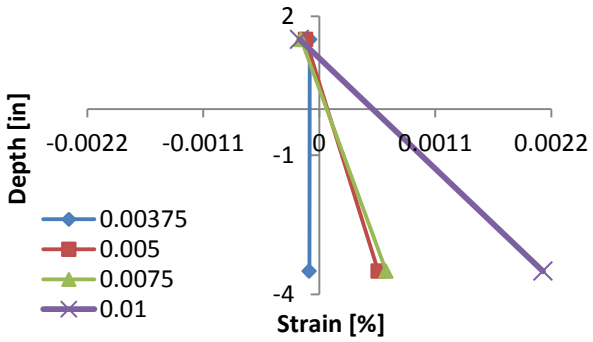

a) South East Flange Positive Maximum

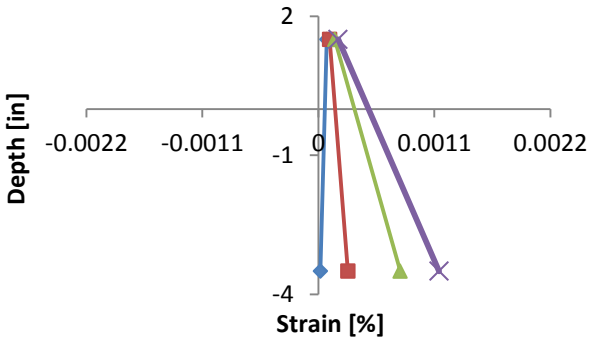

b) South West Flange Positive Maximum

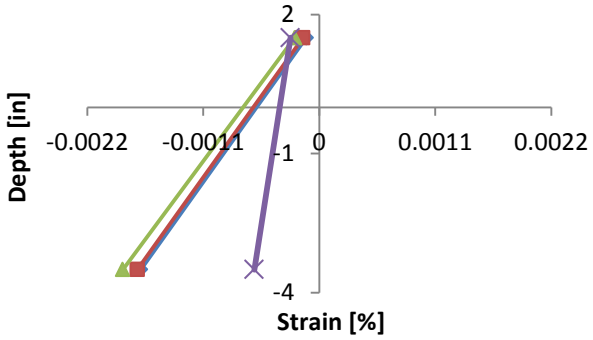

c) North East Flange Positive Maximum

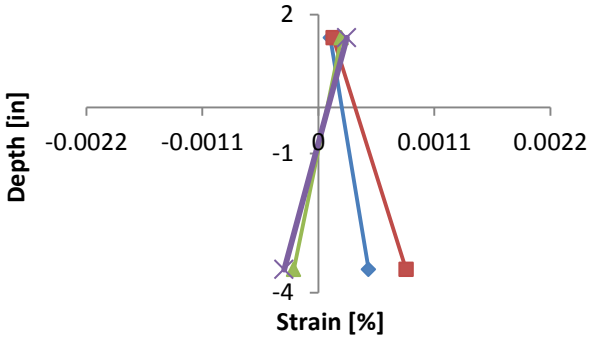

d) North West Flange Positive Maximum

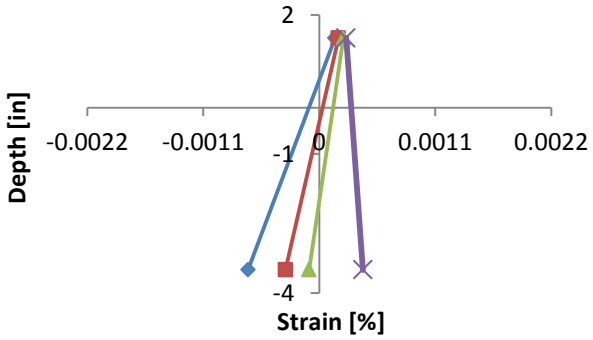

e) South East Flange Negative Maximum

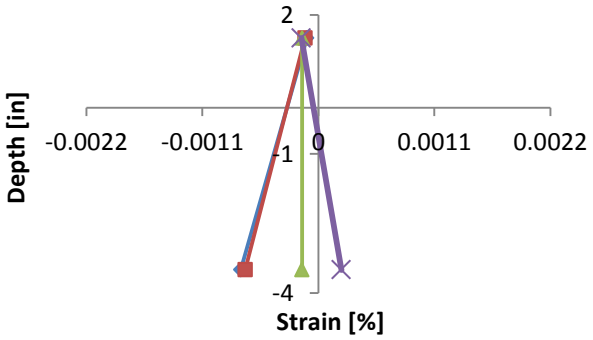

f) South West Flange Negative Maximum

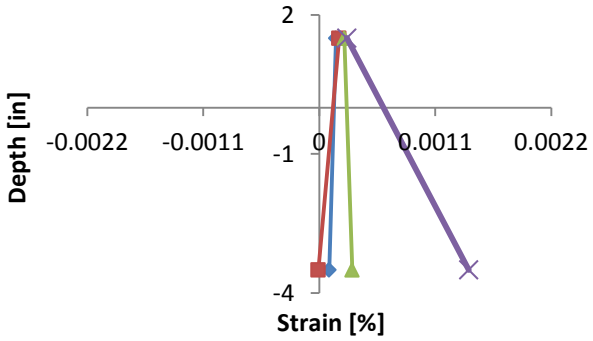

g) North East Flange Negative Maximum

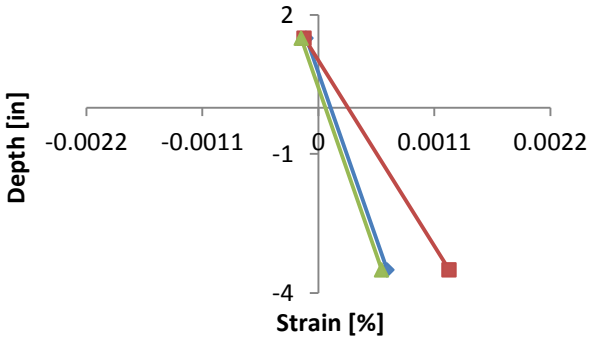

h) North West Flange Negative Maximum

Figure C-10: Strain Gauge Data for Specimen DA2

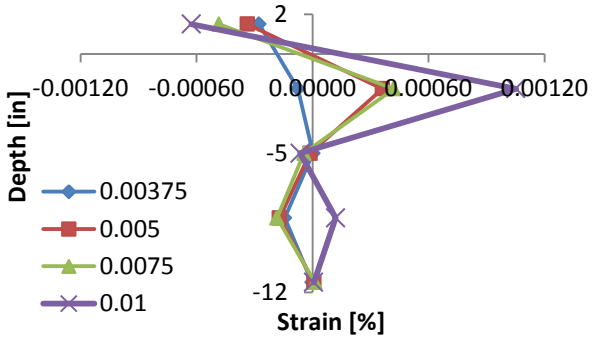

a) South East Flange Positive Maximum

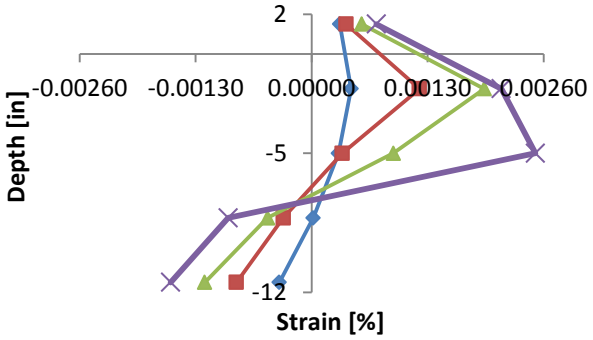

b) South West Flange Positive Maximum

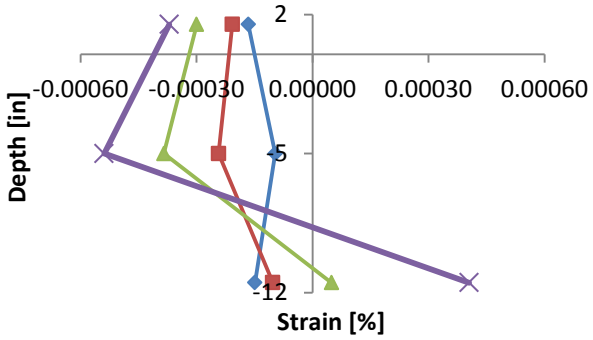

c) North East Flange Positive Maximum

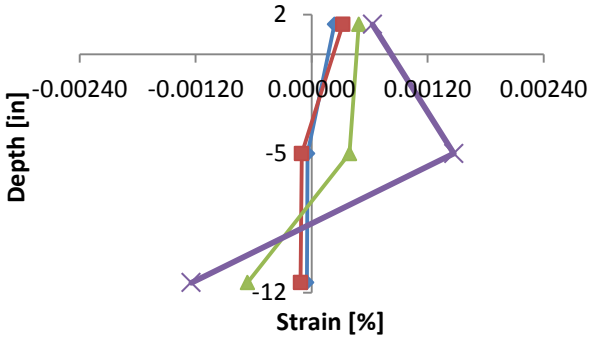

d) North West Flange Positive Maximum

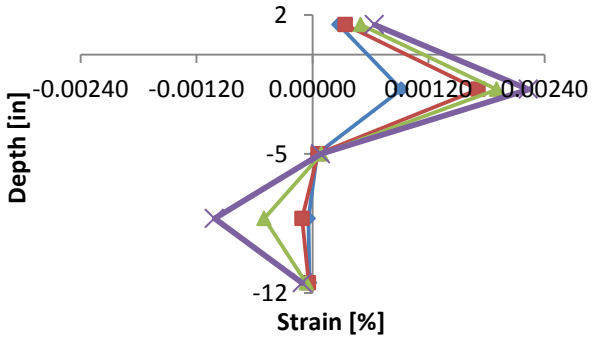

e) South East Flange Negative Maximum

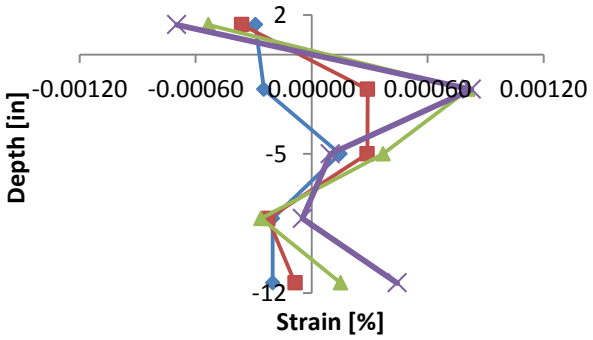

f) South West Flange Negative Maximum

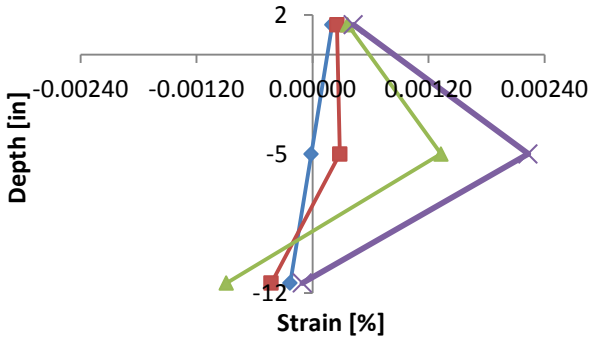

g) North East Flange Negative Maximum

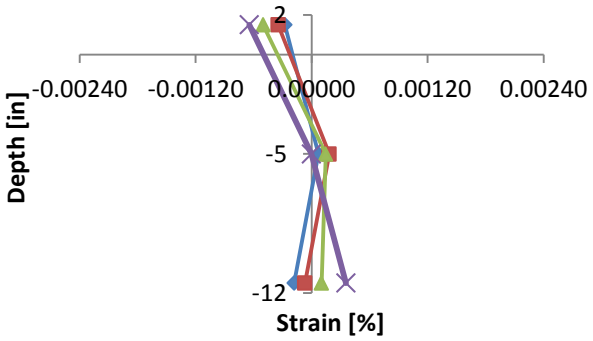

h) North West Flange Negative Maximum

Figure C-11: Strain Gauge Data for Specimen CB2

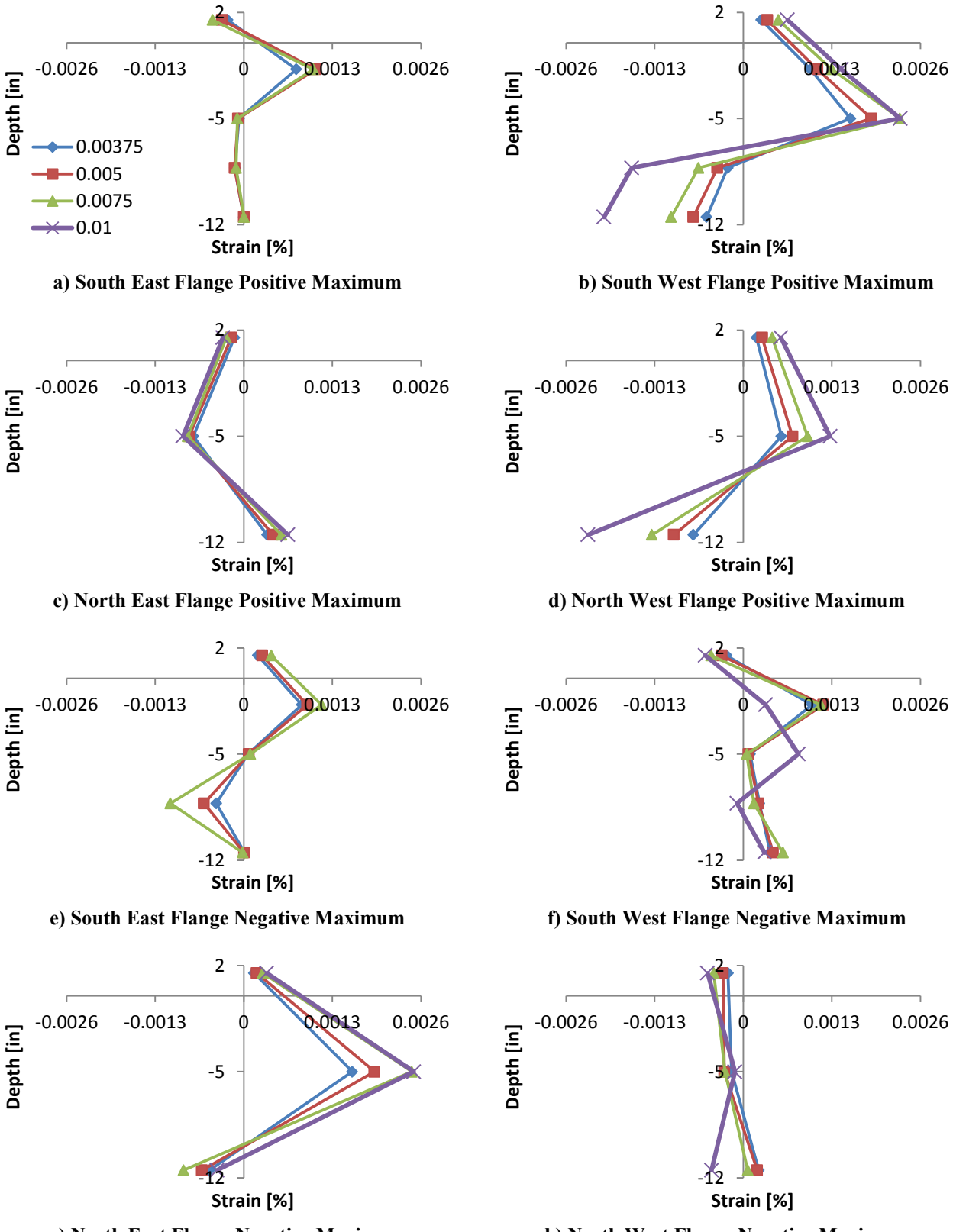

a) South East Flange Positive Maximum

b) South West Flange Positive Maximum

c) North East Flange Positive Maximum

d) North West Flange Positive Maximum

e) South East Flange Negative Maximum

f) South West Flange Negative Maximum

g) North East Flange Negative Maximum

h) North West Flange Negative Maximum

Figure C-12: Strain Gauge Data for Specimen DB2

APPENDIX D. MATERIAL PROPERTIES

For all of the materials used during the test, material tests were conducted. These tests are summarized in the following sections along with the material properties.

Concrete

For each concrete pour cylinders were made for compression testing. Starting with the footing four 8" tall and 4" diameter concrete cylinders we made corresponding to each specimen. These were left in the molds for 24 hours and then removed and placed in the lab near the test specimens so they would dry in similar conditions. This same process was repeated for the concrete in the block-out although it also included the two specimens that were jack hammered out and re-poured. Getting data for the slab from each specimen was not essential so only four cylinders were taken from each pour. Lastly, for each of the pours 4 cylinders were taken of the same dimensions as before. Only this time they were placed them in the fog room after one day of being in the mold and then tested 28 days later to get the 28-day compressive strength.

All the samples were tested in accordance with ASTM C39 [14]. The ultimate load was read from the machine and then the compressive strength was found using the cross sectional area of the cylinders. These compressive strengths are summed up in Table D-1 and the 28-day strengths are summarized in Table D-2.

Table D-1: Compressive Strength and Unit Weight of Block-out, Footing and Grout for Each Specimen

		Compressive Strength [psi]			*Unit Weight [pcf]*	
Specimen	Test Date	Block-out	Footing	Grout	Block-out	Footing
A1	23-Jun	1725	3054	6723	124	132
A2	24-Jun	1578	3013	7360	123	131
A3	23-Jun	1643	2991	6723	125	130
A4	20-Aug	3836	-	-	140	-
B1	19-Jun	1799	3325	7070	125	138
B2	18-Jun	1622	3214	7070	123	136
B3	20-Jun	1780	3488	5895	125	136
B4	21-Aug	4331	-	-	142	-
CA2/DA2	11-Jun	1711	3266	7360	124	132
CB2/DB2	17-Jun	1501	3395	5895	123	136

Table D-2: 28-day Strength of each Concrete Pour

Date	Truck	Location	Slump	Test Date	28-day Comp [psi]	γ_c [pcf]
21-Apr	1	Footing	4	19-May	4312	144
21-Apr	2	Footing	5.5	19-May	4095	141
23-Apr	1	Slab	5.25	21-May	4688	145
6-May	1	Block-out	6.5	3-Jun	2419	133
22-Jul	-	Block-out - A4	5	19-Aug	4149	148
22-Jul	-	Block-out - B4	5	19-Aug	4396	148

Anchor Rods

The anchor rods were tested in tension in accordance with ASTM A370 [14]. The yield stress and ultimate stress of the rod tests are summarized in Table D-3.

Table D-3: Anchor Rod Properties

	Anchor Rod 1	Anchor Rod 2	Average
F_y [ksi]	45.21	45.76	45.49
F_u [ksi]	81.14	81.19	81.17

Steel Columns

Steel coupons were taken from one of the W8×48 columns and one of the W8×35 columns according to ASTM A370 [14]. The coupon design is shown in Figure D-1. The coupons were then tested in accordance with ASTM A370 [14]. Once the data was acquired the field yield stress and ultimate stress of the steel were determined. These values are summarized in Table D-4.

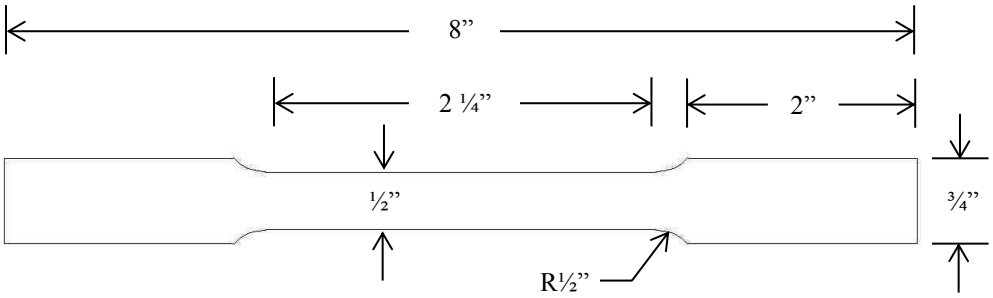

Figure D-1: Steel Coupon Dimensions

Table D-4: Steel Properties

	W8X35	W8X48
F_y [ksi]	52.01	51.56
F_u [ksi]	69.40	73.30